University of Leipzig
Fakulty for Physics and Geoscience
Leipzig Institute for Meteorology

Master Thesis

The effect of cities on aerosol and cloud properties concerning the planetary boundary layer observed with rural and urban lidar and sun photometer measurements in Melpitz and Leipzig

Stefanie Emmrich
Matriculation number: 2509521

Consultant: Prof. Dr. Andreas Macke
Second consultant: Jun.-Prof. Dr. Bernhard Pospichal
Tutor: Dr. Holger Baars

Leipzig, the 6th November 2015

Contents

Abstract

Strong urban-rural contrasts in the aerosol optical thickness (AOT) have been observed during two measurement campaigns in autumn (September to October) 2013 and summer (May to July) 2015. These campaigns took place simultaneously in Leipzig and Melpitz. Whereas Leipzig characterizes an urban influenced area, Melpitz is characterized by rural influence. In the framework of these campaigns, amongst others, lidar and sun photometer measurements were performed. The data from these campaigns are used to determine and quantify the differences in the AOT, planetary boundary layer (PBL) top height and PBL cloud base height as well as cloud cover. Thereby, it was found that the AOT in Melpitz is higher compared to Leipzig during both campaigns. The reason for this is the relative humidity which was significantly higher in Melpitz for both campaigns. Contrarily, the total particle number concentration was mostly higher in Leipzig than in Melpitz. Additionally, the air mass advection during the two campaigns and for different case studies has been investigated but no significant influence on the AOT and only little seasonal difference was found. Additionally, statistical results from the campaigns were analyzed. It turned out that there was a good correlation between both sites for the PBL top and cloud base height. Nevertheless, both quantities were found to be higher during the summer campaign, which is due to the higher temperatures leading to stronger vertical fluxes and thus a larger vertical extent of the boundary layer. Also, during the autumn campaign in 2013 a higher cloud amount was observed more frequently in Leipzig. For the summer campaign, the reverse case was seen.

1 Introduction

In 1950 nearly 30 % of the world's population lived in urban areas. This number increased to 54 % in the year 2014. The UN predicts further increasing numbers of people living in urban areas up to nearly 66 % in year 2050. The urbanization will grow particularly strong in the developing and emerging countries of the world. The strongest growth is expected to be in cities of China, India and Nigeria (UN, 2014). In the Federal Republic of Germany, in 2014 75 % of the inhabitants lived in cities. This number is also expected to grow to 83 % until year 2050 (UN, 2014).
Also connected to the urbanization is the change of meteorological quantities. Among other things, the increased aerosol concentration in the municipal atmosphere leads to reduced surface radiation (Jin et al., 2011). Some aerosols may also absorb radiation (e.g. soot) and change the downward terrestrial radiation. Additionally, there is a change of land surface parameters such as surface albedo, surface emissivity or surface temperature. The increasing urbanization changes the vertical fluxes of sensible and latent heat (Jin et al., 2011). Those fluxes are especially important for development of local and regional weather and they occur in the PBL.
Another important meteorological effect in connection with urbanization is the urban heat island (Oke, 1982). Cities are both at night and day warmer than the surrounding areas and they produce less evaporation compared to planted landscape areas (www.epa.gov, Status: 22.06.2015). This effect points to the fact that the heat flux from the surface into the atmosphere is much higher over the urban area than over the rural area. The higher temperatures in cities can be explained by this fact (Angevine et al., 2003).
In previous studies it was found that the urban PBL provides enhanced surface heat fluxes which leads to a deeper PBL and mostly higher PBL clouds over the urban area (Eresmaa et al., 2009). Nevertheless, the maximum PBL does not only depend on the surface heat flux but also on temperature and relative humidity (Barlow et al., 2014). This indicates the complexity of the urban-rural interaction.
Aerosols are of special interest for research concering differences between urban and rural areas as they are spatially and temporally very complex and variable and hence represent one of the major uncertainties in our understanding of climate, local weather and also air pollution. They lead to changes in the atmospheric radiation

budget by scattering and absorption and play an increasing role in questions of air quality and health (Wiedensohler et al., 2002 and Wiegner et al., 2006).
The differences between the city of Leipzig and the rural village of Melpitz with respect to aerosol properties has been investigated in the framework of this master thesis. Leipzig is a city of about half a million inhabitants with an urbanization area of about 300 km^2 and is representative for continental flat land climate of central Europe. It is characterized by an urban influenced area with high concentrations of particulates (Engler et al., 2012). Melpitz is situated 45 km northeast of Leipzig, characterized by mainly cultivated land and grass (see Spindler et al., 2010 and Spindler et al., 2013). Two measurement campaigns with several instruments, e.g. lidar and sun photometer, were performed in autumn 2013 and summer 2015 to quantify the differences between the two locations. This is of particular interest as the site of Melpitz is planned to become one of the new European supersites in the frame of ACTRIS (www.actris.eu, Status: 26.10.2015) and the remote sensing equipment which is now permanently in Leipzig is planned to be moved to Melpitz. For that reason, it is of high interest to find out if the data taken in Leipzig in the past is representative for Melpitz, too, and vice versa.
In this work, the AOT as well as the PBL top height and PBL cloud base height has been examined to find out urban-rural differences. By analyzing and comparing these quantities during the two campaigns, differences between the sites and maybe the seasons shall become visible.
In the following, the most important measurement instruments during the campaigns will be introduced. A focus is put on the lidar and the sun photometer and the results are linked to ground-based in-situ data (relative humidity, total number concentration). Subsequently, theoretical basics are explained. Aerosol particles and their growth as well as the lidar equation and the PBL will be introduced theoretically. Additionally, the methods used for data analysis and the urban climate will be explained. Afterwards, a detailed explanation of the measurement sites and the two campaigns is given. Last but not least, the results are presented and analyzed concerning the PBL top and cloud base height, the AOT and the relative humidity. Here, the focus is only on PBL clouds. The two campaigns are compared statistically and in the end, a short conclusion is given.

2 Measurement Instruments

In this Chapter, the most important measurement instruments used in the framework of two measurement campaigns in Leipzig and Melpitz in 2013 and 2015 are introduced and their mode of operation is explained in detail. The main focus is put on the lidar and the sun photometer.
Different quantities can be determined by the use of sun photometers or lidars such as the AOT, the Ångstrom exponent, the sky brightness, particle phase function and particle size distribution as well as PBL top height, cloud height and cloud cover (www.tropos.de, Status: 13.02.2015). Here, the sun photometer data are analyzed concerning the AOT whereas the lidar provides backscatter profiles from which the PBL top height, the cloud base height or the cloud cover can be determined. The AOT is a measure for extinction of sunlight by aerosols in the atmosphere such as sea salt, dust or smoke. Additionally, ground-based in-situ data are available. These data are analyzed concerning temperature, relative humidity or dry particle number concentration.

2.1 Lidar Polly^{XT}

Lidar measurements were performed during the two measurement campaigns both in Leipzig and Melpitz. 'Lidar' is the acronym for 'LIght Detection And Ranging'. The principle consists of sending light pulses into the atmosphere where a scatterer is detected by its backscattered radiation. The distance R of the scatterer from the lidar can be determined by the speed of light and the time span between the emission and the detection of the laser light pulse (Kreipl, 2006).
Measurements done by three different lidars of type Polly took place during the two campaigns. The principle and mode of operation is similar for all three used lidars and will be explained in detail for the lidar Polly^{XT} (compare Althausen et al., 2009) of Leibniz-Institute for Tropospheric Research (TROPOS).
The model Polly^{XT} is a multiwavelength-Raman and polarization lidar. Multiwavelength means that the system is able to operate at several defined wavelengths and polarization describes the direction of the electromagnetic field component of an

electromagnetic wave. Raman characterizes the inelastic scattering of light where the molecules that scatter the light absorb a part of the photon's energy and add additional energy to it. This causes a change in frequency and phase (wavelength) of the scattered light.
The open Polly instrument is shown in Fig. 2.1 (Althausen et al., 2009). The lidar is situated in a weatherproof telecommunication cabinet which is thermically insulated by double walls. Six wheels have been installed for better transportation so that the system is easy to handle. Inside the cabinet the laser head, the emitter optics and the receiver optics with the telescope and the seven channels are mounted on an optical laser table. The table has a tilt of 5°. The precipitation sensor on the roof ensures correct shutdown of the system during precipitation. The roof covering protects the quartz plates on top of the roof. Those plates avoid air exchange between the inner of the cabinet and the environment (Althausen et al., 2009).

Figure 2.1: Illustration of the open Polly^{XT} instrument. (1): Laser head, (2): power supply for laser, (3): beam expander, (4): receiver telescope, (5): receiver with seven channels, (6): power supply for PMT cooling unit for the 1064 nm channel, (7): computer with data acquisition and interface card, (8): uninterruptible power supply (UPS), (9): air conditioner, (10): sensors for measurements of temperature and rain outside, (11): roof cover (Althausen et al., 2009).

The optical setup of the lidar Polly^{XT} is shown in Fig. 2.2. The emitter parts are marked by 'E' while the receiver optics are marked by 'R'. The laser is a Nd:YAG

Type Inlite III (Continuum). The repetition rate of the laser pulses is 20 Hz and the energy per laser pulse is 450 mJ at 1064 nm. By use of second harmonic generation (SHG) and third harmonic generation (THG) crystals, laser pulses at 355 nm, 532 nm and 1064 nm are generated and simultaneously emitted. The transferred energy is nearly 180 mJ at 1064 nm, 110 mJ at 532 nm and 60 mJ at 355 nm. The emitted radiation is linear polarized at 532 nm.
After emission, the laser beam is directed upwards by two quartz prisms ('E1' and 'E2'). An achromatic beam expander ('E3') enlarges the beam diameter from 6 mm up to nearly 45 mm before the beam is emitted into the atmosphere. In the atmosphere, the light pulse interacts by scattering and/or absorption with molecules and particles. A part of the scattered light is scattered in direct backward direction. This means that light is scattered at 180° backward. The intensity of the scattered light is wavelength dependent.

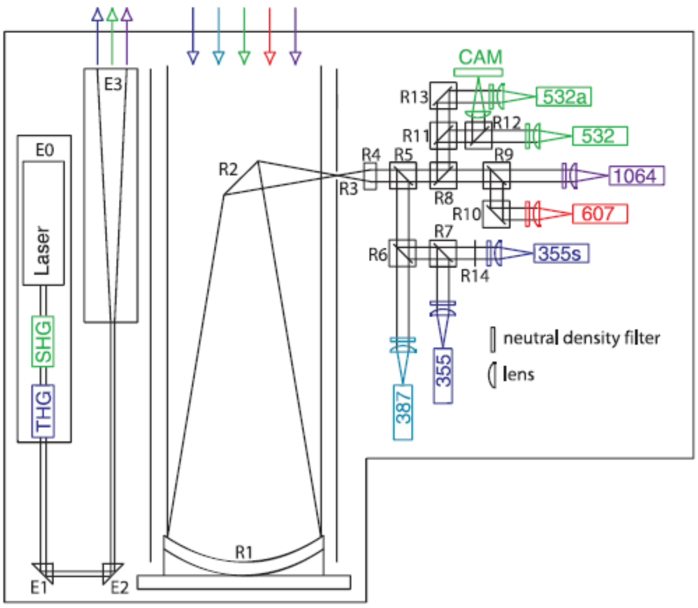

Figure 2.2: Optical setup of the multiwavelength-Raman and polarization lidar Polly^{XT}. The receiver optics are marked by 'R', the emitter optics by 'E' (Althausen et al., 2009).

The backscattered light is collected by a Newton telescope ('R1' and 'R2'). Its main mirror has a diameter of 300 mm and 900 mm focal length. The secondary mirror is a flat, elliptic one. Its main- and minor axis have lengths of 76,2 and 107,77 mm, respectively. The backscattered light is directed through a pinhole ('R3') which defines the field-of-view of 1 mrad. Behind the pinhole an achromatic lens ('R4') aligns the beam and leads the light into the seven detection channels. The focal length

of the achromatic lens is 60 mm. Different filters and dichroitic beamsplitters ('R5' to 'R13') separate and detect the light by its wavelengths. The beamsplitters were chosen to reflect light with shorter wavelengths and to transmit light with longer wavelengths. Furthermore, there is a polarizer ('R14') located in front of the 532 nm channel to ensure the proof of cross-polarized light at only 532 nm.
Behind each interference filter, a plano-convex lense with a 60 mm focal length in front of each photomultiplier tube (PMT) is mounted, except for the 1064 nm channel where a lense with a 100 mm focal length is located. The PMT's detect the light and count the photons. Furthermore, absorbing neutral density filters are mounted in front of each detection channel to damp the received light to the corresponding counting rate. The installed camera (CAM) is used for supervising and setting of the overlap of the emitted beam to the receiver field-of-view.
As already mentioned, the three used lidars are part of the Polly generation. In Table 2.1, the capabilities of the different lidars are shown. Here, α denotes the extinction, β the backscatter and δ characterizes the depolarization channels. During the campaign in 2013, the 'IfT' lidar was located in Leipzig. This 'IfT' lidar is the above explained lidar Polly^{XT}. During the campaign in 2015, the 'Prototype' lidar measured in Leipzig. The 'Oceanet' lidar performed measurements during both campaigns in Melpitz.
It can be seen from Table 2.1 that all three lidars contain measurement channels at 532 nm. Since the 'Prototype' lidar contains only channels at this wavelength, this wavelength is mainly chosen for data analysis. The other two lidars contain in addition UV and IR channels as well as a water vapor channel. The 'Oceanet' lidar also contains a near-range telescope. Due to the differences in the Polly systems, differences concerning the overlap showed up. The height where the laser beam and the receiver field-of-view completely coincide is defined as overlap. The 'IfT' lidar has a higher altitude of complete overlap (1500 m) compared to the other two lidars ('Prototype' lidar with 600-700 m and 'Oceanet' with 800 m height of complete overlap; Engelmann et al., 2015).

2.2 Sun Photometer

Beside the lidar measurements also sun photometer measurements took place in the framework of the field campaigns in Melpitz and Leipzig. These measurements are part of the AERONET-project (AErosol RObotic NETwork, Holben et al., 1998)

System	UV	VIS	IR	W/V	N/R	Overlap height	Resolution
Prototype		α, β				600-700 m	37.5m
IfT	α, β	α, β, δ	β	x		1500 m	30 m
Oceanet	α, β, δ	α, β, δ	β	x	x	800 m	7.5 m

Table 2.1: Measurement capabilities of the three different Polly systems at UV (355 nm), VIS (532 nm) and IR (1064 nm) wavelengths. Additionally, a water vapor (W/V) channel has been installed in two of the three systems. The 'Oceanet' lidar contains a near-range (N/R) telescope in addition. α denotes the extinction, β the backscatter and δ characterizes the depolarization channels. The x indicates whether this feature is available or not (adapted from Engelmann et al., 2015).

which is a worldwide network of ground-based sun photometers.
A sun photometer of the CIMEL company at Melpitz is shown in Fig. 2.3. It determines the intensity of solar radiation at different predetermined wavelengths and measures the difference of incoming solar radiation between the top of atmosphere and the surface and thus provides the AOT. Therefore, a constant radiation of the sun is assumed. A detailed description of the theory is given in the following. By use of this assumption, the atmosphere's opaqueness is calculated from the ratio of the incoming solar radiation on the ground to the radiation outside the atmosphere (Ehrlich, 30.03.2012).
This is done by use of the Lambert-Bouguer law (see Wendisch, 19.12.2013). It describes the extinction or attenuation of the spectral radiance I_λ along a slant path s through an atmospheric volume. Here, no multiple interactions such as multiple scattering or anything else is considered. The change of the relative radiance is given in differential form by:

$$\frac{dI_\lambda}{I_\lambda} = -b_{ext}(\lambda, s)ds, \tag{2.1}$$

where $b_{ext} = b_{sca} + b_{abs}$ describes the volumetric extinction coefficient. The integration of eq. 2.1 delivers an exponential decrease of the irradiance:

$$I_\lambda(s) = I_\lambda(s=0) \cdot exp\left[- \int_0^s b_{ext}(\lambda, s')ds' \right]. \tag{2.2}$$

This is the exponential form the Lambert-Bouguer law.
The Lambert-Bouguer law is preferably defined as a function of the aerosol optical thickness AOT as vertical coordinate and the radiance I_λ is replaced by the solar

irradiance $S_{dir,\lambda}$. It can be obtained from geometry

$$ds = -\frac{dz}{cos\theta_0} = -\frac{dz}{\mu_0}. \tag{2.3}$$

The negative sign denotes the downward direction and the index '0' indicates the direction from the sun.
Using equations 2.1 and 2.3 and replacing the radiance I_λ by the direct solar irradiance $S_{dir,\lambda}$ it can be obtained:

$$\frac{dS_{dir,\lambda}}{S_{dir,\lambda}} = -b_{ext}(\lambda, z)\left(-\frac{dz}{\mu_0}\right) = b_{ext}(\lambda, z)\frac{dz}{\mu_0}. \tag{2.4}$$

By this relation the slant path s is replaced by the geometric altitude z. In addition, the optical thickness AOT is used instead of the geometric altitude z. It is definded as:

$$dAOT(\lambda, z) = [b_{ext}(\lambda, z \to \infty) - b_{ext}(\lambda, z)]dz = -b_{ext}(\lambda, z)dz. \tag{2.5}$$

So it follows:

$$dz = -\frac{dAOT(\lambda, z)}{b_{ext}(\lambda, z)}. \tag{2.6}$$

From equations 2.3 and 2.6, the relative solar direct irradiance change is given by:

$$\begin{aligned}\frac{dS_{dir,\lambda}}{S_{dir,\lambda}} &= b_{ext}(\lambda, z)\frac{dz}{\mu_0} \\ &= b_{ext}(\lambda, z) \cdot \frac{1}{\mu_0} \cdot \left[-\frac{dAOT(\lambda, z)}{b_{ext}(\lambda, z)}\right] \\ &= -\frac{dAOT(\lambda, z)}{\mu_0}.\end{aligned} \tag{2.7}$$

Finally, it follows:

$$S_{dir,\lambda}[AOT(\lambda, z)] = S_{dir,\lambda,TOA} \cdot exp\left[-\frac{AOT(\lambda, z)}{\mu_0}\right]. \tag{2.8}$$

This means that the direct solar spectral irradiance incident at the top of atmosphere is attenuated exponentially with respect to the spectral optical thickness. The attenuation is stronger for a low sun which is due to the longer path length the photons need to travel through the atmosphere (Wendisch, 19.12.2013). By use of this theory, CIMEL is able to calculate the AOT.
The optical sensor head of the instrument includes two detectors. They measure the current incoming solar radiation and cover the spectrum from 340 nm to 1020 nm.

Figure 2.3: Illustration of the sun photometer used in Melpitz. Photo taken by Patric Seifert.

Each detector has a very narrow field-of-view (www.cimel.fr, Status: 20.04.2015). During the two campaigns, two different sun photometers were used. One was located at TROPOS, the other one in Melpitz. They performed more or less simultaneous measurements during the campaigns. After the campaign in 2015, the sun photometer from Melpitz was set up next to the sun photometer at TROPOS to do comparison measurements. The result of this measurement is shown in Fig. 2.4. It can be seen that there is a small offset in the correlation plot. This means that the sun photometer from Melpitz (#649) is measuring slightly enhanced values compared to the one measuring in Leipzig. This means that slightly higher AOT values are measured in Melpitz than actually were present. Nevertheless, since the offset is very small it can be neglected for data analysis.

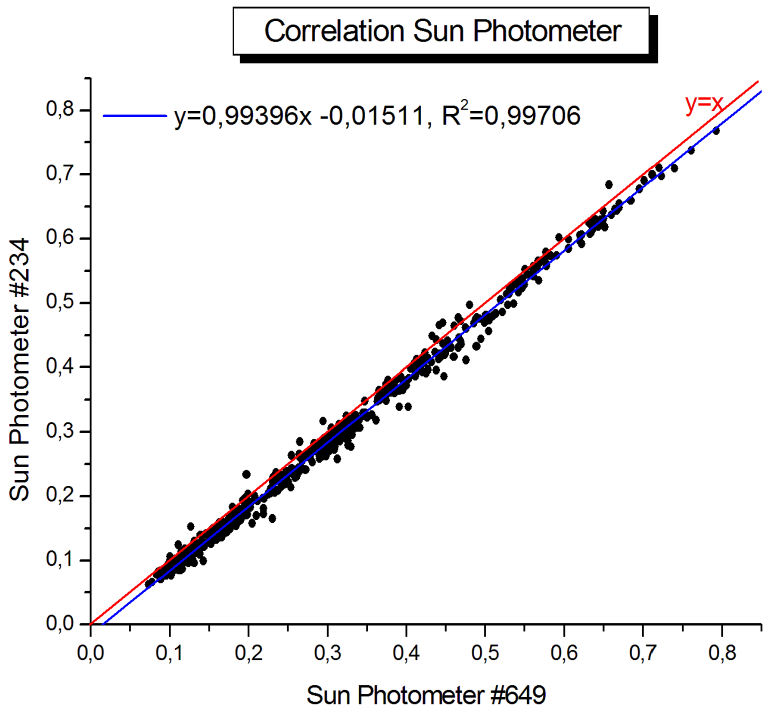

Figure 2.4: Correlation of the sun photometers used in Leipzig and Melpitz. #649 performed measurements in Melpitz and #234 in Leipzig. Formula for linear regression (blue line) and 1:1 line (red line) is also shown.

3 Theory

In this Chapter, theoretical basics and the methods concerning data analysis used in the master thesis are introduced.
At first, the aerosol particles and their growth are explained. Next, the lidar equation is introduced and the PBL will be explained. After this, the determination of PBL top height as well as PBL cloud base height is explained because it is used for data analysis. The urban climate is introduced and the HYSPLIT program is shown because it is also used for analysis. Additionally, statistical metrics are introduced shortly.

3.1 Aerosol particles and their growth

An atmospheric aerosol is defined as a solid and/or liquid particle, suspended in a gas (in our case the air, Wiedensohler, 13.12.2013). Atmospheric aerosols particles have different sizes that range from clusters of some few molecules to particles of 100 μm and larger. Atmospheric aerosols can also be classified into different size classes. The first class characterizes ultrafine particles with a diameter smaller than 100 nm. On their part, this class consists of the Nucleation mode (d = 1 - 10 nm) and the Aitken mode (d = 10 - 100 nm). The next class enfolds fine particles with a diameter smaller than 1 μm and includes the Accumulation mode (d = 100 - 1000 nm). The last class is described by coarse particles (d > 1 μm, Wiedensohler, 13.12.2013).
The concentration of the aerosol particles varies strongly with time and location. It also depends on the vicinity of the source, the rate of emission, the strength of diffusive or convective transfer rates, various removal mechanisms or meteorological parameters. The last two dependencies affect the horizontal and vertical distribution of aerosol particles. The concentration of atmospheric aerosol particles is usually decreasing with increasing height because the majority of aerosol particle sources is on the earth's surface and removal mechanisms operate continuously within the atmosphere. Pruppacher and Klett (1997) suggested that, on average, nearly 80 % of the total aerosol particle mass is contained in the lowest kilometer of the tropo-

sphere.
There are two major sources for aerosol particles. These sources are spatial and widespread surface sources. The spatial sources contain gas to particle conversion which may occur by heterogeneous or homogeneous nucleation, clouds that serve as source of aerosol or extraterrestrial sources such as cosmic dust or particles from meteorite showers. The widespread surface sources contain biogenic sources (living or dead biological particles), volcanoes (dust and ash), oceans and fresh water (mainly sea salt), crustal and cryospheric aerosols such as desert dust and particles from biomass burning (Hobbs, 1993).
Additionally, Hobbs (1993) investigated urban and rural aerosols. The author found out that the aerosols in rural areas are mostly continental but with a moderate impact from anthropogenic sources. Indeed, the aerosols over urban areas have a special character. This is due to the dominant influence of anthropogenic emission such as industries, households or traffic.
The aerosol particle growth, especially at a high relative humidity, is very important for the further investigations. The growth of natural aerosol particles with increasing relative humidity occurs comparatively continuous. This means, with higher relative humidity the particles become larger. This holds only true for natural aerosol particles which consist of a mixture of soluble and insoluble particles (Skupin, 2013). With increasing relative humidity there is also a change in particle size distribution as well as refractive index. These changes also lead to changes in the optical properties of the particles such as the extinction coefficient. This coefficient is composed of the particle absorption coefficient and the particle scattering coefficient. The extinction coefficient itself depends on the refractive index and a change in this quantity also leads to changes in scattering and absorption properties (Skupin, 2013).

3.2 Lidar equation and evaluation algorithms

A lidar measures the intensity of the backscattered light. This intensity depends on several atmospheric and instrumental properties and is described by the lidar equation which will be explained in detail in the following (compare www.tropos.de, Status: 06.01.2015 and Ansmann and Müller, 2005). The general lidar equation is given by:

$$P(R) = \frac{E_0 \eta_L}{R^2} \cdot O(R) \cdot \beta(R) \cdot T(R). \tag{3.1}$$

This equation describes the strength $P(R)$ of the backscattered light from the location R at a certain wavelength. The signal $P(R)$ depends on four quantities. The first term describes the system constant, $O(R)$ is the overlap between the leaving laser beam and the receiver field-of-view of the telescope, $\beta(R)$ describes the backscatter coefficient and $T(R)$ characterizes the transmission term.
The system constant is a quantity which is hard to determine experimentally, with E_0 the transmitting laser pulse energy and η_L, which contains parameters for description of optical and detectional units.
The backscatter coefficient $\beta(R)$ determines the strength of the lidar signal and indicates how much light is scattered in backward direction. It is given by:

$$\beta(R, \lambda) = \beta_{mol}(R, \lambda) + \beta_{aer}(R, \lambda), \tag{3.2}$$

where the laser beam in the atmosphere is scattered both at air molecules and particles. The scattering at air molecules mainly depends on the air density. The contribution by particles is both temporally and spatially variable.
The last term of equation 3.1 is given by:

$$T(R, \lambda) = \exp\Big[-2\int_0^R \alpha(r, \lambda)dr\Big]. \tag{3.3}$$

This equation describes the part of the light that is lost on the way through the atmosphere and it follows from the special form of the Lambert-Bouguer law (compare Section 2.2). The integral describes the path of the light from the lidar to the place where backscatter occurs. The factor two contains the way towards the target and back to the lidar. $\alpha(R, \lambda)$ is the extinction coefficient and results from the absorption and scattering of light by molecules and particles:

$$\alpha(R, \lambda) = \underbrace{\alpha_{mol,sca}(R, \lambda) + \alpha_{mol,abs}(R, \lambda)}_{ext} + \underbrace{\alpha_{aer,sca}(R, \lambda) + \alpha_{aer,abs}(R, \lambda)}_{ext}. \tag{3.4}$$

As already seen from the equations above, α and β depend on the wavelength of the laser light.
To obtain further information about the particle extinction and particle backscatter coefficient from these measured lidar data, evaluation algorithms have to be applied. In the following, the Klett method (Klett, 1981) as well as the Raman method (Mitev et al., 1992) will be introduced and explained.
The lidar signal still contains the background signal. This has to be subtracted from the measured values first.
Afterwards, for determination of the particle properties, the lidar equation has to

be solved for the backscatter and extinction coefficient. Now, the Klett method is introduced first.
The equations 3.1, 3.2 and 3.4 can be summarized to:

$$S(R) = E_0\eta_L[\beta_{aer}(R) + \beta_{mol}(R)]exp\Big[-2\int_0^R[\alpha_{aer}(r) + \alpha_{mol}(r)]dr\Big], \tag{3.5}$$

with the range-corrected signal $S(R) = R^2P(R)$. The molecular scattering properties, $\beta_{mol}(R)$ and $\alpha_{mol}(R)$, can be obtained from the available meteorological data of pressure and temperature or they are estimated under use of the standard atmosphere. This means that only the aerosol backscatter and extinction properties, $\beta_{aer}(R)$ und $\alpha_{aer}(R)$, remain for determination. The problem with this method is that the lidar displays only one signal P but there exist two unknown quantities (α_{aer} and β_{aer}). For that reason the lidar ratio

$$L_{aer}(R) = \frac{\alpha_{aer}(R)}{\beta_{aer}(R)} \tag{3.6}$$

has to be chosen a priori. The particle lidar ratio depends, in comparison to the molecular lidar ratio ($L_{mol} = \frac{8\pi}{3}sr$), on the size distribution, the shape and the chemical composition.
Likewise, another term is introduced:

$$Y(R) = L_{aer}(R)[\beta_{aer}(R) + \beta_{mol}(R)]. \tag{3.7}$$

The following equation is obtained after substitution of $\alpha_{aer}(R)$ and $\alpha_{mol}(R)$ in eq. 3.5 with the expression from eq. 3.6 and the insertion of eq. 3.7:

$$S(R)L_{aer}(R)exp\Big\{-2\int_0^R[L_{aer}(r)-L_{mol}]\beta_{mol}(r)dr\Big\} = E_0\eta_L Y(R)exp\Big[-2\int_0^R Y(r)dr\Big]. \tag{3.8}$$

After applying the logarithm to both sides of the equation and the differentiation with respect to R, the Bernoulli equation is obtained. This one is at last solved for the boundary conditions

$$Y(R_0) = L_{aer}(R_0)[\beta_{aer}(R_0) + \beta_{mol}(R_0)] \tag{3.9}$$

and the following final equation is obtained:

$$\beta_{aer}(R) + \beta_{mol} = \frac{S(R)exp\Big\{-2\int_{R_0}^R[L_{aer}(r) - L_{mol}]\beta_{mol}(r)dr\Big\}}{\frac{S(R_0)}{\beta_{aer}(R_0)+\beta_{mol}(R_0)} - 2\int_{R_0}^R L_{aer}(r)S(r)T(r,R_0)dr} \tag{3.10}$$

with

$$T(r, R_0) = exp\Big\{ -2 \int_{R_0}^{r} [L_{aer}(r') - L_{mol}]\beta_{mol}(r')dr' \Big\}.$$

The profiles of the particle extinction coefficients can be determined from the solution $\beta_{aer}(R)$ by:

$$\alpha_{aer}(R) = L_{aer}(R)\beta_{aer}(R). \tag{3.11}$$

Equation 3.10 can be integrated starting from the reference value R_0. This value either describes the near end ($R > R_0$, forward integration) or the far end ($R < R_0$, backward integration) of the measurement range. Numerical stability can only be guaranteed for backward integration. Usually the reference range R_0 in equation 3.10 is chosen so that at point R_0 the particle backscatter coefficient is negligible compared to the known molecule backscatter coefficient.
The advantage of this method is the high spatial and temporal resolution (Ansmann, 10.12.2014). The most critical parameter is the lidar ratio $L_{aer}(R)$. This has to be assumed first. This quantity depends on the microphysical, chemical and morphological properties of the particles. On their part, these properties depend on the relative humidity. The lidar ratio can vary strongly with height since the relative humidity varies with height.

This problem can be avoided by the use of the Raman method (Ansmann and Müller, 2005). This method measures the air molecules and particles elastically backscattered and the nitrogen or oxygen molecules inelastically backscattered lidar signal. The Raman method can be used mainly only at night in the abscence of the bright sky background whereas the Klett method can be used during day time (Ansmann and Müller, 2005).
With the Raman method, the particle extinction coefficient can be determined from the Raman backscatter signal. By use of this method, no lidar ratio assumptions are needed. The advantage of this method becomes apparent from the equivalent lidar equation for the Raman backscatter signal:

$$P(R, \lambda_{Ra}) = \frac{E_0 \eta_{\lambda_{Ra}}}{R^2} O(R, \lambda_{Ra})\beta_{Ra}(R, \lambda_0) \times exp\Big\{ - \int_0^R [\alpha(r, \lambda_0) + \alpha(r, \lambda_{Ra})]dr \Big\}. \tag{3.12}$$

The coefficient β_{Ra} describes the Raman backscatter coefficient, $\alpha(R, \lambda_0)$ characterizes the extinction coefficient on the way to the region of backscatter and $\alpha(R, \lambda_{Ra})$ describes the extinction coefficient on the way back to the lidar. The advantage of this method is that the lidar provides one signal for solving one unknown (α).

It arises from equation 3.12 that no particle backscatter occurs. The only particle scattering effect on the signal strength contains the attenuation.
The Raman backscatter coefficient can be calculated from the molecular number density N_{Ra}. This corresponds to the number density of the nitrogen or oxygen molecules:

$$\beta_{Ra}(R, \lambda_0) = N_{Ra}(R)\frac{d\sigma_{Ra}}{d\Omega}(\pi, \lambda_0). \tag{3.13}$$

$\frac{d\sigma_{Ra}}{d\Omega}(\pi, \lambda_0)$ is the molecular (differential) cross section of the scattering process at the laser wavelength λ_0 and the scattering angle π. The molecular number density profiles are obtained from current radiosonde observations or the standard atmosphere.
The following equation is obtained after inserting eq. 3.13 into eq. 3.12, the appliance of the logarithm to both sides of the new equation, the differentiation with respect to R and the rewriting:

$$\alpha(R, \lambda_0) + \alpha(R, \lambda_{Ra}) = \frac{d}{dR} ln \frac{N_{Ra}(R)}{S(R, \lambda_{Ra})} + \frac{d}{dR} lnO(R, \lambda_{Ra}). \tag{3.14}$$

Here, $S(R, \lambda_{Ra}) = R^2 P(R, \lambda_{Ra})$ is again the range-corrected molecule signal. The total laser beam and receiver field-of-view overlap is lidar specific and ,e.g., not guaranteed for ranges under 1500 m in case of Polly^{XT}. For this reason, the measurement range has to be increased by a correction of the overlap function. This correction is based on measurements of the overlap profile with the same lidar on cloudfree days. However, it follows that the determination of the extinction coefficient near the lidar is very sensitive to the overlap uncertainties near the lidar. The overlap near the lidar is small and changes rapidly with distance.
For this reason, the optimal measurement range is considered in the following. This means that an exact overlap correction is assumed and thus the overlap term in eq. 3.14 can be neglected. With eq. 3.4 it can be written:

$$\alpha_{aer}(R, \lambda_0) + \alpha_{aer}(R, \lambda_{Ra}) = \frac{d}{dR} ln \frac{N_{Ra}(R)}{S(R, \lambda_{Ra})} - \alpha_{mol}(R, \lambda_0) - \alpha_{mol}(R, \lambda_{Ra}). \tag{3.15}$$

The Ångstrom exponent å(R) is introduced to obtain the extinction coefficient at the transmitted wavelength. This describes the wavelength dependency of the particle extinction coefficient

$$\frac{\alpha_{aer}(\lambda_0)}{\alpha_{aer}(\lambda_{Ra})} = \left(\frac{\lambda_{Ra}}{\lambda_0}\right)^{å(R)}. \tag{3.16}$$

In the end it follows:

$$\alpha_{aer}(R,\lambda_0) = \frac{\frac{d}{dR}ln\frac{N_{Ra}(R)}{S(R,\lambda_{Ra})} - \alpha_{mol}(R,\lambda_0) - \alpha_{mol}(R,\lambda_{Ra})}{1+\left(\frac{\lambda_0}{\lambda_{Ra}}\right)^{å(R)}}. \tag{3.17}$$

Here, in comparison to the Klett method, no critical assumptions are necessary. Besides the extinction coefficient, the backscatter coefficient can be determined from the ratio of the aerosol backscatter signal to the molecular backscatter signal. The particle backscatter coefficient, $\beta_{aer}(R,\lambda_0)$, as a function of the laser wavelength λ_0, can be determined both by the use of the total (particle plus molecule) and the pure molecular backscatter signal. Therefore, two measured signal pairs $P(R,\lambda_0)$ and $P(R,\lambda_{Ra})$ at R and R_0 are required. A solution for the backscatter coefficient $\beta_{aer}(R,\lambda_0)$ is obtained from the two lidar signals $P(R,\lambda_0)$ and $P(R_0,\lambda_0)$ of the total backscatter (see eq. 3.1) and two other lidar signals $P(R,\lambda_{Ra})$ and $P(R_0,\lambda_{Ra})$ from the Raman backscatter (eq. 3.12). Therefore, the following ratio is needed:

$$\frac{P(R_0,\lambda_{Ra})P(R,\lambda_0)}{P(R_0,\lambda_0)P(R,\lambda_{Ra})}. \tag{3.18}$$

In the end, the solution for the backscatter coefficient results from inserting the correspondant lidar equations for the four signals and rewriting the resulting equations:

$$\begin{aligned}\beta_{aer}(R,\lambda_0)+\beta_{mol}(R,\lambda_0) = {}&[\beta_{aer}(R_0,\lambda_0)+\beta_{mol}(R_0,\lambda_0)]\frac{P(R_0,\lambda_{Ra})P(R,\lambda_0)}{P(R_0,\lambda_0)P(R,\lambda_{Ra})}\frac{N_{Ra}(R)}{N_{Ra}(R_0)}\\ &\times\frac{exp\{-\int_{R_0}^{R}[\alpha_{aer}(r,\lambda_{Ra})+\alpha_{mol}(r,\lambda_{Ra})]dr\}}{exp\{-\int_{R_0}^{R}[\alpha_{aer}(r,\lambda_0)+\alpha_{mol}(r,\lambda_0)]dr\}}.\end{aligned} \tag{3.19}$$

The overlap effect cancels out in case both signal channels are aligned to each other. Hence, the backscatter coefficient can even be determined for height ranges close to the lidar.

As already seen at the Klett method, a reference value for the particle backscatter needs to be determined. The reference height is chosen in the upper troposphere where particle scattering is negligible compared to Rayleigh scattering. For solving eq. 3.19, only the air density, the molecule backscatter and atmospheric extinction properties have to be determined. They result from meteorological profiles or the standard atmosphere.

The particle transmission ratio for the height range between R_0 and R is determined from the measured particle extinction profiles assuming the wavelength dependency

$\lambda^{å}$. The height profile of the particle lidar ratio yields from the profiles of $\alpha_{aer}(R, \lambda_0)$ and $\beta_{aer}(R, \lambda_0)$:

$$L_{aer}(R, \lambda_0) = \frac{\alpha_{aer}(R, \lambda_0)}{\beta_{aer}(R, \lambda_0)}. \tag{3.20}$$

For vertically aligned lidars it follows $R \equiv z$ (Ansmann and Müller, 2005).
The advantage of this method consists in the exact determination of the vertical profile of the extinction coefficient and the lidar ratio. The disadvantage comprises the poor temporal and spatial resolution (Ansmann, 10.12.2014).
Following, after determining the particle backscatter and the extinction coefficient by one of the introduced algorithms, further quantities can be derived such as the linear depolarization ratio after Freudenthaler et al. (2009). The linear depolarization ratio provides information about the particle shape. Spherical particles do not change the polarization of the emitted light but non spherical particles produce a depolarization.
The Ångstrom exponent provides information about the particle size. The bigger this exponent, the smaller the particles are.
Furthermore, the PBL top height, the PBL cloud height as well as the PBL cloud fraction can be determind and derived from lidar profiles. In this work, the automatically determined backscatter and extinction profiles obtained as described in Baars et al. (2015) are used. In the following, the terms backscatter and extinction coefficient always refer to the particle backscatter and particle extinction.

3.3 Planetary boundary layer

As next step, the PBL will be further introduced.
The earth's atmosphere consists of several layers. The most important layer for weather is the troposphere. This layer can be devided into two layers. The upper one is the free troposphere, whereas the lower part is the PBL. In the free troposphere, the geostrophic wind equilibrium can be approximated and frictional forces are of little importance. The PBL, the lowest layer of the atmosphere, is much more turbulent and friction plays an important role. It is defined as the layer of air which is directly above the earth's surface. The effects of the surface like heating and cooling or friction can be felt directly on time scales less than a day. Within this layer, significant fluxes of momentum, heat or matter take place and they are carried by turbulent motions (Garratt, 1992).
The PBL at day extends from roughly some hundreds of meters until two to three

kilometers. This height depends strongly on the time of day, the season of year as well as the geographical position. The PBL is influenced by the diurnal cycle of day (surface heating and cooling) and the presence of clouds. During stable night conditions, the PBL reaches heights of roughly 50 - 100 m. The PBL is in every sense very important for humanity since we spend nearly the whole lifetime within this layer. In a meteorological way it is also important with regard to trace gases getting captured within this layer and the mixing of aerosol, water vapor or other material into the free troposphere (Garratt, 1992).
The upper part of the convective PBL is defined at the transition zone between the convective PBL and the free troposphere. There is often a temperature inversion which prevents the vertical distribution of the turbulent momentum in the PBL into the free troposphere (Garratt, 1992).
The PBL has some characteristical properties, such as a high degree of turbulence, high energy dissipation because of the high friction and fast vertical mixing of trace gases. The most important feature is the turbulent flow and mixing. The convective mixing of the PBL is mainly caused by two mechanisms: 1) a strong heating of the earth's surface due to the sun which leads to convective rising of air masses and 2) the actinic cooling at upper cloud top which leads to local sinking of air parcels. Additionally, turbulence can be produced by strong vertical wind shear.
The PBL undergoes mainly three parts during the diurnal cycle of a day. The first part is the 'Mixed Layer' during day (see Fig. 3.1). The production of turbulence weakens shortly before sunset though the already turbulent air remains as so-called 'Residual Layer'. This layer is mostly layered thermodynamically neutral and the turbulence is roughly isotropic. The so-called 'Stable Nocturnal Boundary Layer' is the layer closest to the surface and a very stable one during nighttime (Garratt, 1992).
Barlow et al. (2014) made some investigations about the PBL top height over London and a rural area where they found out that the diurnal cycle of PBL top height is strongly linked to the surface heat flux, both in the city and the rural site. In the morning the evolution of PBL height starts at nearly the same time as the increase of surface heat flux. They found out that there are four different phases of PBL stability over the city. The first phase is characterized by a rapid growth of the convective urban PBL, the second phase by a fully developed PBL. In the third phase the decay of the convective PBL occurs, whereas in the fourth phase a transition from the unstable to the more stable PBL (the nocturnal PBL) happens. In the last phase, a stable nocturnal layer can be found. For the rural PBL, the first

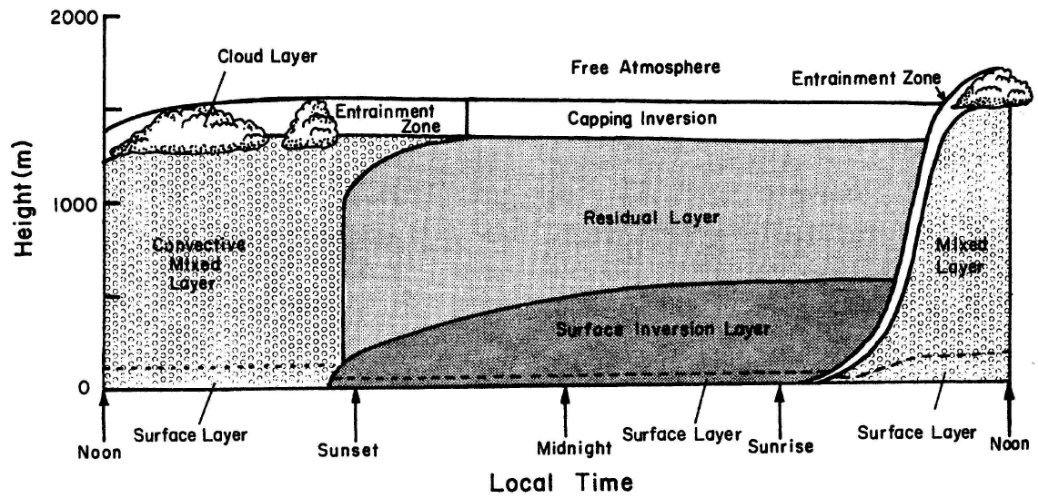

Figure 3.1: The typical diurnal setup of the PBL. It consists of mainly three parts: (1) a very turbulent 'Mixed Layer' during day, (2) a less turbulent mixed 'Residual Layer' which contains some parts of the former turbulent air and (3) a 'Nocturnal Stable Layer' where the turbulence is very low (Garratt, 1992).

two phases are similar whereas the decay of the PBL is more rapid for the rural site and the transition to the stable nocturnal layer occurs already in phase three. This means that stable conditions over the rural site occur up to three hours before the urban site. Nevertheless, they found out that the PBL top height over the city was in most cases higher compared to the rural measurement site.

3.4 Determination of boundary layer top

The following Chapter adresses the determination of the PBL top by use of different lidar techniques. The gradient method, the variance analysis as well as the wavelet covariance transform technique and the gradient Richardson scheme will be explained. The gradient method as well as the wavelet covariance method assume that the PBL contains more aerosol particles than the free troposphere. This results in a strong decrease of the backscatter signal on top of the PBL. However, the variance analysis uses the strong temporal variation of the lidar signal on top of the PBL. This is caused by entrainment of particle free air from the free troposphere into the PBL. The gradient method, the variance analysis and the gradient Richardson scheme are shown in Fig. 3.2 (Baars et al., 2008).
The idealized profile of a lidar measurement is depicted in Fig. 3.2 a). The drawn

profile could be assumed as concentration of atmospheric aerosol particles. High values of backscatter are visible in the PBL as well as distinct lower values in the free troposphere. Likewise, the strong decrease of the lidar signal on top of the PBL is discernible.
The gradient method is shown in Fig. 3.2 b). This method makes use of the first or second derivative of the range-corrected lidar signal with respect to the height. The minimum gradient indicates the top of the PBL.
The variance analysis is illustrated in Fig. 3.2 c). Here, a maximum in the profile of the sum of the squares of the deviation of the lidar signal from a mean value, for example a five minute or one hour measurement time span, is searched and the maximum is reached in the middle of the transition zone. The transition zone or entrainment layer is defined as that layer where the mixing of the polluted PBL air and the clean free tropospheric air significantly influences the aerosol concentration in each arbitrary height within this layer (Baars et al., 2008).

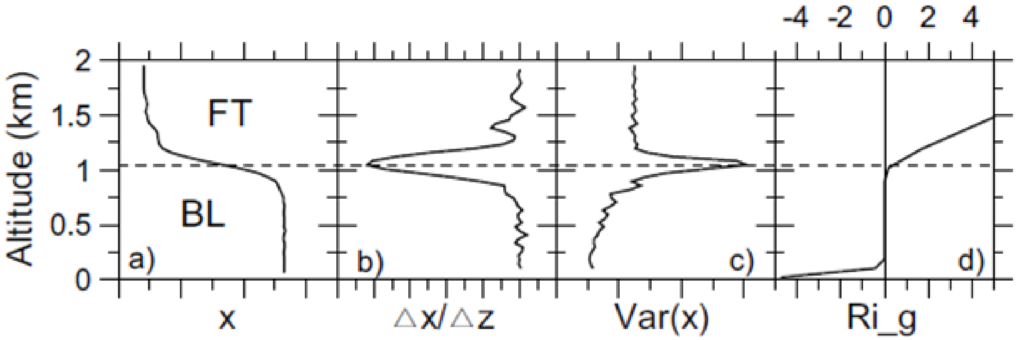

Figure 3.2: Derivation of the PBL top height by different lidar techniques. a) Idealized profile of an atmospheric quantity, b) profile of the gradient method, c) profile of the variance analysis, d) profile of the gradient Richardson number scheme (Baars et al., 2008).

Furthermore, the gradient Richardson scheme is presented in Fig. 3.2 d). Among other things, this approach is used for the numerical prediction model COSMO of the German Weather Service (www.cosmo-model.org, Status: 25.02.2015). This method seeks for a transition from the thermically and dynamically unstable PBL to the more stable overlying layer. Therefore, for identification of the PBL top, a critical Richardson number (0.38 in the COMSO model, Baars et al., 2008) is introduced. In the turbulent PBL, the Richardson number is lower than 0.38. This number exceeds the critical value in case the production of the turbulence signif-

icantly weakens and finally vanishes at the PBL top. This method is not very suitable for measurements during stable stratification that extends from the surface up to three kilometer height. These conditions often occur during nighttime and this method is unable to determine the PBL under these conditions since the method assumes that the PBL is in a steady state (Baars et al., 2008).
There exists another approach to determine the PBL top height. This is done by just fitting an idealized profile to the measured one (see Fig. 3.2 a)). This profile is marked by height-independent backscattering the lower PBL, a decrease of the backscatter signal in the transition zone and at least another height-independent backscatter in the free troposphere. Here, the top of the PBL coincides with the middle of the transition zone (Baars et al., 2008).
The wavelet covariance transform technique (Fig. 3.3) is a very often used algorithm and analyzes the aerosol signature of the range-corrected signal profiles. This methodology is used in this work. It is less influenced by signal noise than the gradient and variance method. The wavelet covariance transform technique is described by the following formula:

$$W_f(a,b) = \frac{1}{a}\int_{z_b}^{z_t} f(z)h\Big(\frac{z-b}{a}\Big)dz,$$

where $f(z)$ is the range-corrected backscatter signal, z is the measurement height and z_b and z_t are the lower and upper boundaries of the lidar backscatter signal gradient, respectively. $h(\frac{z-b}{a})$ describes the Haar- or step function (depicted in Fig. 3.3 b)). The dilation a describes the size of the step function, the translation b determines the position of the step. The covariance transform $W_f(a,b)$ is a measure for the similarity of the range-corrected lidar backscatter signal and the Haar function.
In case of a clear lidar profile signature such as in Fig. 3.3 a) with high backscatter values in the PBL and significantly less backscatter values in the free troposphere, $W_f(a,b)$ supposes a clear local maximum at the height of the PBL top, as is the case for n = 12 in Fig. 3.3 c). The choice of a suitable value of dilation is the biggest challenge in succesfully determing the PBL top by use of the wavelet covariance transform technique. For rather small values of a, signal noise is dominating the vertical profile (see Fig. 3.3 c) for $a = 2\Delta z = 75$ m). On the other hand, a huge dilation leads to the fact that further aerosol layers in the lower free troposphere cannot be detected (Baars et al., 2008).

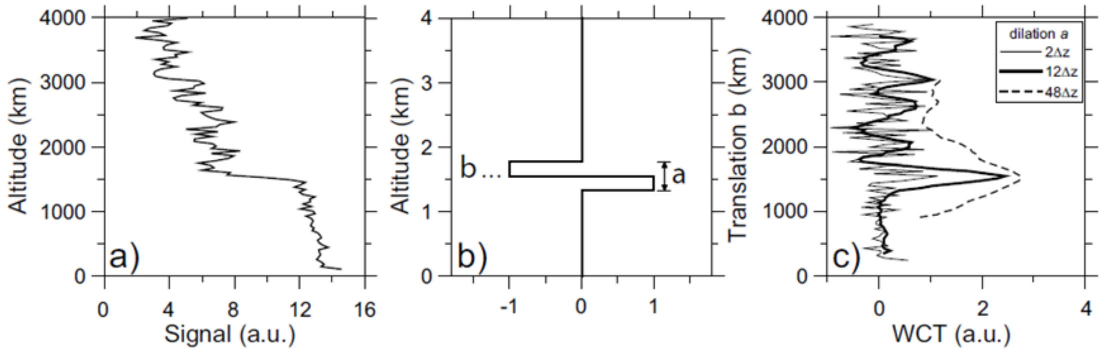

Figure 3.3: Derivation of the PBL top height by use of the wavelet covariance transform technique. a) Lidar signal profile, b) Haar- or step function, c) resulting covariance transform at values of $a = 2\Delta z$, $12\Delta z$ and $48\Delta z$ (Baars et al., 2008).

3.5 Determination of the cloud base height and cloud cover

Beside the PBL top height also the PBL cloud base height as well as the PBL cloud cover is analyzed in this work and thus the methodology explained in the following. For determination of the cloud base height, the lidar equation holds true again (see eq. 3.1). In a homogeneous, undisturbed atmosphere the signal is dropping off monotonically with height. When a cloud occurs, an enhancement in $P(R)$ is due to the presence of cloud droplets. So the PBL cloud base height can easily be detected from the lidar return signal. It can be found at that altitude where the signal shows the highest increase. Another way to determine the cloud base heights works via forming the first derivative of the backscatter intensity dP/dr where this intensity changes sign from negative to positive (compare Pal et al., 1992 and Demoz et al., 1999).

For analyzing the cloud cover, only PBL clouds are taken into account. Here, an algorithm analog to the one used by the German Weather Service (compare DWD, 1998 and DWD, 2010) was applied. The data is averaged over ten bins which corresponds to a time intervall of five minutes. This means that every five minutes backscatter returns in terms of cloud base heights are obtained. The backscatter signals used for cloud cover determination are divided into three categories: no cloud hits, cloud hits or unknown hits. Every time when there is a cloud detected, it is counted as 'cloud hit'. Unknown hits mean events like rain or fog. In this work, only clear cloud hits have been investigated and processed, unknown hits were skipped. After averaging the dataset over five minutes, each hour contains a dataset of twelve cloud base heights. The amount of cloud cover is determined by adding the total number of cloud hits and the calculation of the ratio of these hits to the total possible number of hits.

3.6 Urban climate

Now some fundamentals about the so-called 'Urban Heat Island' (Oke, 1982) are introduced. This term is used for urban areas, which are usually warmer than surrounding rural areas. The annual mean air temperature of a city with around one million people can be up to 1 °C to 3 °C higher compared to the rural area. The effect of the urban heat island increases also with increasing size of the city (Oke, 1982).

The urban heat island occurs over the city, both at the surface and in the atmosphere above the city and is present both at day and night. It is strongest during day, when sun is shining and weakest during the late morning and starts to grow after sunrise (www.epa.gov, Status: 22.06.2015).

The effect of the urban heat island is caused by the changes in thermal and radiative properties of the urban infrastructure and the development of it. Buildings, streets and other things have an impact on the urban climate and huge buildings for example can slow down the rate at which the city is cooling down at night (Oke, 1982).

In rural areas, natural vegetation clearly dominates the landscape. Usually, this results in a lower surface temperature compared to the city. The natural vegetation reduces the air temperature due to the evapotranspiration which describes the transfer of latent heat via evaporating water. During this process, plants release water to the surrounding air which dissipates ambient heat. Due to this effect, the relative humidity over rural areas is higher than over the urban area. On the other hand, the city is characterized by much less natural vegetation and significantly more dry and impervious surfaces such as roads, buildings, roofs, parking lots and other things. Thus, less evapotranspiration can take place over the city due to the lower natural vegetation cover. As a result, the urban area cannot cool down so much and gets warmer than the rural area due to the higher surface and air temperature (Bornstein, 1968).

Additionally, the urban heat island is influenced by the geographic location of the

city (e.g. if there are rivers or mountains near the city), special weather patterns and their changes on a daily and seasonal basis. Especially in summer, on dry, hot and sunny days, the incoming solar radiation can heat the urban surfaces to higher values than the ambient air temperature. In comparison, at rural sites the surface temperature remains closely to the air temperature. The magnitude of this effect varies with seasons due to changes in the intensity of incoming solar radiation. This means that the urban heat island gets largest in summer. Other facts that may have an influence on this effect are cloud cover and the weather in general. Most intense urban heat islands occur on calm and sunny days in summer. Heavy cloud cover can block the solar radiation and reduces the warming. Increased atmospheric mixing is caused by strong winds and thus the rural-urban temperature difference is lowered (Bornstein, 1968).
Another fact that has to be taken into account is that urban areas lead to changes in different quantities such as albedo, thermal emissivity or the heat capacity. The color of the surface is of matter for the albedo. Darker surfaces reflect less of the solar radiation compared to brighter surfaces which leads to a decrease of albedo for the city. This causes less reflection and thus more absorption in urban areas and thus, again, higher surface and air temperatures. Another quantity that is different in an urban area compared to the rural one is the thermal emissivity. Most of the construction materials in a city have high thermal emittance values, which means that they cannot stay cool for a long time since they release heat quite badly and thus store the heat. Additionally, the heat capacity of a material is very important since this quantity describes the ability to store heat. Usually, urban material has a higher heat capacity compared to rural materials such as soil, sand or trees. This means, cities can store the energy of the sun in terms of heat more effective than rural sites. Urban materials can store and absorb twice the amount of heat compared to the rural area (www.epa.gov, Status: 22.06.2015).
At least, anthropogenic heat is also an issue, which refers to heat produced by human activities. It is estimated by totaling all the energy used in everyday life, such as light or, especially in summer, air conditioning. More energy intense buildings produce more heat. This mostly contributes to the winter heat island (www.epa.gov, Status: 22.06.2015).

3.7 HYSPLIT

In this work, backward trajectories are simulated with HYSPLIT program (Hybrid Single Partial Langrangian Integrated Trajectory Model). This is a complete system for calculating trajectories of an airparcel up to complex dispersion and deposition models such as dispersion of volcanic ash, dust or particles from forest fires. It has been developed by the National Oceanic and Atmospheric Administration (NOAA, USA) and the Australian Bureau of Meteorology (www.arl.noaa.gov, Status: 18.02.2015).
In this work, a cluster analysis has been performed to get an idea about the air flow direction during the two campaigns. The knowledge about the origin of the air mass is important for their characterization. This means, e.g., whether it has passed over huge cities and was influenced by them.
In the following, it is explained in short how such a cluster analysis is done. Thereby, GDAS (Global Data Assimilation System) data are used for calculation. GDAS is an atmospheric model that uses already existing meteorological data and combines them with calculations of numerical weather prediction models (Hänel, 2011).
For the cluster analysis, the backtrajectories for all days during September and October 2013 and May to July 2015 are calculated. Therefore, in the first iteration step each trajectory is defined as separate cluster (Hänel, 2011). This means there exists N cluster and N trajectories. Afterwards, it has to be clarified which two clusters are matched together. For each combination of trajectory pairs the spatial deviation of the cluster (σ_r) is calculated. This is defined as follows:

$$\sigma_r = \sum_{j=1}^{N} D_j^2.$$

D_j describes the distance between the end point of the trajectory (cluster component) and the middle cluster end point. N describes the number of trajectories in a cluster. As next step, the total spatial deviation of the cluster (σ_t) will be calculated. It follows from the sum of the single σ_r:

$$\sigma_t = \sum_{i=1}^{M} \sigma_{r,i}.$$

Afterwards, the clusters where σ_t is lowest are matched together. After this first iteration, the number of clusters has decreased to $N-1$. At the second iteration, the clusters consist of either individual trajectories or paired trajectories. Again, for each combination of clusters the σ_r and the σ_t are calculated and the two clusters with the lowest σ_t are matched. The cluster analysis is done until the last two clusters have been combined. Then only one cluster with N trajectories exists (Hänel, 2011). As next step, four different clusters have been chosen to indicate the backward trajectories for the two campaigns. The results will be explained in detail in Chapter 4.4.

3.8 Statistical metrics

First, the correlation is explained in short. It analyzes the connection between two metric variables. However, the correlation only describes the quantitative connection without assuming a cause-effect-relation. The correlation always is undirected. This means that there is no information obtained about which variable causes the other since both are equal. The correlation coefficient describes the strength of the connection and varies between -1 and 1 (Bamberg et al., 2012).
Additionally, the coefficient of determination for a linear regression is introduced. This value indicates the part of the variance of the dependent variable which can be explained by the independent one. It describes how good the variance of the dependent variable can be explained or predicted by the independet variable. The closer these values lie to one, the higher is the probability of a linear correlation. This means, the coefficient of determination is an index for the quality of alignment. Indeed, a coefficient of determination does not proof a linear correlation (Bamberg et al., 2012).

4 Campaign Overview

In this Chapter, the two measurement campaigns in Leipzig and Melpitz as well as the two sites are going to be introduced and first results are presented.

4.1 Measurement Sites

In autumn 2013 and summer 2015, two measurement campaigns in Leipzig and Melpitz took place where, among other things, parallel lidar and sun photometer measurements were performed (Fig. 4.1). The difference and impact of the city of Leipzig on different meteorological quantities was investigated and compared to the measurements of the surrounding unurbanized countryside (Melpitz).

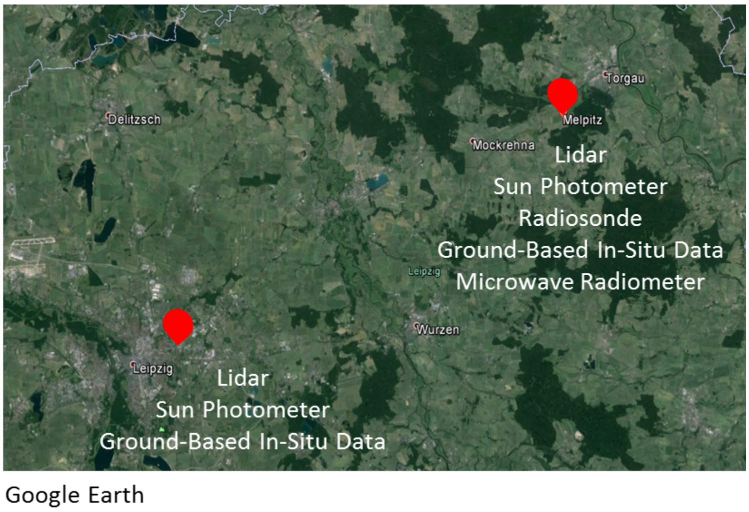

Figure 4.1: Location of the measurement sites Leipzig/TROPOS and Melpitz. In Leipzig and Melpitz lidar and sun photometer measurements took place. Additionally, microwave radiometer measurements as well as radiosonde launches and aerosol measurements were performed in Melpitz. Also surface data (relative humidity, particle number concentration and particle size distribution) from both sites are available. Both sites are nearly 45 km away from each other (Google Earth).

The measurement site at TROPOS in Leipzig is located in the northeast of the city (see Fig. 4.2). This means that the measurements are strongly influenced by the city of Leipzig during westerly and southwesterly wind directions. This could lead to different measurement values compared to the surrounding land. However, when the wind is coming from an eastern direction, TROPOS is less influenced by the city (Spindler et al., 2010).

The second measurement site, Melpitz, was founded in 1992 as an air chemistry and micrometeorological energy balance station to examine the effect of atmospheric long-range transport on local air quality (Poulain et al., 2011 and Spindler et al., 2013). It is an urban background area in Central Europe (Spindler et al., 2010) and representative for the conditions there. The Melpitz site is located on a meadow and surrounded by agricultural fields in the glacial valley of the river Elbe between Leipzig (45 km southwest from Melpitz) and the city of Torgau (12 km to the east). The main wind direction is southwest (60 % of the time). When air is advected from this direction, maritime air masses that passed over a large area of Germany and the city of Leipzig arrive in Melpitz. These air masses have a low particulate mass concentration. The second main wind direction is east (17 % of the time) with long-range transport from Poland, Belarus, Ukraine, Slovakia or the Czech Republic. The easterly (continental) air masses contain high particle mass concentrations (Spindler et al., 2010).

Also, the impact of the surface coverage is very important. Leipzig is characterized by an urban influenced area with lots of dark and impervious surfaces, whereas Melpitz is characterized by rural influence with mainly cultivated land, grass and forest. This brings along lots of differences. Those differences will be further investigated in the following Chapters.

4.2 Campaign 2013

The first campaign took place in September and October 2013 in Leipzig and Melpitz. In the framework of the campaign HD(CP)^2 (High Definition Clouds and Precipitation for advancing Climate Prediction), different measurements were performed (see Fig. 4.1). This German-wide campaign is funded by the BMBF (Bundesministerium für Bildung und Forschung) to obtain a better understanding of cloud and precipitation processes and their impact on different climate scenarios (www.hdcp2.zmaw.de, Status: 22.07.2015).

Google Earth

Figure 4.2: Location of the measurement site at TROPOS. TROPOS is located in the northeastern part of Leipzig (Google Earth).

Figure 4.3: Location of the measurement site at Melpitz. It is located roughly 45 km in the northeast of Leipzig. Here, the measurement containers are shown.

In the following Section, first results of the measurement campaign in 2013 will be presented to give an overview about the prevailing atmospheric conditions. In the next Section, the summer campaign in 2015 is introduced and first results from this campaign are presented. In the end, a wind cluster analysis for both campaigns is shown.

4.2.1 Measurement data

In Fig. 4.4 the time series for the AOT at 500 nm and the total number concentration for particles from 100 to 300 nm and 300 to 800 nm for both sites are depicted. Already here, important differences between the measured AOT and total number concentration can be seen. In the upper part it becomes apparent that most of the measured AOT values are between 0,05 and 0,2. Only some days showed clearly higher values. The mean AOT at 500 nm for Melpitz (black line) is 0,111 and the mean AOT for Leipzig (red line) is 0,107. The differences can be seen comparatively good since a rash of values in Melpitz is significantly higher than in Leipzig. These higher values in Melpitz are caused by the higher relative humidity in Melpitz.
On the other hand, Fig. 4.4 b) shows cleary higher values in Leipzig compared to Melpitz. The mean number concentration in Leipzig (red line) for particles from 100 to 300 nm is 1042 $\#/cm^{-3}$ compared to 794 $\#/cm^{-3}$ in Melpitz (black line). The same effect holds true for the particle sizes from 300 to 800 nm.

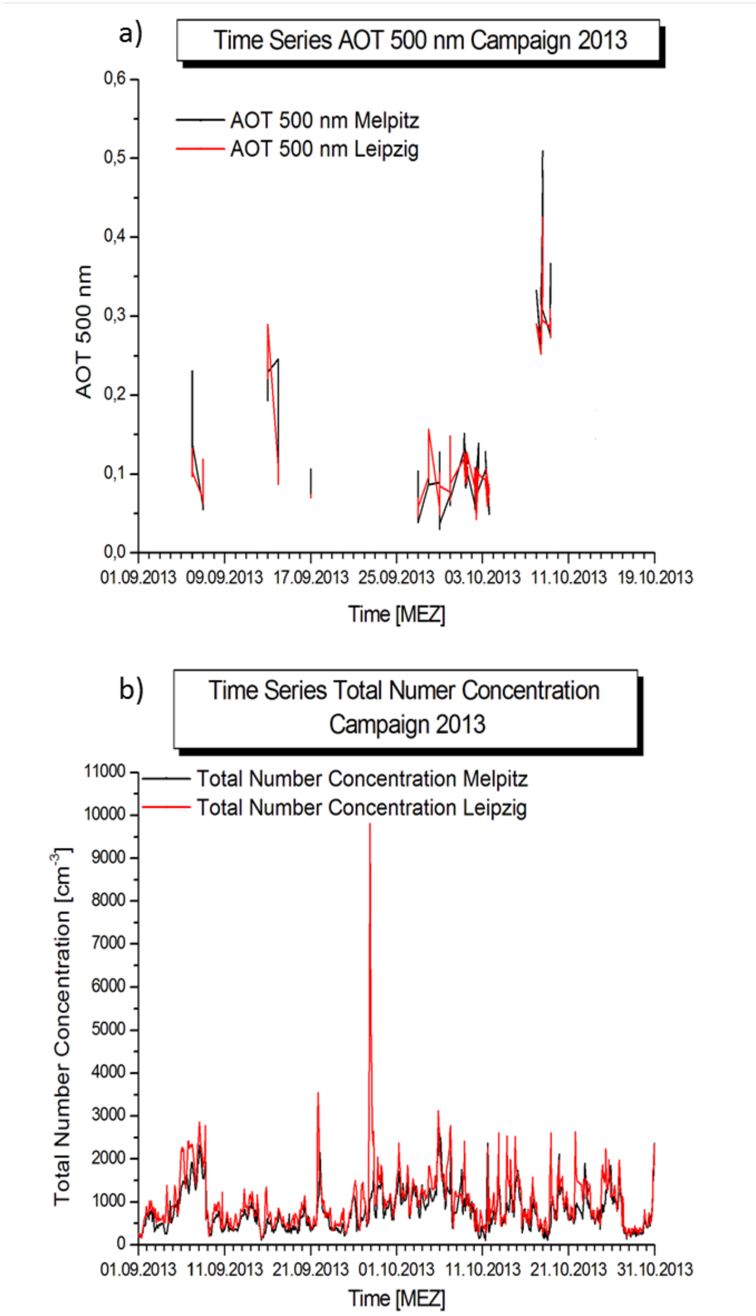

Figure 4.4: Time series for a) the AOT at 500 nm and b) the total number concentration for particle sizes from 100 to 300 nm for September and October 2013. The red line indicates the measurements from Leipzig, the black line the measurements from Melpitz. The data is obtained hourly.

4.3 Campaign 2015

The second measurement campaign lasted from May to July 2015. The aim of this campaign was the investigation of aerosol particles from the ground to the overlying atmospheric layers up to three kilometers height. Besides measurements of the chemical and physical properties at the ground running continuously, during this campaign additional experiments were done. They served for investigation of the aerosol particles in the air masses above the measurement site. Again, lidar and sun photometer measurements were performed during this campaign both in Leipzig and Melpitz (www.tropos.de, Status: 24.07.2015).

4.3.1 Measurement data

Here, the first results from the measurement campaign in 2015 are presented.
The time series for the AOT at 500 nm is depicted in Fig. 4.5. Here, it can be seen that on most of the days during the campaign the AOT at both sites was nearly equal. Only on single days the AOT in Melpitz was significantly higher than in Leipzig. Some huge deviations occured at the beginning of the measurement campaign. They were caused by a wrongly adjusted sun photometer in Melpitz.

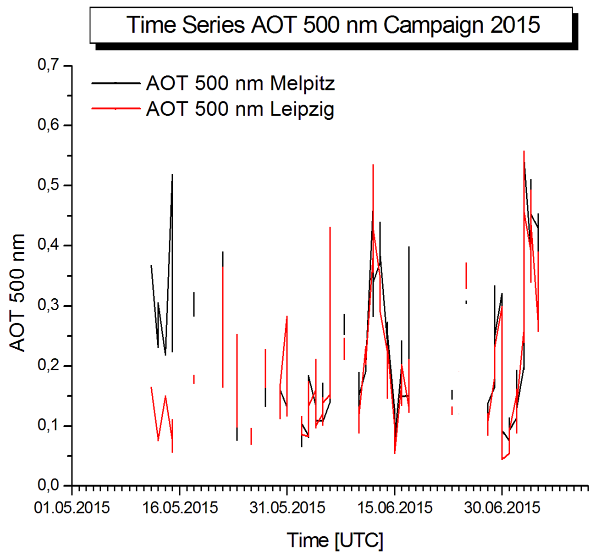

Figure 4.5: Time series of the AOT at 500 nm between Leipzig and Melpitz for May to July 2015. The red line shows the measurements from Leipzig, the black indicates measurements from Melpitz.

4.4 Cluster Analysis

Now, after the campaigns and the measurement sites were presented, the origin of the air masses shall be analyzed. Therefore, HYSPLIT simulations have been performed. 120-h backward trajectories have been calculated for every day of September and October 2013 as well as May and June 2015 for both sites at 1000 m height and a cluster analysis has been performed (see Chapter 3.7). The height of 1000 m was chosen because this height lies within the PBL and characterizes it.
The backward trajectories for September and October for Leipzig (left part of Fig. 4.6) and Melpitz (right part of Fig. 4.6) have been calculated and the frequency of occurence is indicated. Here, four different cluster can be seen. The first cluster (green) characterizes air masses coming from 290° - 360° and the second cluster (yellow) from 260° - 290°. The third cluster (blue) describes the eastern one and indicates air masses coming from 0° - 180° whereas the last cluster (red) shows the flow direction from 180° - 260°.
This graphic shows that the major part of the trajectories came from a westerly direction, as can be expected. Nearly a quarter of the air masses originated from a southwestern direction. For Leipzig it becomes apparent that more than ten percent of the backward trajectories came from a more northeastern flow direction compared to Melpitz where roughly one third came from north to northeast. By means of this graphic, first differences between the two measurement stations become apparent. The differences based on occurrence of air masses from southwest to northwest are relatively small but they are considerable when looking at the north to northeast direction.
Additionally, a cluster analysis to determine the origin of the air masses has also been done for the campaign in 2015. The first cluster (green) characterizes air masses coming from 230° - 260° and the second cluster (yellow) from 260° - 300°. The third cluster (blue) describes air masses coming from 300° - 360° whereas the fourth cluster (red) shows that air masses are coming from 0° - 230°. It can be seen that the air masses came from a clearly western wind direction. A small part of the air masses came over a more southern direction to the two measurement sites and some of the trajectories show a northwestern component. In comparison to the air mass origin from the autumn campaign (compare Fig. 4.6) there is no significant eastern flow direction visible. For this campaign, the differences between both sites are also comparatively small.
Since the two measurement sites are located quite close to each other and the dif-

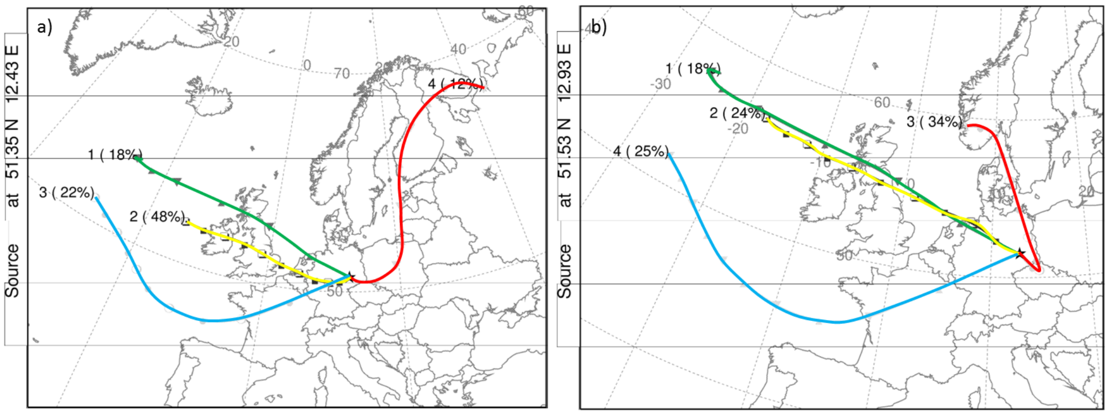

Figure 4.6: Flow for September and October 2013 for a) Leipzig and b) Melpitz at 1000 m height. For each day of the two months 120-h backward trajectories have been calculated and were clustered (frequency of occurence) to four main air flow directions. The first cluster (green) characterizes air masses coming from 290° - 360° and the second cluster (yellow) from 260° - 290°. The third cluster (blue) describes the eastern one and indicates air masses coming from 0° - 180° whereas the last cluster (red) shows the flow direction from 180° - 260°.

ferences during both campaigns are comparatively small it can be assumed that advection of aerosol from outside the observation area has no major impact on the AOT.

Summing up it has been shown that the dominant air mass origin between Melpitz and Leipzig is not differing so much. The only larger difference has become visible between the two campaigns. In autumn 2013 a minor part of the trajectories had an eastern to northeastern origin whereas this effect was less significant during the summer campaign. Nevertheless, this effect is comparatively small and it can be suggested that this is not the major reason for the differences in the measured AOT between both sites.
In the following Chapters, some case studies from the two measurement campaigns are analyzed concerning the PBL top and PBL cloud base height. Additionally, statistical investigations are done.

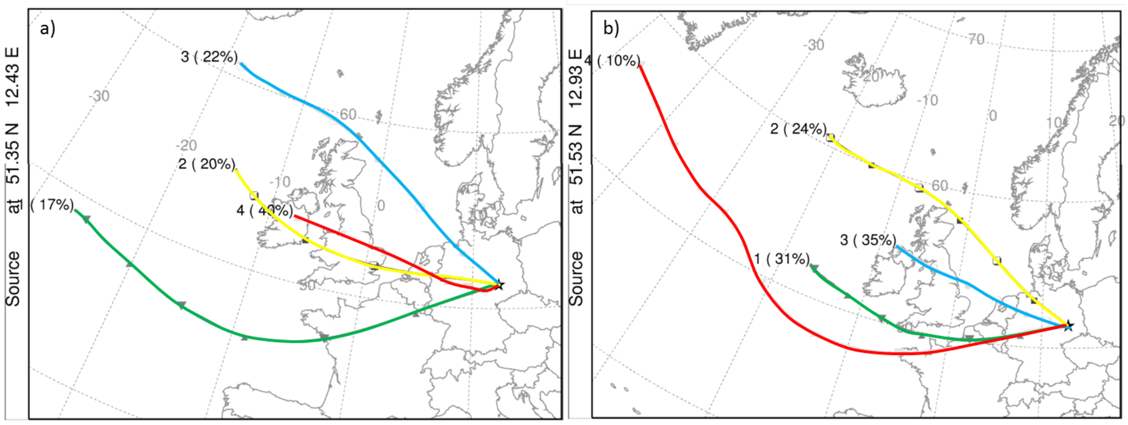

Figure 4.7: Flow for May and June 2015 for a) Leipzig and b) Melpitz at 1000 m height. For each day of the two months 120-h backward trajectories have been calculated and were clustered (frequency of occurence) to four main air flow directions. The first cluster (green) characterizes air masses coming from 230° - 260° and the second cluster (yellow) from 260° - 300°. The third cluster (blue) describes air masses coming from 300° - 360° whereas the fourth cluster (red) shows that air masses are coming from 0° - 230°.

5 Case Studies

In this Chapter, some case studies of the two measurement campaigns will be presented. At first, the PBL top height and air mass origin during three days in 2013 will be shown as well as some case studies for different PBL cloud base heights. Next, case studies for PBL top and PBL cloud base heights for the summer campaign in 2015 are investigated.

5.1 Case Studies 2013

In the following, three case studies of varying AOT are presented and analyzed in detail. Those case studies represent diverse cases with different AOT values measured in Leipzig and Melpitz.

5.1.1 First Case: 06. September 2013

The first case deals with the 06. September 2013 (Fig. 5.1). This was one of the days when the mean AOT (measured by sun photometer) was much higher in Melpitz (0,142) than the mean AOT measured in Leipzig (0,114). Also the lidar profile of this day has been analyzed to find out if the lidar receives similar results as the sun photometer (Fig. 5.1 a)). In the lidar profile the backscatter coefficient is shown. This indicates how strong the particles scatter the light in different heights back to the lidar. From Fig. 5.1 a) it can be seen that the lidar also measures clearly enhanced backscatter values in the PBL with higher values in Melpitz. This might be an indicator for a higher aerosol concentration within this height in Melpitz.
The backtrajectories (Fig. 5.1 b) and c)) of this day indicate that they first came from a northwestern and afterwards a southeastern direction. The trajectories passed over the Czech Republic. The pollution there is higher compared to Germany (www.welt.de, Status: 23.05.2015) so it could be assumed that polluted air and other aerosol from the Czech Republic came to the sites. Nevertheless, the direction of flow for Leipzig and Melpitz shows similar patterns and since these differences are small, this is not the reason for the differences in the measured AOT.

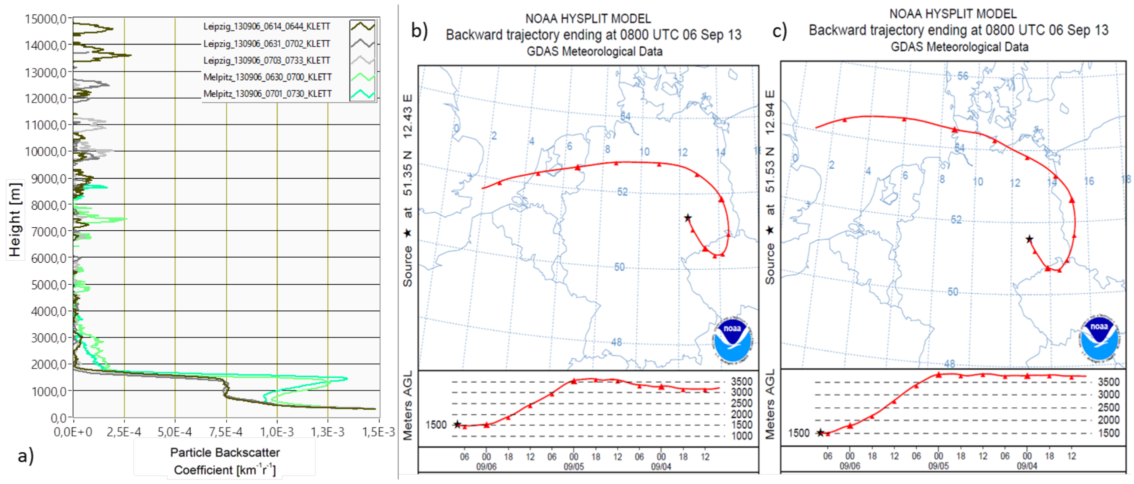

Figure 5.1: Case study of 06. September 2013. a) Lidar profile of this day from 06 to 08 UTC, the green-blue lines characterize the measurements from Melpitz, the grey-black lines characterize the measurements from Leipzig. The backscatter coefficient is plotted with respect to the height, b) HYSPLIT 3-day backward trajectories for Leipzig in 1500 m height, c) HYSPLIT 3-day backward trajectories for Melpitz in 1500 m height (www.arl.noaa.gov, Status: 18.02.2015).

Furthermore, the PBL top height measured with lidar has been analyzed (Fig. 5.2). Here, the corresponding range-corrected lidar signal of this day from the two measurement sites is depicted. The ups and downs of the PBL in the range-corrected lidar signal indicate convection. When there is increase in the signal of the PBL the air masses rise due to convection, when there is decrease then the air masses are sinking in this area. Therefore, most of the used data is averaged over a certain time period. For the PBL top height cases the data is averaged over five minutes, for the PBL cloud base heights over one minute.
It can be seen that the convective PBL development starts both in Melpitz (left part of Fig. 5.2) and Leipzig (right part of Fig. 5.2) at nearly 08 UTC. Also, there are no significant differences during the evolution between 08 UTC and 12 UTC visible. It can be seen that the PBL decay in Leipzig is starting at around 15 UTC and between 18 and 19 UTC a residual layer has formed. Comparing these observations to the one from Melpitz it becomes visible that the transition between convective PBL and residual layer occurs more or less smooth. For Melpitz, a clear decay and transition of PBL to the resiudal layer is not as good visible as for Leipzig. This shows the different behavior during the decay of PBL in Melpitz and Leipzig, as already mentioned in Section 3.3. Therefore, only measurement data until 14 UTC

is used in this case.
When reckoning the correlation plot 5.3, there are some differences visible. During the development of the PBL (blue dots, from 08 to 11 UTC) on this day, it was almost always higher in Leipzig than in Melpitz. This is due to the enhanced growth of PBL in Leipzig compared to Melpitz (see Fig. 5.2) which could be caused by the effect of the urban heat island. The surface heat flux from the earth into the atmosphere over the city could be enhanced compared to the rural site which could result in a stronger convection over Leipzig than in Melpitz (www.epa.gov, Status: 22.06.2015).
In the late afternoon the PBL height was nearly equal in Leipzig and Melpitz with slightly higher values in Leipzig. This is due to the fact that PBL at both sites is fully developed at that time whereas the growth of PBL in the morning happens to be with a different speed and strength at both sites.

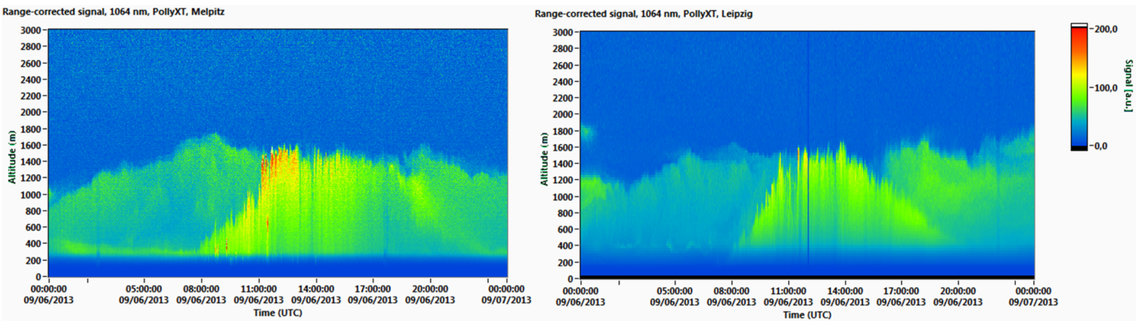

Figure 5.2: Lidar profile of the 06. September 2013 for 24 hours. Left part of the Figure: profile from Melpitz, right part of the Figure: profile from Leipzig. The red color indicates higher backscatter values compared to the blue color.

The relative humidity of this day was much higher in Melpitz compared to Leipzig (Fig. 5.4 a). Nevertheless, the total number concentration (for particles from 100 to 300 nm and from 300 to 800 nm, Fig. 5.4 b) and c)) at this day was mainly higher in Leipzig than in Melpitz. From this it could be assumed that the higher relative humidity in connection to the lower total number concentration in Melpitz may have produced particles there that grow stronger compared to Leipzig. The water vapor in Leipzig has to adsorb on comparatively many particles whereas the water vapor in Melpitz can adsorb on comparatively few particles. Thus, the particles in Melpitz can get bigger because they get more water vapor but they are less in number than in Leipzig. These huge particles could produce the higher AOT values in Melpitz.

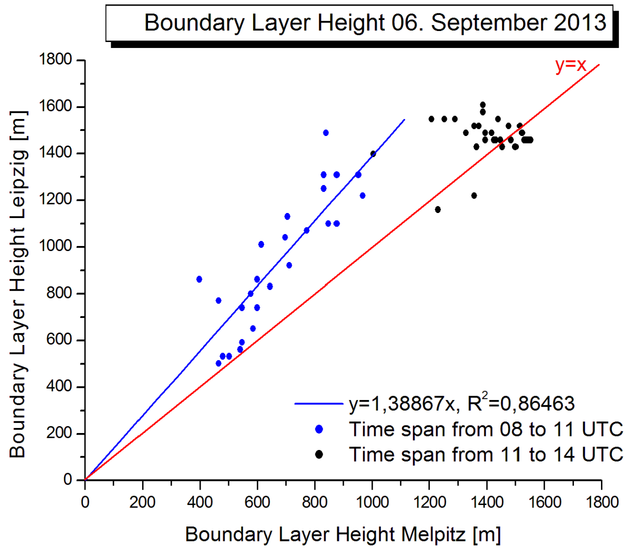

Figure 5.3: Correlation of the PBL top height from the 06. September 2013 between Melpitz and Leipzig. The blue dots mark data from 08 to 11 UTC, the black dots from 11 to 14 UTC. Formula for linear regression (blue line) and 1:1 line (red line) is also shown. The data is averaged over five minutes.

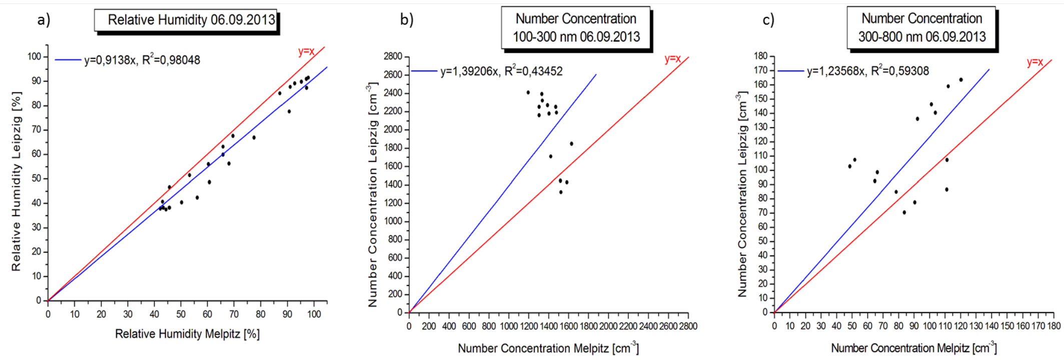

Figure 5.4: Correlation of a) the relative humidity, b) the total number concentration for particles from 100 to 300 nm and c) the total number concentration for particles from 300 to 800 nm for the 06. September 2013. Formula for linear regression (blue line) and 1:1 line (red line) is also shown. The data is obtained hourly.

5.1.2 Second Case: 28. September 2013

The second analyzed case is the 28. September 2013 (Fig. 5.5). This day characterizes the 'typical' case with a high mean AOT in Leipzig (0,117) compared to a lower mean AOT in Melpitz (0,091). The lidar measurement of this day also reveals

higher backscatter values measured in Leipzig than in Melpitz (Fig. 5.5 a)).
When reckoning the backward trajectories (Fig. 5.5 b) and c)) it shows that they came from a northwestern direction towards the sites and thus they corresponded more to the main wind direction. The air masses moved slightly over the city of Leipzig but were not influenced too much by the city. The measurement site at TROPOS is located in the northeastern part of the city and will be more strongly influenced by the city at a western or southwestern flow. The direction of flow for both sites was similar on that day. This also indicates that the reason for these differences is not preferential the flow direction.

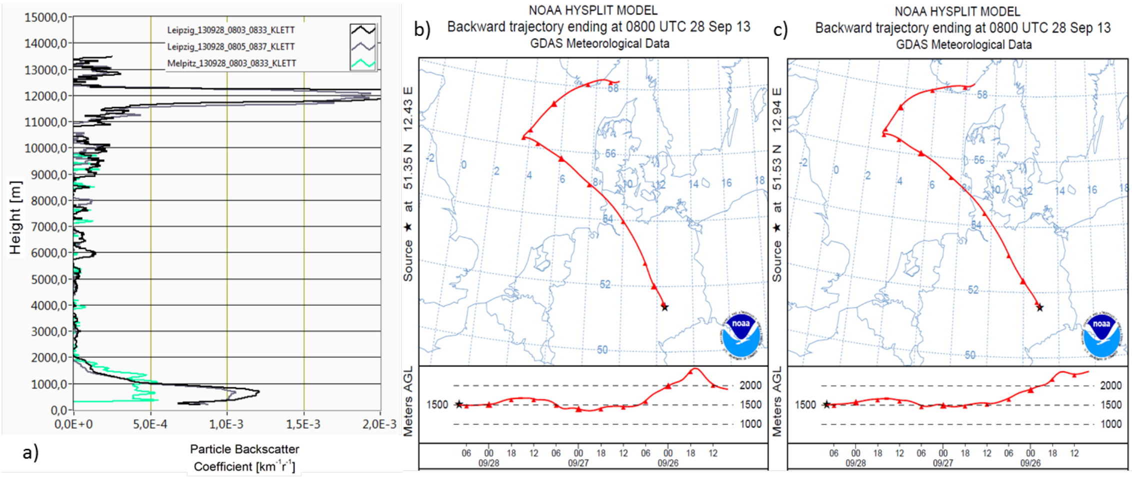

Figure 5.5: Case study of 28. September 2013. a) Lidar profile of this day from 08 to 09 UTC, the green-blue lines characterize the measurements from Melpitz, the grey-black lines characterize the measurements from Leipzig. The backscatter coefficient is plotted with respect to the height, b) HYSPLIT 3-day backward trajectories for Leipzig in 1500 m height, c) HYSPLIT 3-day backward trajectories for Melpitz in 1500 m height (www.arl.noaa.gov, Status: 18.02.2015).

The PBL top height from the range-corrected lidar signal (Fig. 5.6) shows the start of the convective PBL development for both sites at around 09 to 10 UTC whereas a clear determination of the start of PBL evolution in Leipzig is hard to determine because of the higher altitude of complete overlap between the laser beam and the receiver field-of-view. On this day, small convective PBL clouds occured at around 11 UTC and lasted on until 15 UTC in Melpitz and nearly 16 UTC in Leipzig. They will be not investigated here. The PBL in Leipzig started to decay at around 16 to 17 UTC whereas a clear determination in Melpitz is not possible. Therefore, only measurement data until 16 UTC is used.

However, when considering the correlation plot (see Fig. 5.7) it becomes apparent that the convective PBL during the development in the morning hours (from 08 to 11 UTC) is slightly higher in Leipzig than in Melpitz. The reason for these differences is the different speed of growth at both sites but the effect of the urban heat island could also play a role. In the late afternoon, the PBL top height in Melpitz is higher compared to Leipzig. The higher PBL top in Melpitz could be caused by the earlier decay of convective PBL in Leipzig, although a clear start of PBL decay in Melpitz is hard to determine.

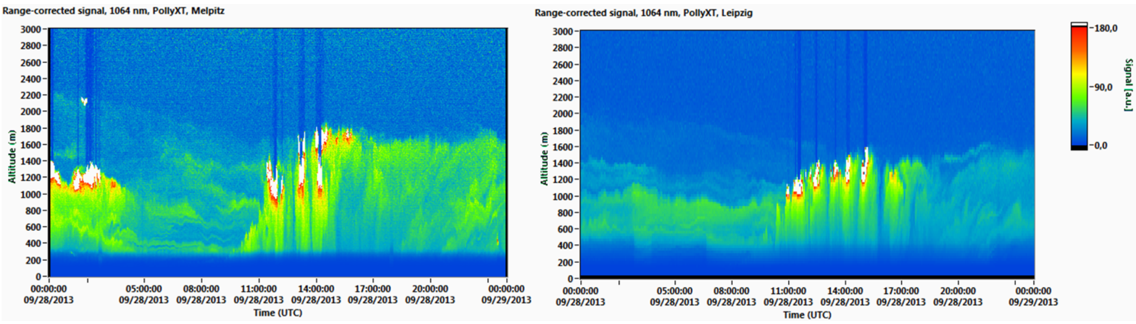

Figure 5.6: Lidar profile of the 28. September 2013 for 24 hours. Left part of the Figure: profile from Melpitz, right part of the Figure: profile from Leipzig. The red color indicates higher backscatter values compared to the blue color.

The relative humidity as well as the total number concentration for particles from 100 to 300 nm and from 300 to 800 nm are shown in Fig. 5.8. Here, again, the relative humidity was higher in Melpitz than in Leipzig. The total number concentration shows higher values in Leipzig compared to Melpitz for the two particles sizes (100 to 300 nm and 300 to 800 nm). The measured aerosol particle number concentration values in Melpitz from this case are comparatively equal to the values from the other two cases. Comparing the values from this day measured in Leipzig to the values in Leipzig from the other two cases, it turns out that the total number concentration on this day is nearly twice as high for both particle sizes compared to the other two cases. As a result, for this case not only the relative humidity caused those differences in the AOT but also the significantly higher aerosol number concentration in Leipzig.

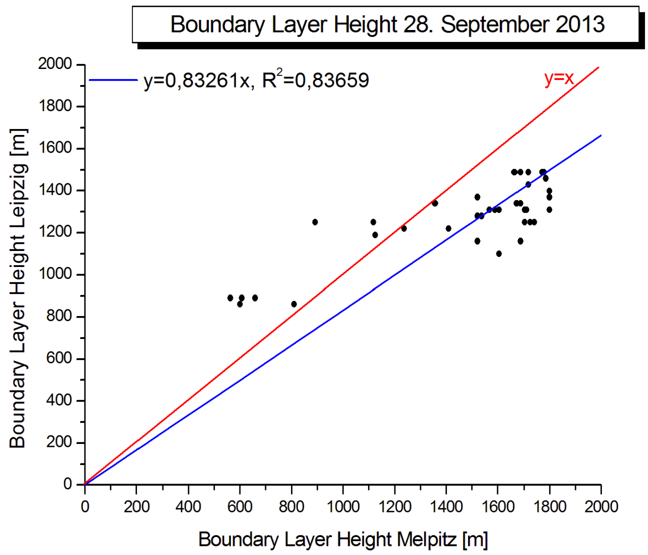

Figure 5.7: Correlation of the PBL top height from the 28. September 2013 between Melpitz and Leipzig. Formula for linear regression (blue line) and 1:1 line (red line) is also shown. The data is averaged over five minutes.

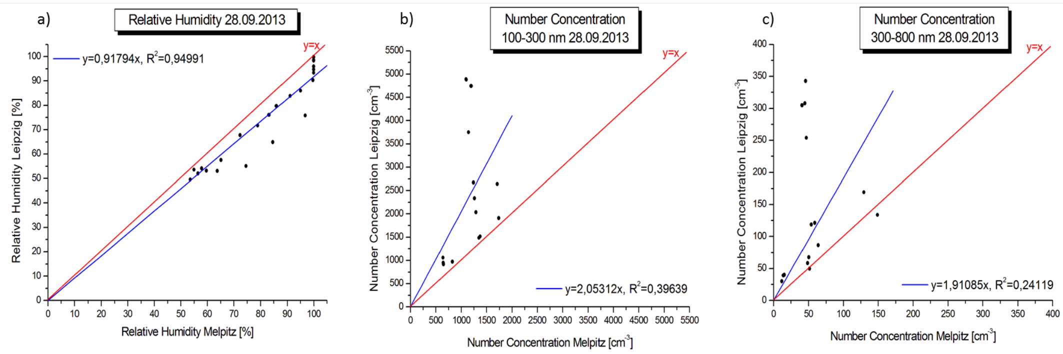

Figure 5.8: Correlation of a) the relative humidity, b) the total number concentration for particles from 100 to 300 nm and c) the total number concentration for particles from 300 to 800 nm for the 28. September 2013. Formula for linear regression (blue line) and 1:1 line (red line) is also shown. The data is obtained hourly.

5.1.3 Third Case: 29. September 2013

The third analyzed case is the 29. September 2013 (Fig. 5.9). This day characterizes a case when the mean AOT between Leipzig (0,072) and Melpitz (0,068) was nearly equal. The lidar profile confirms this since there is no significant difference in the PBL visible between both measurement sites (Fig. 5.9 a)).

When reckoning the backward trajectories (Fig. 5.9 b) and c)) it can be seen that they first came from a northeastern direction towards the sites and then changed to an eastern direction. This means that the two measurement sites are nearly completely unaffected by larger cities or industry. This is especially true for the site of TROPOS since it is not influenced by the city of Leipzig. The direction of flow in Leipzig was similar to the one in Melpitz on that day.

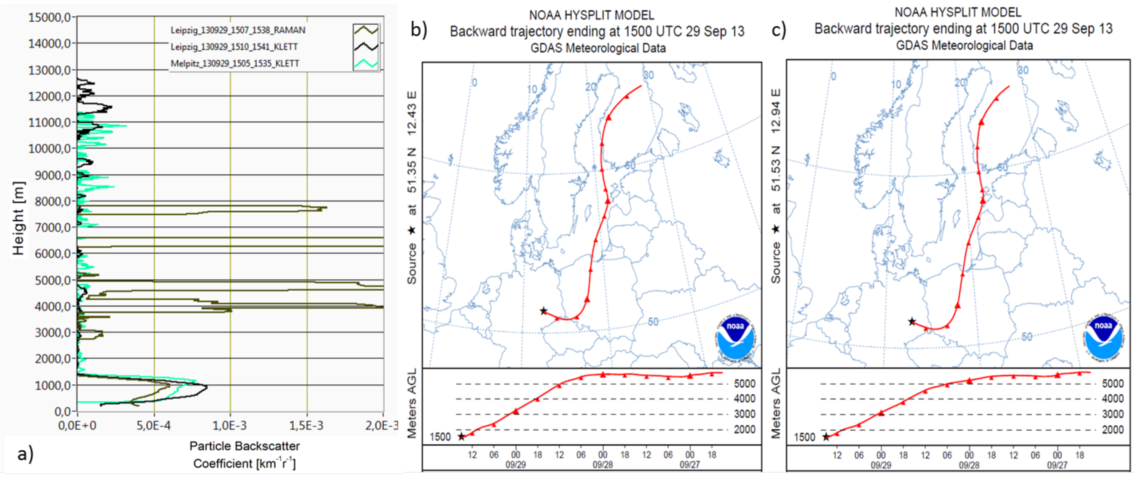

Figure 5.9: Case study of 29. September 2013. a) Lidar profile of this day from 15 to 16 UTC, the green-blue lines characterize the measurements from Melpitz, the grey-black lines characterize the measurements from Leipzig. The backscatter coefficient is plotted with respect to the height, b) HYSPLIT 3-day backward trajectories for Leipzig in 1500 m height, c) HYSPLIT 3-day backward trajectories for Melpitz in 1500 m height (www.arl.noaa.gov, Status: 18.02.2015).

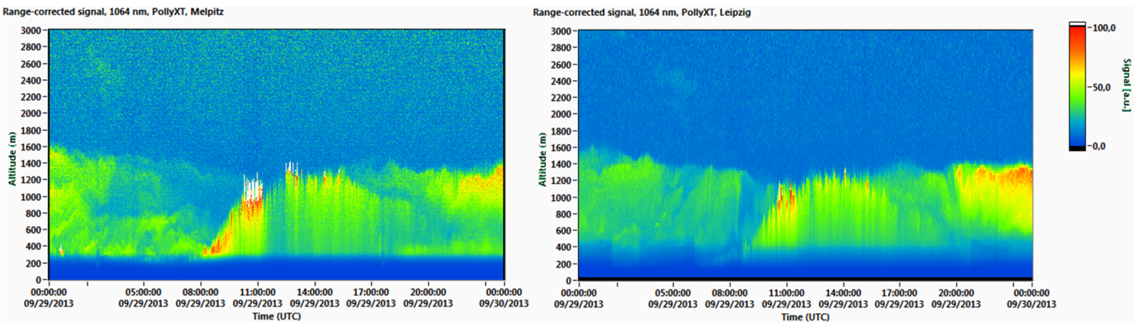

Figure 5.10: Lidar profile of the 29. September 2013 for 24 hours. Left part of the Figure: profile from Melpitz, right part of the Figure: profile from Leipzig. The red color indicates higher backscatter values compared to the blue color.

The convective PBL top development from the range-corrected lidar signal of this case has also been investigated (Fig. 5.10). The PBL evolution starts in Melpitz at nearly 08 UTC whereas it is starting a little bit later in Leipzig (at around 09 UTC). Nevertheless, it has to be considered that the altitude of complete overlap between the laser beam and the receiver field-of-view for the lidar measuring in Leipzig is higher compared to Melpitz (see Section 2.1). This makes a clear determination of the start of the convective PBL evolution harder for Leipzig. Additionally, some small PBL clouds showed up at both sites at around 10 UTC but they will not be investigated further here. The decay of PBL starts between 15 and 16 UTC in Leipzig and afterwards the stable residual layer forms. The transition between convective PBL and residual layer for Melpitz is starting at nearly the same time as in Leipzig. Here, only measurement data until 15 UTC is used.
With a view to the correlation of the PBL top height (Fig. 5.11) of this day, a rather good correlation between both sites can be seen. There are only small differences between both measurement sites. The differences are caused by the different behavior and speed of growth between Leipzig and Melpitz as well as the slightly different start of decay of PBL. The effect of the urban heat island might also play a role but this cannot be proven here.

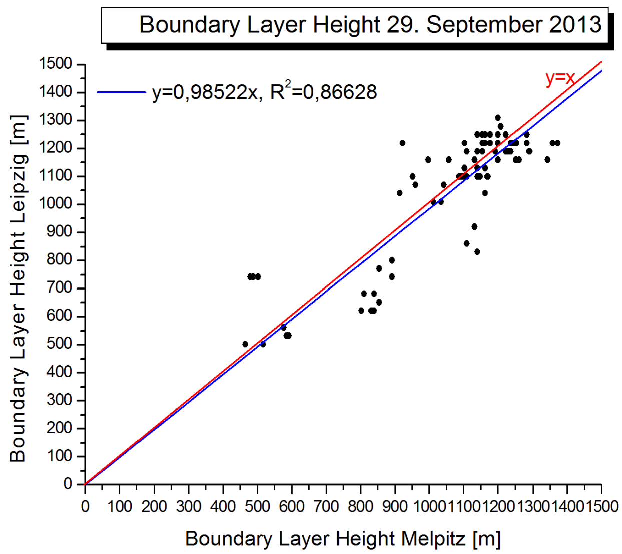

Figure 5.11: Correlation of the PBL top height from the 29. September 2013 between Melpitz and Leipzig. Formula for linear regression (blue line) and 1:1 line (red line) is also shown. The data is averaged over five minutes.

Again, the relative humidity as well as the total number concentrations for particles from 100 to 300 nm and 300 to 800 nm are depicted in Fig. 5.12. The relative humidity is higher in Melpitz, as already seen in the previous cases. On the other hand, the total number concentrations for both particle sizes are higher in Leipzig, although they are only slightly higher with a very good correlation compared to the first two observed cases (compare 5.4 and 5.8). The high relative humidity in Melpitz and the only slightly enhanced number concentrations in Leipzig lead to the result that the particles at both sites can grow to nearly the same size. Thereby, the AOT values which were nearly equal at the rural and urban site can be explained.

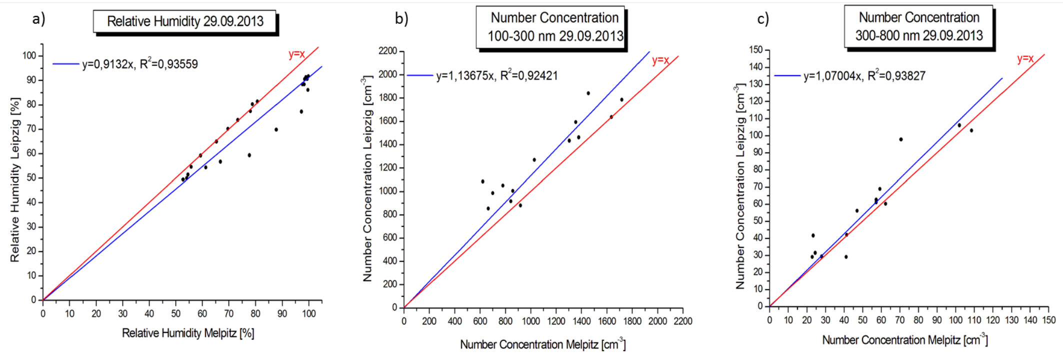

Figure 5.12: Correlation of a) the relative humidity, b) the total number concentration for particles from 100 to 300 nm and c) the total number concentration for particles from 300 to 800 nm for the 29. September 2013. Formula for linear regression (blue line) and 1:1 line (red line) is also shown. The data is obtained hourly.

The PBL on those three observed days showed different behaviour. The first case showed clearly higher values in Leipzig caused by the stronger growth there compared to Melpitz. The second case showed enhanced PBL top heights in Melpitz caused by the higher relative humidity in Melpitz. The last case illustrated nearly the same PBL top heights for both sites.
As next, PBL cloud base heights during the campaign in 2013 are analyzed for a few days.

5.1.4 Boundary layer cloud base height

In this Chapter, the cloud base heights of two chosen days with convective PBL clouds are going to be examined.
The first analyzed day was the 14. September 2013. Here, the convective PBL development started both in Melpitz and Leipzig at nearly 08 UTC, as can be seen

from the respective range-corrected lidar profile (see Fig. 5.13). At around 15 UTC, a frontal system passed over the two sites, first affecting Leipig and then Melpitz. For this reason, only cloud base heights until 15 UTC have been taken into account. The first clouds over Leipzig started to develop at nearly 11 UTC whereas the first PBL clouds in Melpitz did not start to develop before 12 UTC. On this day, the cloud evolution over the city started earlier.

The corresponding correlation plot is shown in Fig. 5.14. The data has been separated into two different time spans: one from 13 to 14 UTC and the second from 14 to 15 UTC. During the whole day, the cloud base height over Melpitz is slightly higher compared to Leipzig. Additionally, the differences between the two time spans are quite small. This shows that the changes during day are small both in Leipzig and Melpitz.

Additionally, the relative humidity (Fig. 5.15) between both sites shows mostly higher values over Melpitz compared to Leipzig. The higher cloud base height in Melpitz could be caused by this higher relative humidity in Melpitz. This is due to the larger amount of water vapor that may favor cloud evolution.

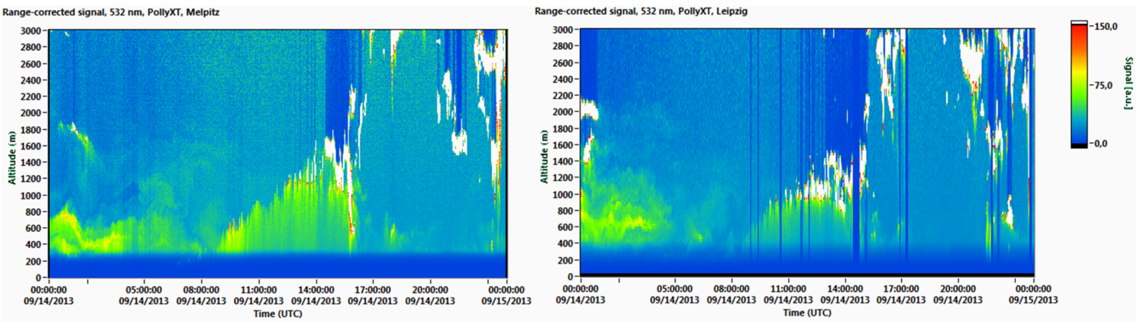

Figure 5.13: Lidar profile of the 14. September 2013 for 24 hours. The left Figure indicates the measurement from Melpitz, the right one from Leipzig. The white areas indicate the clouds.

The second case with observed PBL clouds was the 01. October 2013. A strong development of PBL can be seen in Fig. 5.16, starting between 08 UTC and 09 UTC both in Leipzig and Melpitz. The clear determination in Leipzig is harder due to the higher altitude of complete overlap between the laser beam and the receiver field-of-view (see Section 2.1). PBL clouds started to develop at around 10 UTC at both sites and lastet on until nearly 17 to 18 UTC whereat the clouds lived longer in Leipzig. Here, only measurement data until 17 UTC is analyzed.

The correlation (Fig. 5.17) between both sites shows nearly equal PBL cloud base

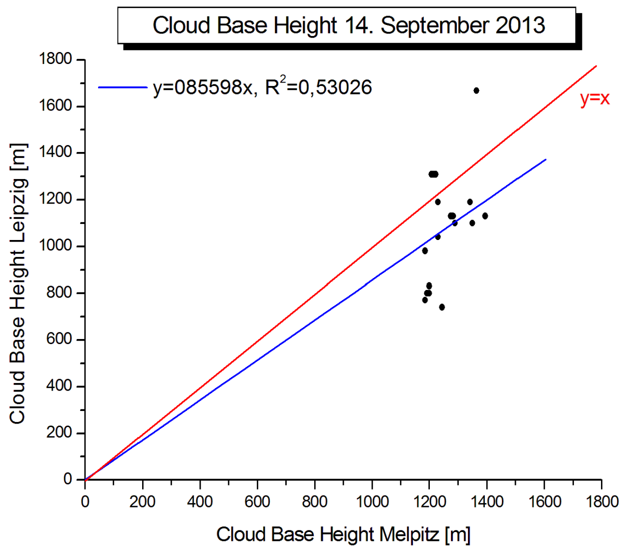

Figure 5.14: Correlation of the cloud base height of the 14. September 2013 between Leipzig and Melpitz. Formula for linear regression (blue line) and 1:1 line (red line) is also shown. The data is averaged over one minute.

heights and no huge differences have been found. The cloud base height over Melpitz was only slightly higher than in Leipzig.
Additionally, the time series for this day is shown from 08 to 13 UTC in Fig. 5.18. Here, it can be seen that the PBL top height during the evolution is significantly higher in Melpitz until nearly 13 UTC which is not the typical case. After this, the PBL top height between both sites was similar. Here, the stronger growth of PBL as well as the higher relative humidity in Melpitz (not shown here) could be a possible reason for the higher values in Melpitz.

All in all, the PBL cloud base heights between both measurement sites were almost equal. The slightly higher cloud base heights over the rural site may be caused by the higher relative humidity there. The higher humidity may favor or enhance the cloud growth and evolution. Nevertheless, the results for the PBL clouds did not confirm what would be expected from theory - higher PBL clouds over the city due to the effect of the urban heat island.

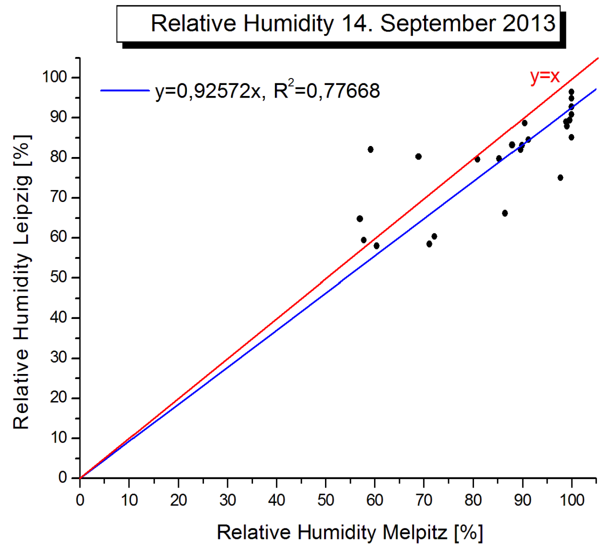

Figure 5.15: Correlation of the relative humidity for the 14. September 2013. Formula for linear regression (blue line) and 1:1 line (red line) is also shown. The data is obtained hourly.

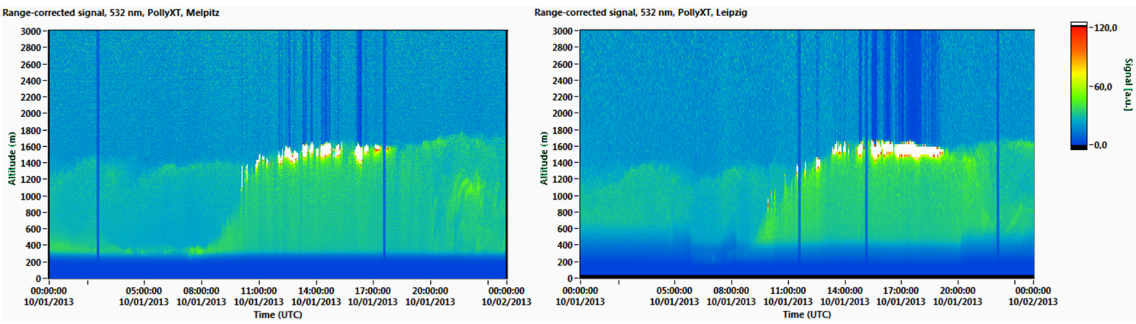

Figure 5.16: Lidar profile of the 01. October 2013 for 24 hours. The left Figure indicates the measurement from Melpitz, the right one from Leipzig. The white areas indicate the clouds.

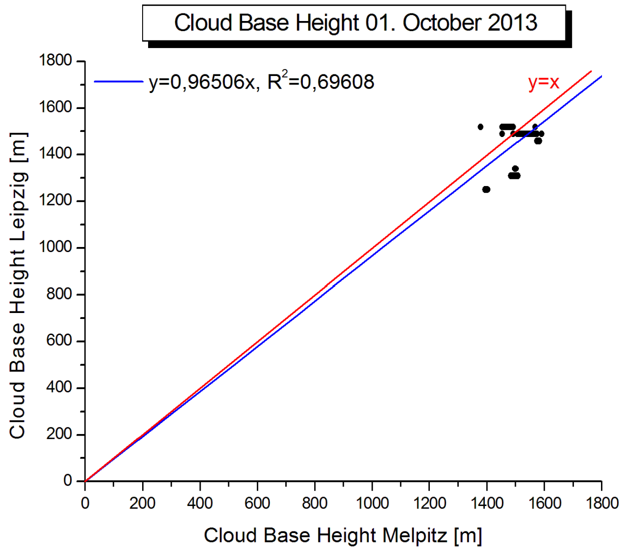

Figure 5.17: Correlation of the cloud base height of the 01. October 2013 between Leipzig and Melpitz. Formula for linear regression (blue line) and 1:1 line (red line) is also shown. The data is averaged over one minute.

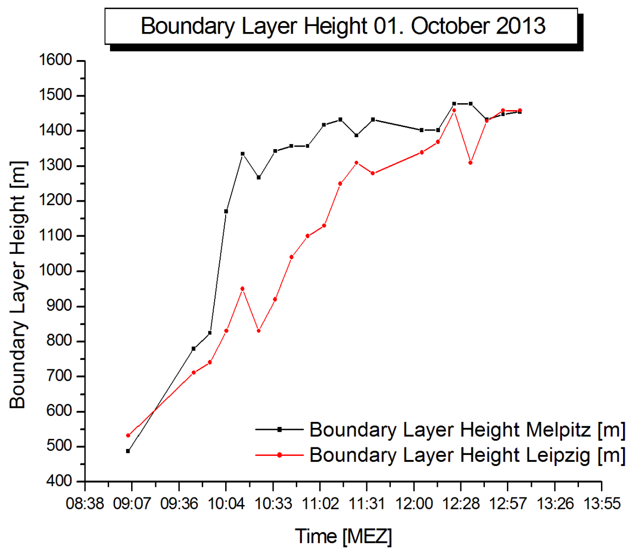

Figure 5.18: Time series of the PBL evolution on the 01. October 2013 from 08 to 13 UTC between Leipzig and Melpitz. The red line shows the measurements from Leipzig, the black line the values measured in Melpitz. The data is averaged over ten minutes.

5.2 Case studies 2015

Also for this campaign, three case studies with varying AOT are examined and the results are compared to the ones from the autumn campaign.

5.2.1 First Case: 05. June 2015

The first case was observed on the 05. June 2015. Here, the mean AOT (measured by sun photometer) in Melpitz (0,134) was nearly equal to the mean AOT measured in Leipzig (0,126). This is confirmed by the lidar profile of this day (Fig. 5.19 a)). It can be seen that the backscatter coefficients in Melpitz and Leipzig are very close to each other.
The backward trajectories (Fig. 5.19 b) and c)) indicate that the air masses first came from the west and then changed to a northern direction. In the end, the air masses reaching the two measurement sites came from the south. Thereby, the trajectories passed over the Czech Republic. Due to the higher pollution there compared to Germany (www.welt.de, Status: 23.05.2015) it could be be assumed that polluted air and other aerosol from the Czech Republic came to the sites. Nevertheless, the flow for Leipzig is similar to the one in Melpitz and since the differences are small, this is not the main reason for the differences in the measured AOT.
The start of PBL evolution for Melpitz is hard to determine (left part of Fig. 5.20). This is due to the very complex and distinct layer that extends from 800 to 1600 m. For Leipzig (right part of Fig. 5.20), the start of PBL development is much easier to determine because this layer is less distinct as in Melpitz. Here, the PBL started to grow at nearly 06 to 07 UTC. The PBL decay in Leipzig is starting around 14 to 15 UTC whereas it starts in Melpitz at around 16 to 17 UTC. Therefore, only measurement data until 15 UTC is used.
The correlation plot (Fig. 5.21) shows nearly equal PBL top heights between both sites. The significantly higher PBL top heights in Melpitz compared to Leipzig (1300 m in Melpitz compared to 700 m in Leipzig) mostly occured during the afternoon when the PBL decay over Leipzig has started a bit earlier than in Melpitz. This causes the higher PBL top heights over Melpitz compared to Leipzig.
The relative humidity measured during this day (Fig. 5.22) shows clearly higher values in Melpitz compared to Leipzig, as already seen from the previous campaign. This may have had an influence on the PBL top height.

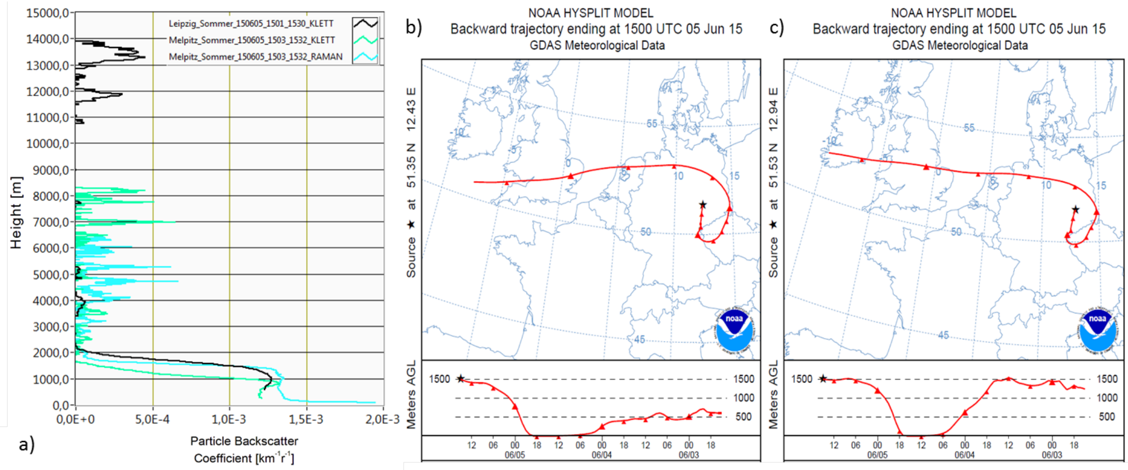

Figure 5.19: Case study of 05. June 2015. a) Lidar profile of this day from 15 to 16 UTC, the green-blue lines characterize the measurements from Melpitz, the grey-black lines characterize the measurements from Leipzig. The backscatter coefficient is plotted with respect to the height, b) HYSPLIT 3-day backward trajectories for Leipzig in 1500 m height, c) HYSPLIT 3-day backward trajectories for Melpitz in 1500 m height (www.arl.noaa.gov, Status: 18.02.2015).

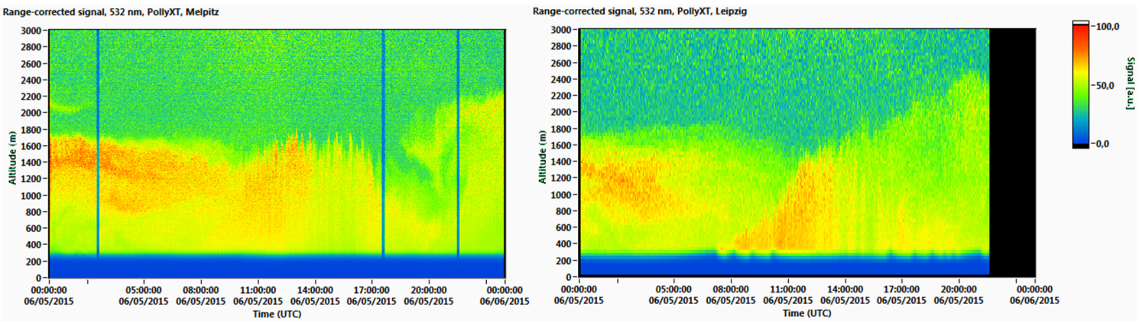

Figure 5.20: Lidar profile of the 05. June 2015 for 24 hours. Left part of the Figure: profile from Melpitz, right part of the Figure: profile from Leipzig. The red color indicates higher backscatter values compared to the blue color.

5.2.2 Second Case: 10. June 2015

The next case was observed on the 10. June 2015. On this day, the measured AOT in Melpitz (0,152) was significantly higher than in Leipzig (0,106). This is also confirmed by the corresponding lidar profile (Fig. 5.23 a)). It can be seen that the particle backscatter coefficient in the lowest 2000 m is clearly higher in Melpitz compared to Leipzig.

When reckoning the backward trajectories (Fig. 5.23 b) and c)) of this day it

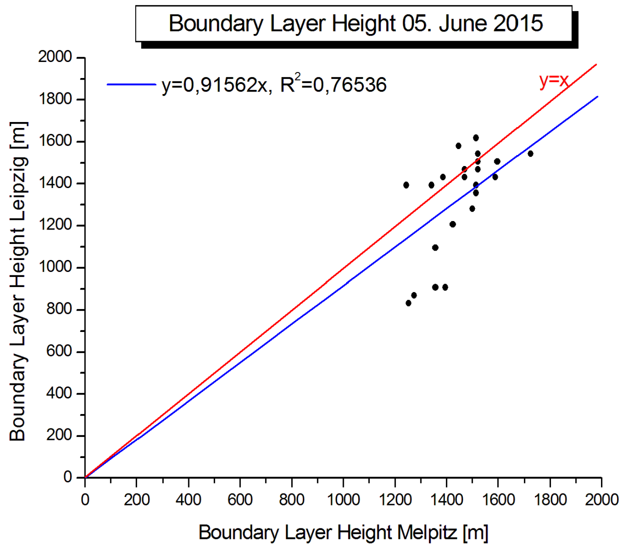

Figure 5.21: Correlation of the PBL top height from the 05. June 2015 between Melpitz and Leipzig. Formula for linear regression (blue line) and 1:1 line (red line) is also shown. The data is averaged over five minutes.

becomes apparent that the air masses first came from a western direction and then changed to an eastern one. This implies that both measurement sites are nearly unaffected by larger cities but the air masses passed over Poland and might have been influenced by the stronger polluted air there (Spindler et al., 2010). The direction of flow in Melpitz was similar to the one in Leipzig.

The PBL development on this day was starting at around 06 UTC both in Melpitz and Leipzig (Fig. 5.24). Unfortunately, a frontal system was passing over both sites in the afternoon on that day, first reaching Leipzig and then Melpitz. For that reason, only measurement data until 14 UTC can be analyzed.

The correlation of the PBL top height between Leipzig and Melpitz (Fig. 5.25) reveals almost equal PBL top heights. Here, the higher values in Leipzig occured during the phase of development in the morning due to the stronger PBL evolution in Leipzig compared to Melpitz. The higher values in Melpitz occured during the afternoon.

The relative humidity on this day (see Fig. 5.26) shows clearly enhanced values over Melpitz compared to Leipzig. The higher relative humidity may be the cause for the higher AOT in Melpitz. Due to the higher amount of water vapor within the atmosphere, larger particles can be formed compared to an atmosphere with a lower relative humidity and this could be the reason for the higher AOT in Melpitz.

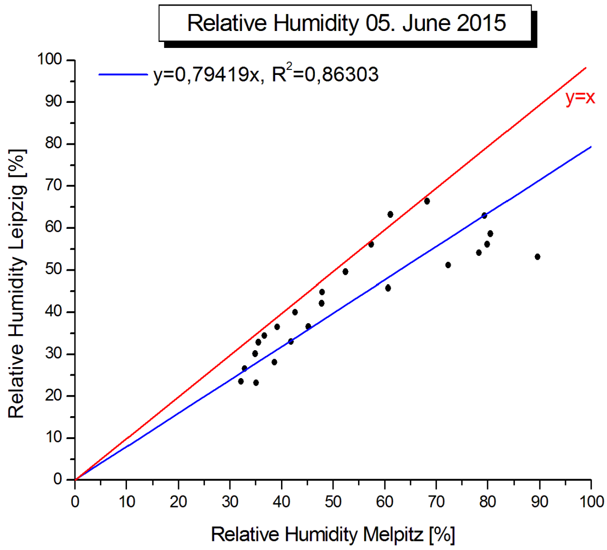

Figure 5.22: Correlation of the relative humidity for the 05. June 2015. Formula for linear regression (blue line) and 1:1 line (red line) is also shown. The data is obtained hourly.

5.2.3 Third Case: 12. June 2015

Another observed case was the 12. June 2015. On this day, the 'typical' case with a significantly higher measured AOT in Leipzig (0,429) compared to Melpitz (0,363) occured. The lidar profile (Fig. 5.29 a)) shows a clearly enhanced particle backscatter coefficient for Leipzig in the lowest 2000 m. This confirms the observations made by the sun photometers.

The backward trajectories (Fig. 5.27 b) and c)) of this day indicate that the air masses mostly came from the southwest. On this day, the air masses reaching TROPOS passed over the city of Leipzig which means that they may be stronger polluted and influenced than the air masses reaching Leipzig during the other two cases. The air mass origin for both sites was almost equal.

On that day, the PBL started to grow at around 06 to 08 UTC whereat it is starting earlier in Leipzig than in Melpitz which is due to precipitation that passed Leipzig first and then Melpitz (Fig. 5.28). The decay of PBL started in Melpitz at around 17 UTC whereas in Leipzig it was starting a little bit earlier. For that reason, measurement data for analysis is only used until 16 UTC.

The correlation plot (Fig. 5.29) shows a generally good correlation. Nevertheless, for this case the PBL top height is slightly higher in Leipzig. This is what would be

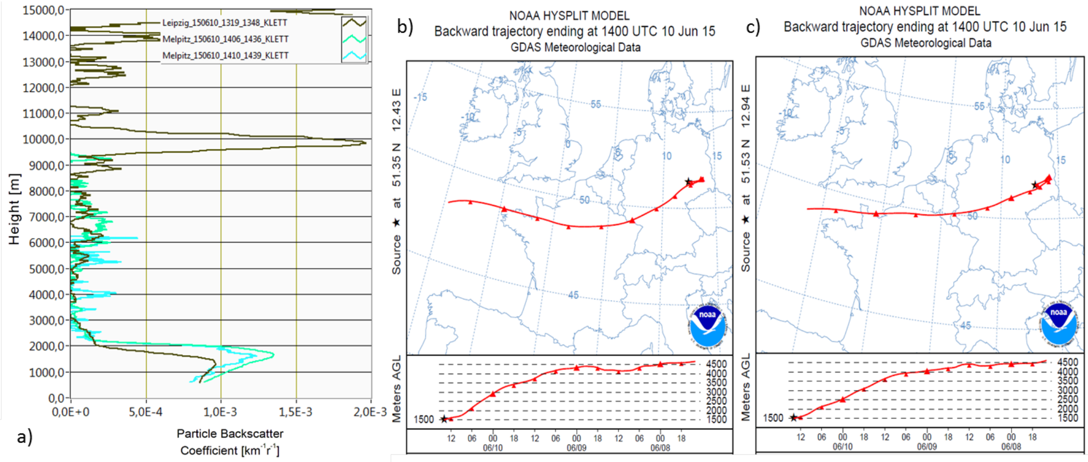

Figure 5.23: Case study of 10. June 2015. a) Lidar profile of this day from 13 to 15 UTC, the green-blue lines characterize the measurements from Melpitz, the grey-black lines characterize the measurements from Leipzig. The backscatter coefficient is plotted with respect to the height, b) HYSPLIT 3-day backward trajectories for Leipzig in 1500 m height, c) HYSPLIT 3-day backward trajectories for Melpitz in 1500 m height (www.arl.noaa.gov, Status: 18.02.2015).

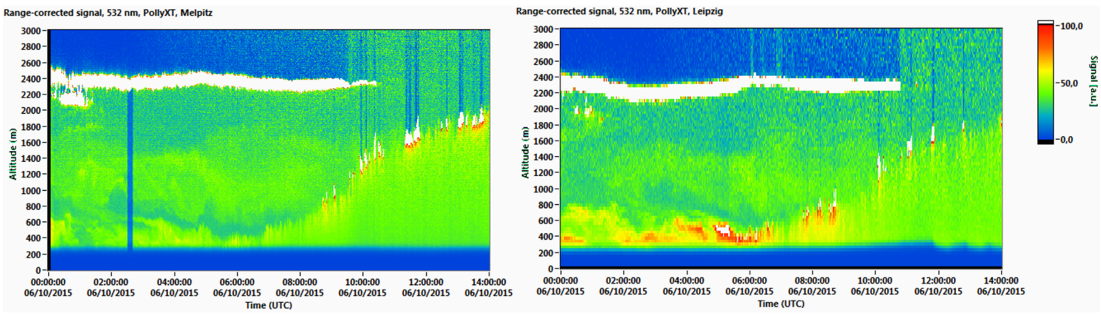

Figure 5.24: Lidar profile of the 10. June 2015 for 24 hours. Left part of the Figure: profile from Melpitz, right part of the Figure: profile from Leipzig. The red color indicates higher backscatter values compared to the blue color.

expected normally because of the effect of the urban heat island with higher heat fluxes and a larger extent of PBL over the urban area. In this case, the higher PBL top heights over Leipzig are caused by the different start of PBL growth due to the precipitation in the morning on that day.
The correlation of the relative humidity between Leipzig and Melpitz reveals a higher relative humidity in Melpitz as in Leipzig (Fig. 5.30). This is what also became visible in the previous cases. This might have an influence on the measured AOT and PBL top height.

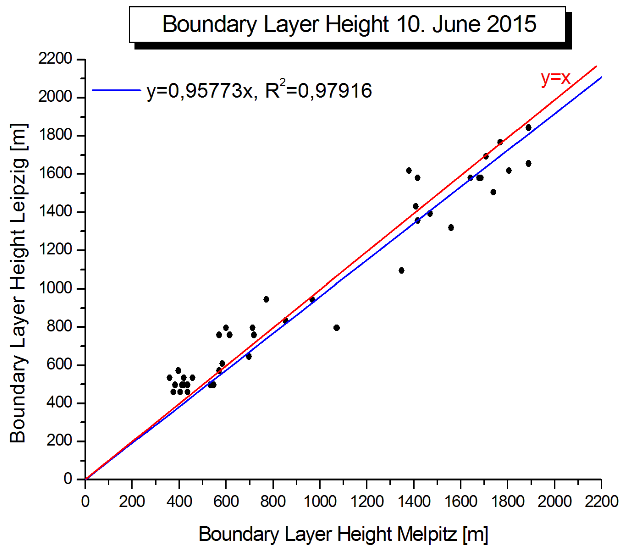

Figure 5.25: Correlation of the PBL top height from the 10. June 2015 between Melpitz and Leipzig. Formula for linear regression (blue line) and 1:1 line (red line) is also shown. The data is averaged over five minutes.

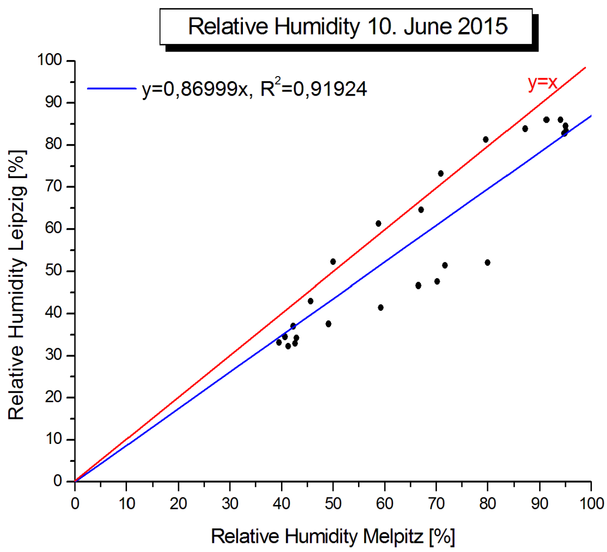

Figure 5.26: Correlation of the relative humidity for the 10. June 2015. Formula for linear regression (blue line) and 1:1 line (red line) is also shown. The data is obtained hourly.

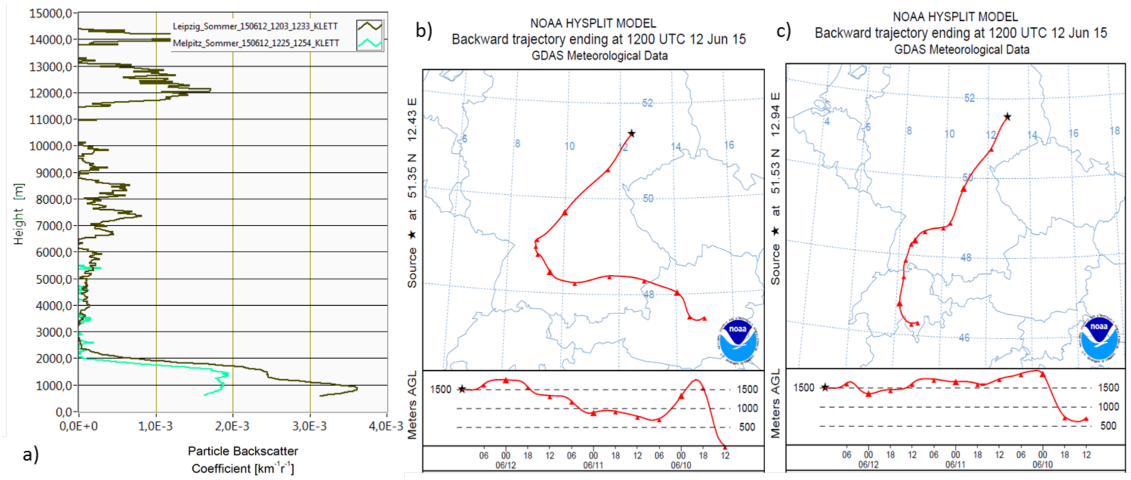

Figure 5.27: Case study of 12. June 2015. a) Lidar profile of this day from 12 to 13 UTC, the green-blue lines characterize the measurements from Melpitz, the grey-black lines characterize the measurements from Leipzig. The backscatter coefficient is plotted with respect to the height, b) HYSPLIT 3-day backward trajectories for Leipzig in 1500 m height, c) HYSPLIT 3-day backward trajectories for Melpitz in 1500 m height (www.arl.noaa.gov, Status: 18.02.2015).

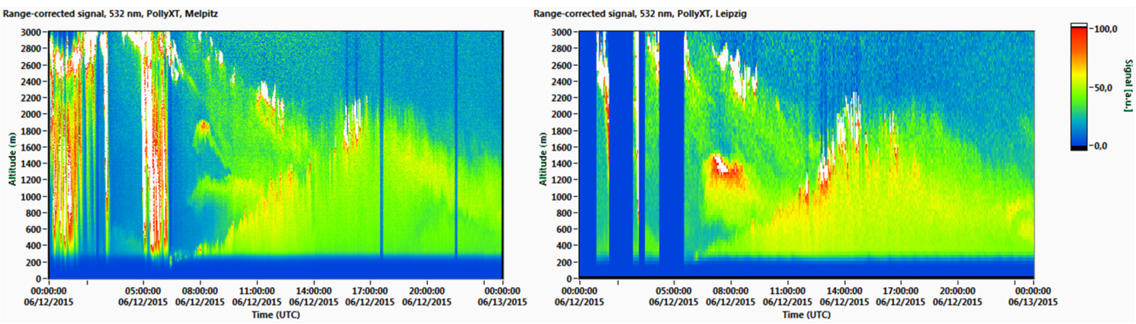

Figure 5.28: Lidar profile of the 12. June 2015 for 24 hours. Left part of Figure: profile from Melpitz, right part of Figure: profile from Leipzig. The red color indicates higher backscatter values compared to the blue color.

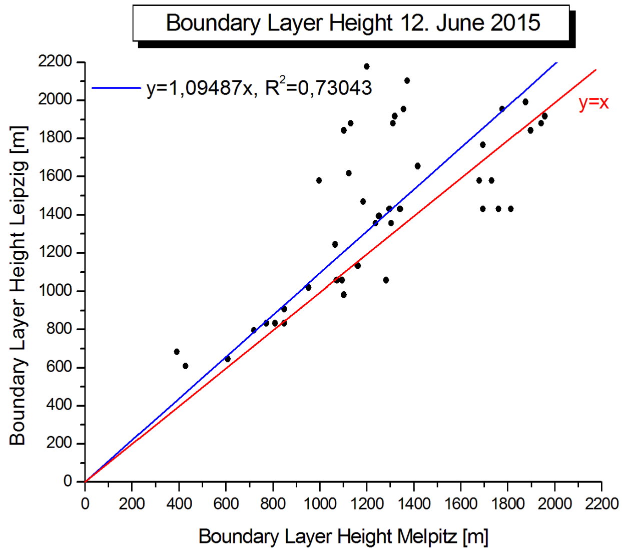

Figure 5.29: Correlation of the PBL top height from the 12. June 2015 between Melpitz and Leipzig. Formula for linear regression (blue line) and 1:1 line (red line) is also shown. The data is averaged over five minutes.

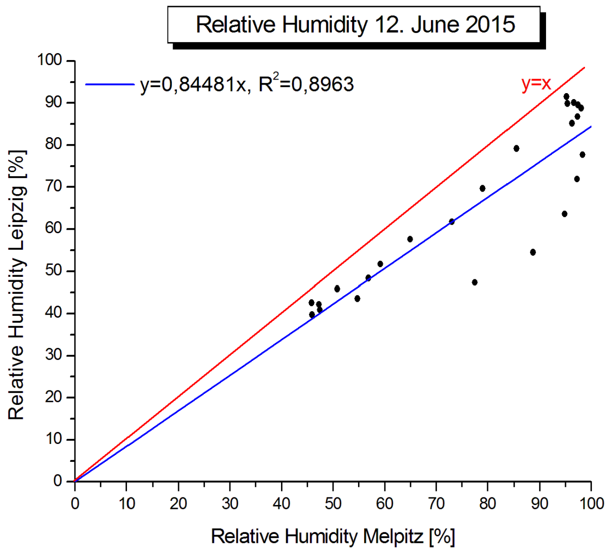

Figure 5.30: Correlation of the relative humidity for the 12. June 2015. Formula for linear regression (blue line) and 1:1 line (red line) is also shown. The data is obtained hourly.

5.2.4 Boundary layer cloud base height

Now, a case with typical PBL clouds will be analyzed. On this day (02. May 2015), the PBL evolution started at around 07 UTC in Melpitz and Leipzig (see Fig. 5.31). A clear determination of the start of PBL development for Leipzig is hard because of the higher altitude of complete overlap between the laser beam and the receiver field-of-view (see Section 2.1). First PBL clouds showed up in Melpitz at around 08 UTC and a little bit later in Leipzig. The clouds lasted in Melpitz until nearly 17 UTC and in Leipzig until 15 to 16 UTC when the PBL started to decay. Here, only measurement data until 16 UTC is used.

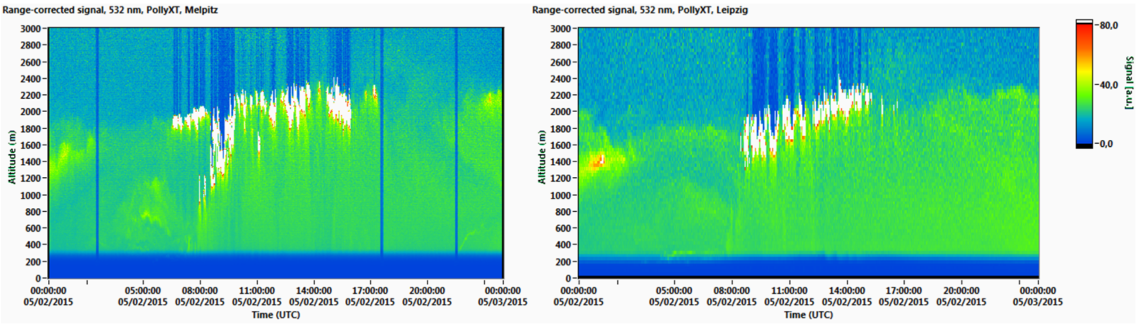

Figure 5.31: Lidar profile of the 02. May 2015 for 24 hours. The left Figure indicates the measurement from Melpitz, the right one from Leipzig. The white areas indicate the clouds.

The correlation plot for both sites (Fig. 5.32) shows nearly equal heights between both sites. Nevertheless, in Melpitz slightly enhanced cloud base heights were observed. This is consistent with the results from the autumn campaign in 2013. Here, on most of the days, the correlation between Leipzig and Melpitz was very good and only slightly enhanced cloud base heights over Melpitz were measured.
The temperature of this day indicates mostly higher values over Leipzig. However, some small differences can be seen. During sunrise from 07 to 11 UTC, the temperature was slightly higher in Melpitz whereas during the rest of the day the temperature reached higher values in Leipzig. The temperature may also have an impact on the cloud base height but this cannot be proven here.

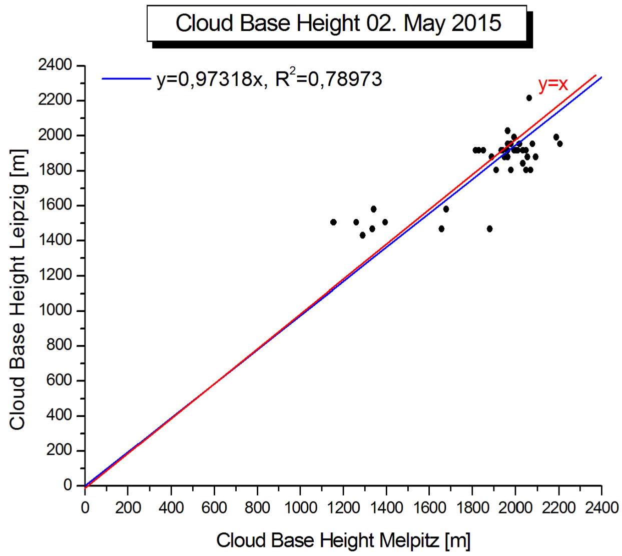

Figure 5.32: Correlation of the PBL cloud base height between Leipzig and Melpitz for the 02. May 2015. Formula for linear regression (blue line) and 1:1 line (red line) is also shown. The data is averaged over five minutes.

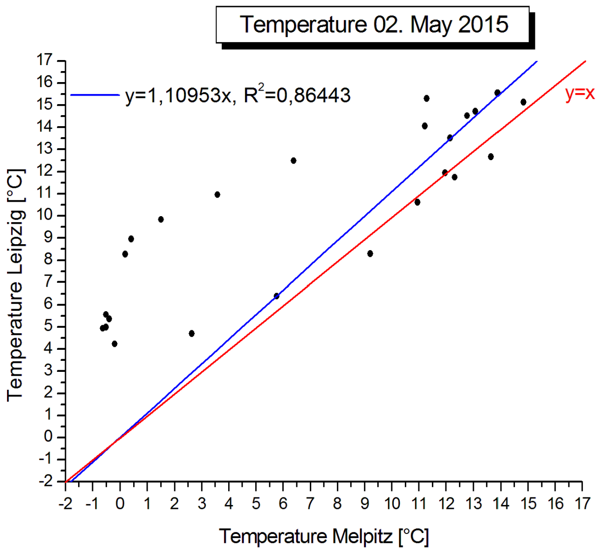

Figure 5.33: Correlation of the temperature of the 02. May 2015 between Leipzig and Melpitz. Formula for linear regression (blue line) and 1:1 line (red line) is also shown. The data is obtained hourly.

5.3 Conclusion

All in all, comparing the results from the two campaigns in 2013 and 2015, some differences can be seen. On the days with a higher AOT in Melpitz, the PBL top height was higher in Leipzig (southeastern flow) in 2013 whereas it was slightly higher in Melpitz in 2015 (western flow). For the case with higher AOT in Leipzig, the reverse case occured. Here, a higher PBL top height in Melpitz compared to Leipzig was observed in 2013 (northwestern flow) and it was almost equal in Leipzig and Melpitz with a southwestern direction in 2015. The last case showed mean AOT values that were almost equal in Leipzig and Melpitz with only slightly enhanced PBL top heights in Melpitz during both campaigns.

However, when comparing the different cases during the two campaigns to each other it has to be considered that the direction of flow was not always equal during the compared cases. This may lead to different results between the measurement campaigns.

On the other hand, the PBL cloud base heights showed mostly almost equal heights with only slightly enhanced values in Melpitz during the two measurement campaigns.

Most of the obtained results are linked to the enhanced relative humidity on these days in Melpitz compared to Leipzig. To find out further differences and seasonal influences between Leipzig and Melpitz and the autumn and summer campaign, statistical analysis of the data has been done in the following Chapter.

6 Statistics

In this Chapter, the results from the two campaigns are analyzed in detail and some statistical investigations will be done. Therefore, the AOT, relative humidity and total number concentration between both campaigns is shown. The correlation of the PBL top height as well as PBL cloud base height during the two campaigns is analyzed and compared concerning four different wind directions. Additionally, the lidar profiles of all days during the campaigns and the cloud cover is shown.

6.1 Aerosol optical thickness, relative humidity and total number concentration

At first, the AOT during the campaign in 2013 is analyzed. The correlation of the AOT measured by AERONET sun photometers between Melpitz and Leipzig is analyzed with respect to three different wavelengths (see Fig. 6.1). One would expect the AOT in Leipzig to be generally higher compared to Melpitz because of the more polluted environment over Leipzig. By means of the three graphics in Fig. 6.1 it becomes apparent that the reverse case has occured. The AOT for all three analyzed wavelength bands (440 nm, 500 nm and 870 nm) was higher in Melpitz than in Leipzig. Additionally, it can be seen that the variance of the measured values is quite small with a coefficient of determination (R^2) of around 0,9. This coefficient of determination is an index for the quality of alignment and may suggest a linear correlation. The analysis of three different wavelengths has been performed to make sure that none of the sun photometer channels was calibrated wrongly and thus led to wrong measurement results.
By means of these graphics it is evident that a bulk of the data is in the range of low AOT ($<$ 0,2 at 440 nm and 500 nm and $<$ 0,1 at 870 nm) and only few of these data showed high AOT ($>$ 0,2 at 440 nm and 500 nm and $>$ 0,1 at 870 nm) during the measurement period. Because of that, the correlation for all three wavelengths between both measurement sites for AOT values smaller and larger than 0,2 (and 0,1 for 870 nm) has been investigated. The results are shown in the Fig. 6.2. It is evident that there is no significant correlation in the range of low AOT values

between both stations (left part of Fig. 6.2). In contrast, a clear correlation with higher values in Melpitz is found for the measurement of high AOT ($>$ 0,2 at 440 nm and 500 nm and $>$ 0,1 at 870 nm). This leads to the assumption that these few but high values cause the differences between Melpitz and Leipzig. For the few but high values it turns out that they were measured only on five days during the campaign. These days were the 06.09.2013, the 13.09.2013, the 14.09.2013, the 08.10.2013 as well as the 09.10.2013. In the following, these interesting results are further discussed.

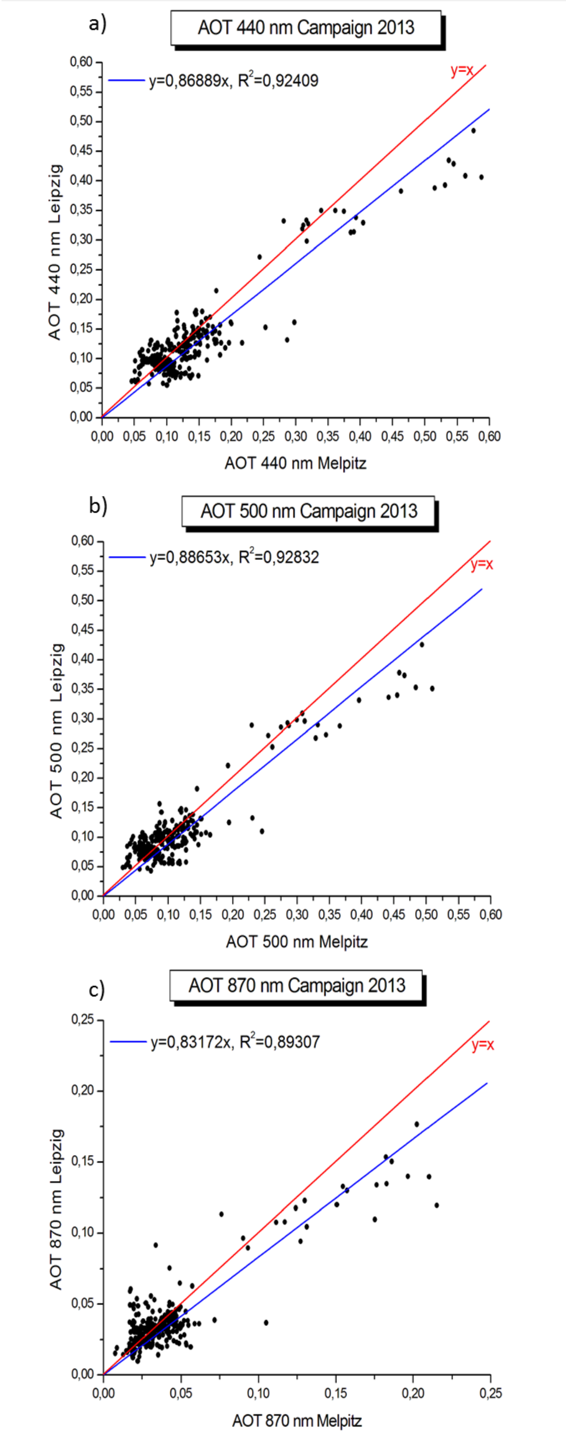

Figure 6.1: Correlation of the AOT at a) 440 nm, b) 500 nm and c) 870 nm between Leipzig and Melpitz for September and October 2013. Formula for linear regression (blue line) and 1:1 line (red line) is also shown.

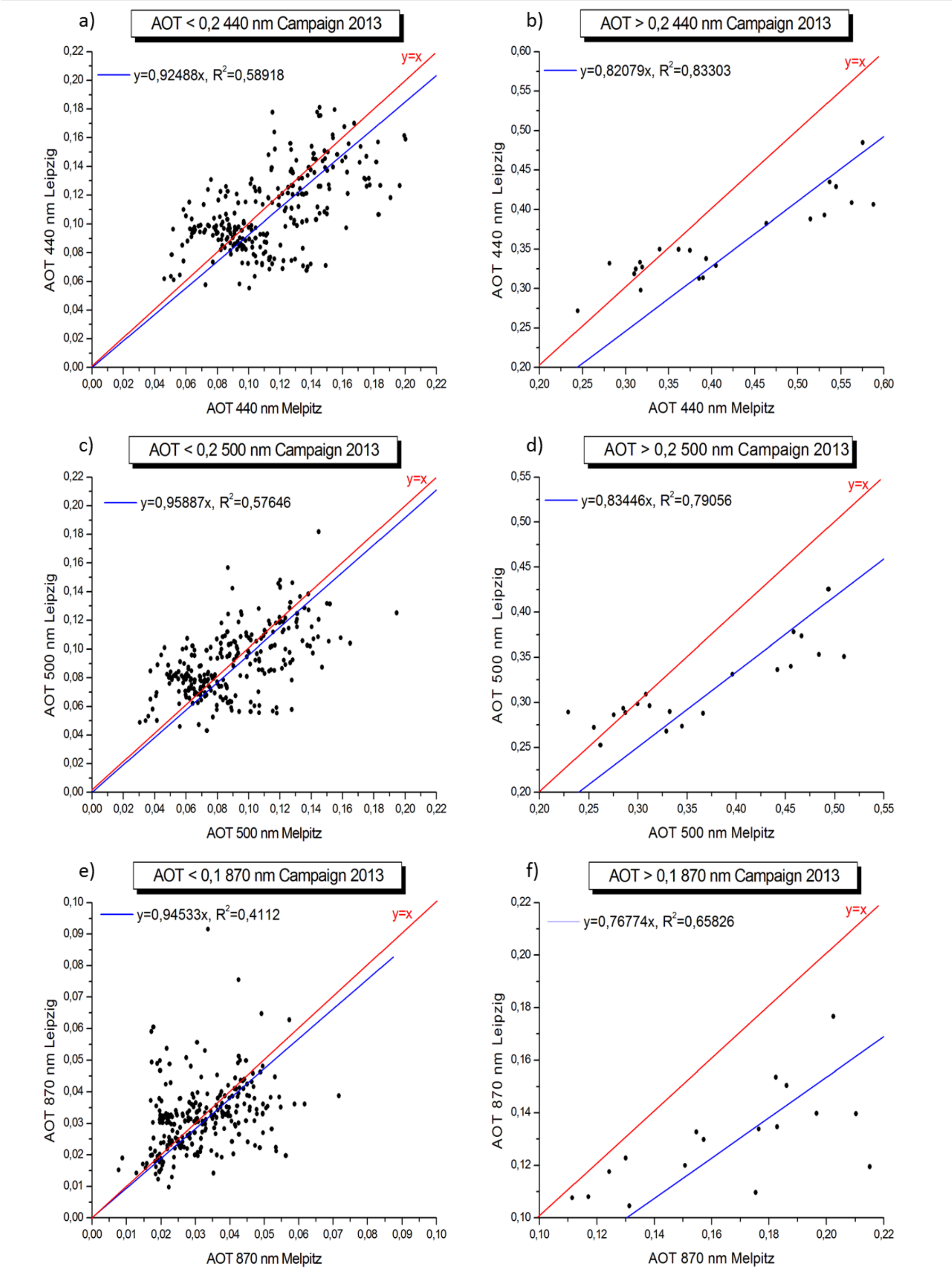

Figure 6.2: Correlation of AOT at 440 nm (upper part), 500 nm (middle part) and 870 nm (lower part) between Leipzig and Melpitz. On the left side values smaller 0,2 (and 0,1 for 870 nm) and on the right side values larger 0,2 (and 0,1 for 870 nm) for September and October 2013 are depicted. Formula for linear regression (blue line) and 1:1 line (red line) is also shown.

Next, the AOT at 500 nm will be examined for the campaign in 2015 (see Fig. 6.3). It becomes apparent that the AOT at 500 nm during this campaign is slightly higher in Melpitz (mean AOT of 0,205) compared to Leipzig (mean AOT of 0,188; compare Fig. 6.1). Again, most of the measured values are in the range of low AOT (0,05 to 0,25). Like in the autumn campaign, the correlation between both sites is very good but the variability of the AOT during this campaign was higher compared to the campaign in 2013. This is indicated by the coefficient of determination of 0,83. The maximum AOT values during both campaigns reached values of up to 0,55 to 0,6. Though, during the summer campaign much more values lie within this range of higher values (from 0,3 to 0,6). In this campaign, as already in the previous one, some of the measured values were significantly higher in Melpitz than in Leipzig (e.g. 0,5 in Melpitz compared to 0,05 in Leipzig). These high outlier values occured only on three days: the 12.05.2015, the 13.05.2015 and the 15.05.2015. On these days, the sun photometer in Melpitz was aligned wrongly what may have caused the strongly deviating values.

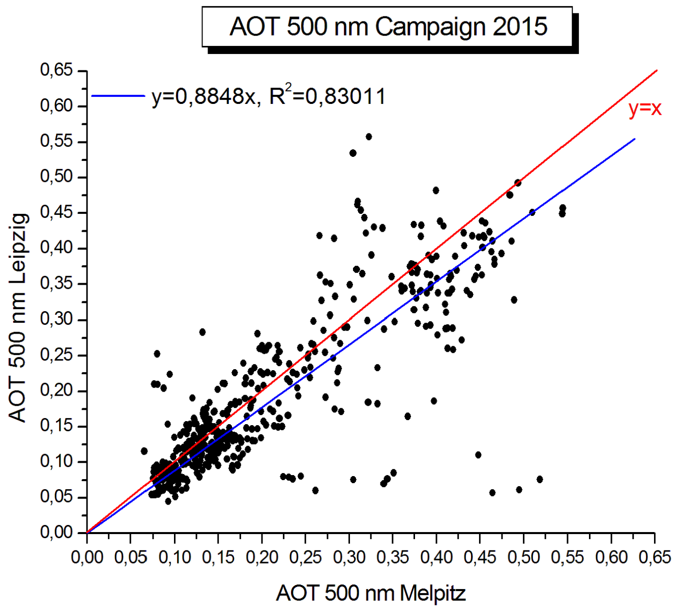

Figure 6.3: Correlation of the AOT at 500 nm between Leipzig and Melpitz for May to July 2015. Formula for linear regression (blue line) and 1:1 line (red line) is also shown.

Furthermore, the relative humidity during both campaigns has been investigated. At first, the relative humidity during the campaign in 2013 will be analyzed (Fig. 6.4).

Already in Fig. 6.4 a) it becomes apparent that the relative humidity during the whole campaign was higher in Melpitz than in Leipzig. The reason for this may be the vicinity of the river Elbe which flows near Melpitz or the different vegetation cover since there is significantly more forest and grass in Melpitz than in Leipzig. The coefficient of determination for the linear regression of around 0,92 could be an indicator for a linear connection and reveals a very good correlation.
A closer look at values from 75 % up to 100 % relative humidity is important (Fig. 6.4 b)) because particles grow strongly at a high relative humidity. This is due to the comparatively continuous particle growth (Skupin, 2013). It arises from Fig. 6.4 b) that more than half of the measured relative humidity values lie within this range. Additionally, the measured relative humidity within this range is significantly higher in Melpitz compared to Leipzig. Since the city of Leipzig contains much less natural vegetation and much more impervious surfaces compared to Melpitz, less evapotranspiration takes place over Leipzig. Additionally, Melpitz is influenced by the river Elbe. These effects in Melpitz increase the relative humidity there whereas it is smaller over the city of Leipzig.
This result also leads to the hypothesis that the higher relative humidity in Melpitz could be the reason for the observed differences in the AOT between both measurement sites. In an environment with a higher relative humidity compared to an environment with a lower humidity but the same dry aerosol number, the aerosol can grow stronger. This means that scattering is increased if one assumes equally dry aerosols in Leipzig and Melpitz.
The relative humidity has also been investigated for the summer campaign in 2015 (see Fig. 6.5). It was higher in Melpitz than in Leipzig during this campaign, as already seen in the previous campaign (compare Fig. 6.4). The lower coefficient of determination during this campaign compared to the autumn campaign indicates a larger variance for the measured relative humidity values with a higher mean relative humidity in Melpitz than in Leipzig for this campaign compared to the other one. A possible reason for this might be the fact that warmer air masses can absorb more water vapor than less warm air masses and as as consequence, more evapotranspiration could have occured over Melpitz.
Also here, the relative humidity for values higher 75 % is analyzed. Figure 6.5 b) indicates that nearly the half of the measured relative humidity values are within this range. Also for this campaign it turned out that significantly higher relative humidities were measured in Melpitz than in Leipzig within this range.
The reason for the higher values of relative humidity in Melpitz are the same as for

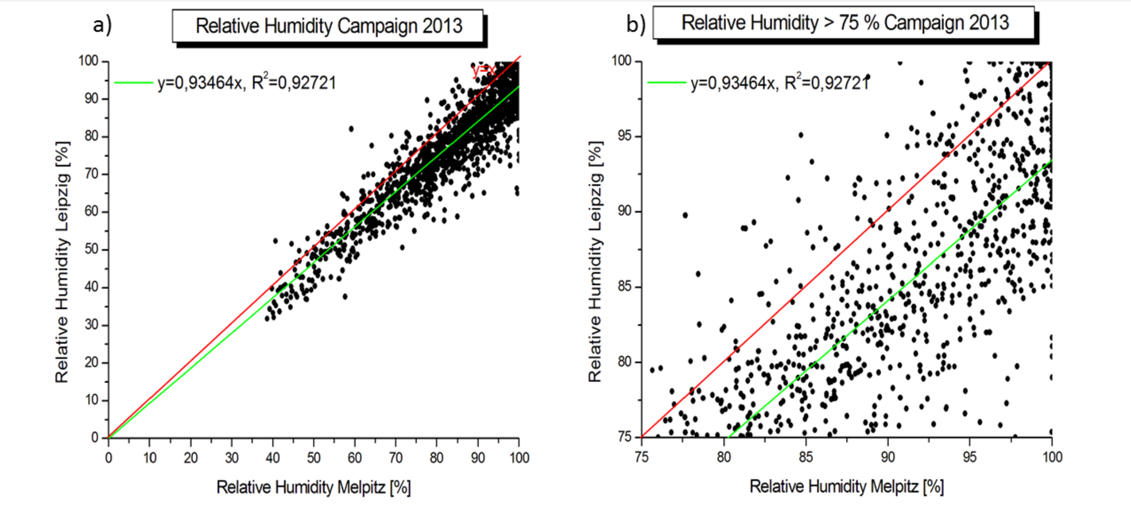

Figure 6.4: Surface relative humidity during the autumn campaign in 2013 for both sites. a) Relative humidity from 0 % to 100 % and b) relative humidity in the range from 75 % to 100 %. Formula for linear regression (blue line) and 1:1 line (red line) is also shown. The data is obtained hourly.

the autumn campaign in 2013. The vicinity of the river Elbe may play a role but the more important fact is the different vegetation between both sites which explains the higher AOT in Melpitz.

The total dry particle number for two particle sizes (100 to 300 nm and 300 nm to 800 nm) during the measurement campaign in 2013 has also been analyzed (Fig. 6.6 and 6.7). Figure 6.6 shows the total number concentration during this campaign only for the five days with the significantly higher AOT in Melpitz compared to Leipzig (06.09.2013, 13.09.2013, 14.09.2013, 08.10.2013 and 09.10.2013). It can be seen that the correlation between the small particle size (100 to 300 nm) is comparatively low with higher values in Leipzig whereas it is high for the larger particle size with nearly equal particle numbers in Leipzig and Melpitz. This shows that more small particles were present in Leipzig whereas the number of larger particles was nearly equal in Leipzig and Melpitz.
The results for the dry particle number for the rest of the days during this campaign (without the five outlier days) is shown in Fig. 6.7. Here, for the two particle sizes it is visible that slightly higher particle concentrations occured in Leipzig than in Melpitz. This is also what would be expected since over Leipzig there is much more pollution. Among other things, this pollution is caused by traffic or industrial

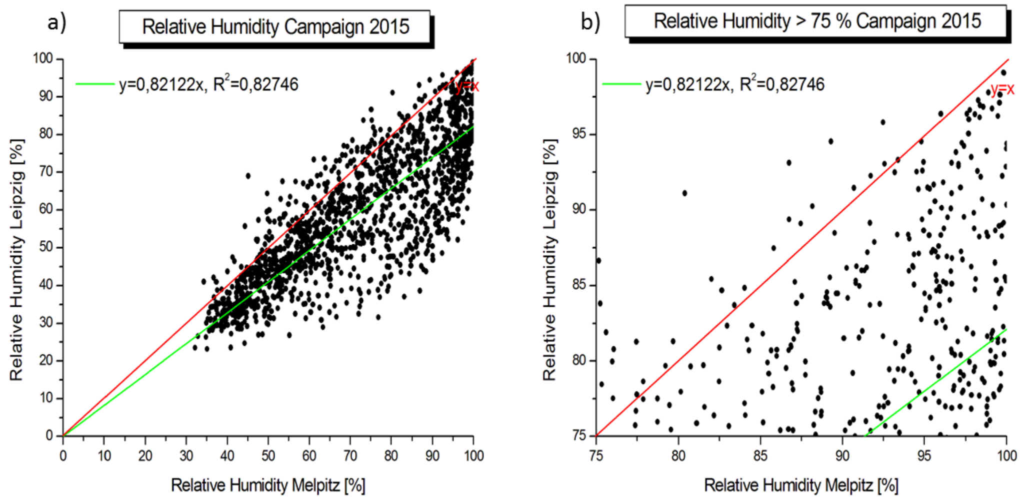

Figure 6.5: Surface relative humidity during the summer campaign in 2015 for both sites. a) Relative humidity from 0 % to 100 % and b) relative humidity in the range from 75 % to 100 %. Formula for linear regression (blue line) and 1:1 line (red line) is also shown. The data is obtained hourly.

pollution.
The outliers in Fig. 6.7 were measured on the 27.09.2013, 28.09.2013, 11.10.2013 and 31.10.2013. Nevertheless, without these four outlier days, the particle number concentration was still higher in Leipzig than in Melpitz.

It might be suggested that the main reason for the higher AOT in Melpitz was the higher relative humidity there. The higher relative humidity in Melpitz compared to Leipzig in connection to the mostly higher particle number concentration in Leipizg may have produced more but smaller particles in Leipzig compared to Melpitz. The particles in Melpitz are less in number but larger and this may have caused the higher AOT values in Melpitz.

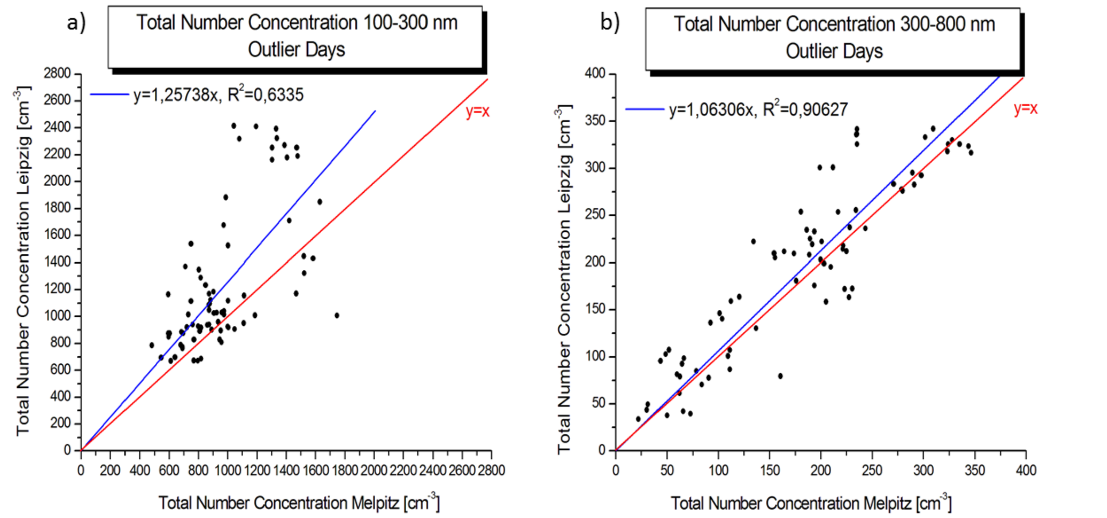

Figure 6.6: Number concentration for the outlier days during the autumn campaign in 2013 for both sites. a) Number concentration in cm^{-3} for particle sizes from 100 to 300 nm and b) number concentration in cm^{-3} for particle sizes from 300 to 800 nm. Formula for linear regression (blue line) and 1:1 line (red line) is also shown. The data is obtained hourly.

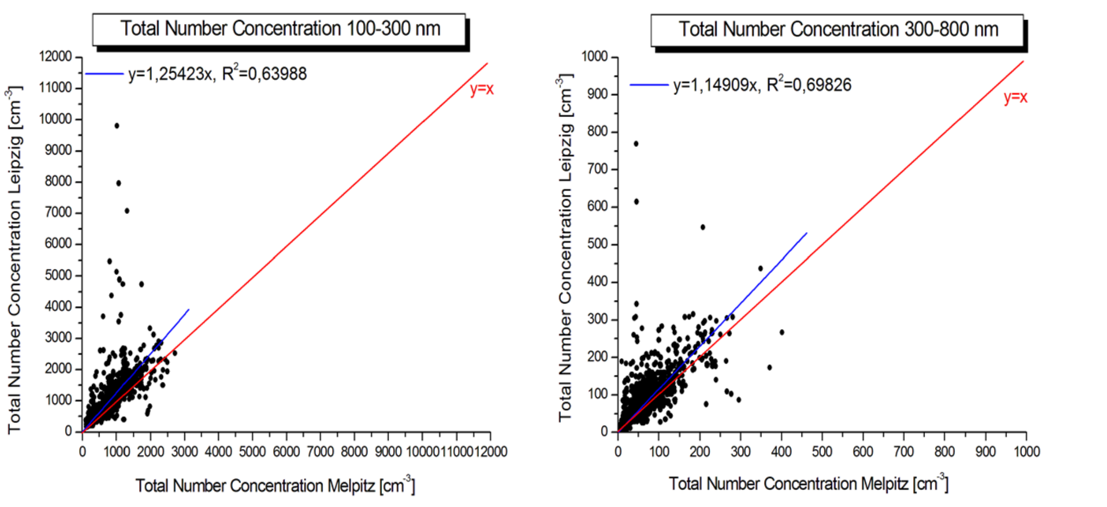

Figure 6.7: Number concentration without the outlier days during the autumn campaign in 2013 for both sites. a) Number concentration in cm^{-3} for particle sizes from 100 to 300 nm and b) number concentration in cm^{-3} for particle sizes from 300 to 800 nm. Formula for linear regression (blue line) and 1:1 line (red line) is also shown. The data is obtained hourly.

6.2 Boundary layer top height

In this Section, the evolution of PBL top height during both campaigns is analyzed and discussed. At first, the time series of the PBL during the autumn campaign in 2013 at both locations is shown (Fig. 6.8). Here, each day is depicted separately. The agreement between both measurement sites is quite well. Nevertheless, the higher PBL top heights in Leipzig compared to Melpitz were mostly measured during the early morning and noon when the PBL started to develop which is most likely due to the effect of the urban heat island with higher heat fluxes and temperatures and thus a higher PBL over the city. During the afternoon, the PBL was sometimes higher in Melpitz compared to Leipzig. This might be due to the different start of decay at both sites.

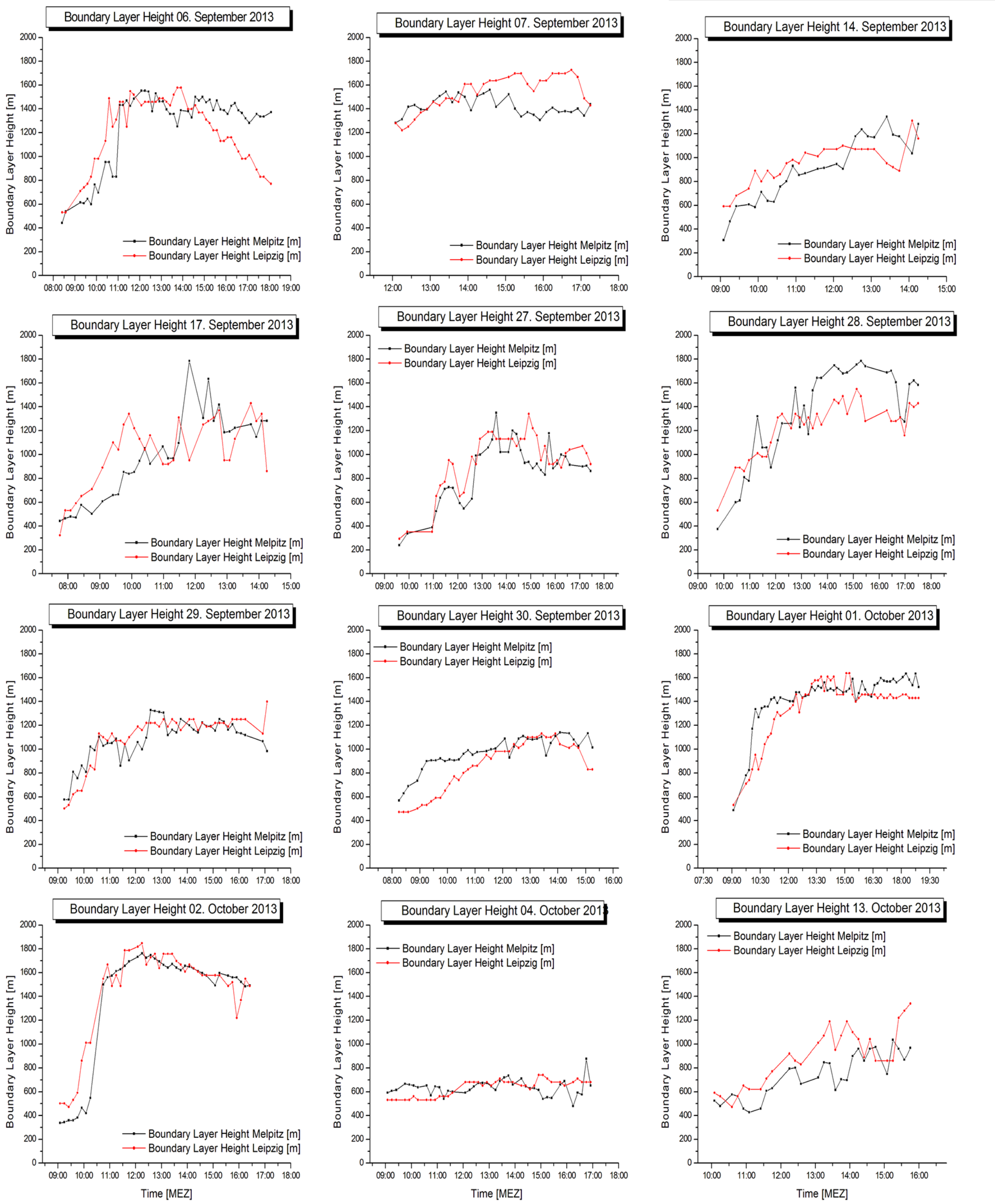

Figure 6.8: Time series of the PBL top height during the measurement campaign in 2013. The red line characterizes the PBL top height of Leipzig, the black line the one in Melpitz. The data is averaged over ten minutes.

The time series for the PBL top height during the summer campaign in 2015 (not shown here) also reveals higher PBL top heights in Leipzig which were mostly measured during the early morning and noon when the PBL starts to evolve. Higher values in Melpitz mostly occured during the late afternoon.
Additionally, almost no seasonal differences between autumn 2013 and spring/summer 2015 in the growth and decay of PBL top heights occured. Only the maximum height during the summer campaign was higher than during the autumn campaign. In Fig. 6.9, the PBL top heights during the autumn (Fig. 6.9 a)) and summer campaign (Fig. 6.9 b)) are correlated. As already seen from the previous Figure, there is no large difference between rural and city. Indeed, the correlation plot shows quite similar heights between both sites and during both campaigns (coefficient of determination of 0,84 in autumn 2013 and 0,83 in summer 2015). Nevertheless, there is no significant trend, maybe a slightly higher PBL top in Melpitz can be seen.

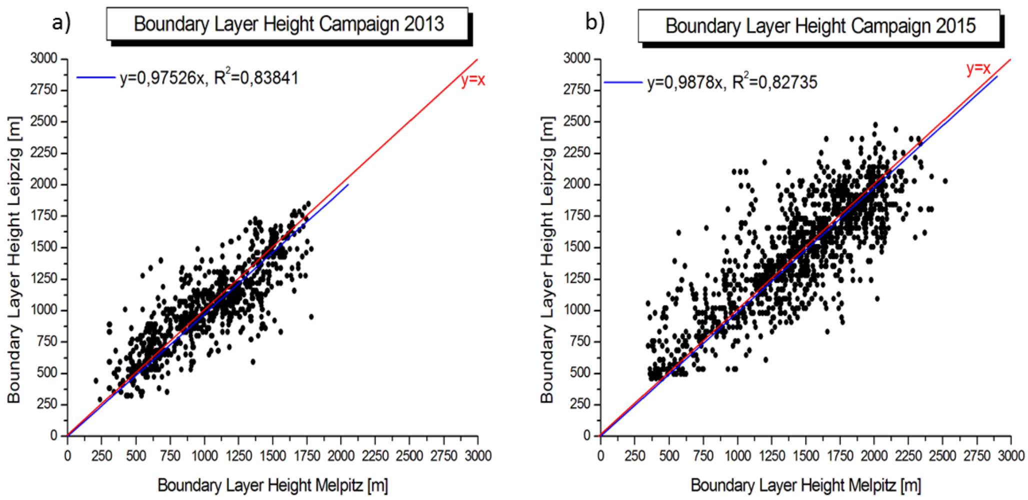

Figure 6.9: Correlation of the PBL top height between Leipzig and Melpitz. a) PBL top height during the campaign in 2013, b) PBL top height during the campaign in 2015. Formula for linear regression (blue line) and 1:1 line (red line) is also shown. The data is averaged over ten minutes.

Additionally, no major differences between the two campaigns can be seen. This leads to the hypothesis that there might be no seasonal difference between the locations. This however, would need to be validated by long-term observations at both sites. Though, it becomes apparent that the maximum PBL top height in summer was higher (up to nearly 600 m) compared to the autumn campaign which is due to higher temperatures and a larger vertical extent of surface air masses caused by stronger vertical fluxes in summer compared to autumn.

6.3 Boundary layer cloud base height

The PBL cloud base height (Fig. 6.10) for the two measurement campaigns is discussed next. Normally, the cloud base height would be expected to be higher in Leipzig than in Melpitz because of higher temperatures with a higher PBL top height and thus higher PBL clouds. However, it becomes apparent that the cloud base height at both sites shows similar heights with a slightly higher cloud base height over Melpitz. This is in slight opposition to theory. The similar cloud base heights between the two campaigns show almost no seasonal influence, as already seen from the previous Figure. Only the maximum cloud base height in summer can be up to 400 meters higher than in autumn. The reason for this is, again, the higher temperature in summer due to higher incoming solar radiation and thus a larger vertical extent of the air masses due to enhanced convection.

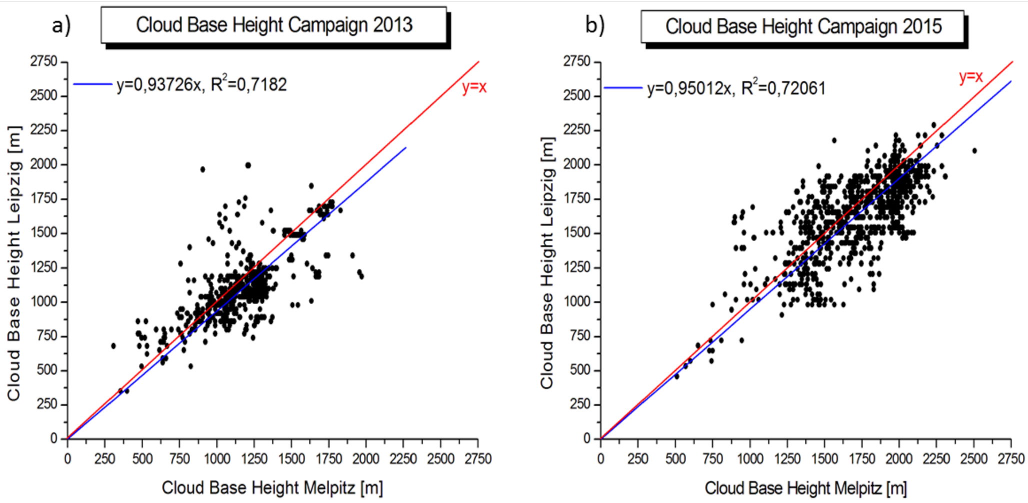

Figure 6.10: Correlation of the PBL cloud base height between Leipzig and Melpitz. a) PBL cloud base height during the campaign in 2013, b) PBL cloud base height during the campaign in 2015. Formula for linear regression (blue line) and 1:1 line (red line) is also shown. The data is averaged over one minute.

6.3.1 Cloud amount

In the next Section, the PBL cloud amount (see Chapter 3.5) at day during both campaigns is investigated. The results are presented in Fig. 6.11. The red bars show the measurement values from Melpitz, the blue ones from Leipzig. During both campaigns it can be seen that most frequent clear sky conditions occured. Additionally, the most frequent cloud amount was at 1/8. Nevertheless, some important differences, especially between the two campaigns, become clear.
During the campaign in 2013 in Melpitz more cloud amounts at 0/8 and 1/8 have been detected whereas in Leipzig more frequent higher cloud amounts (4/8, 5/8 and 7/8) have been determined. Compared to the campaign in 2015 the reverse case can be seen. Here, more frequent lower cloud amounts (0/8, 1/8, 2/8 and 3/8) appeared in Leipzig and higher cloud amounts (4/8, 5/8, 7/8 and 8/8) were more often visible in Melpitz.

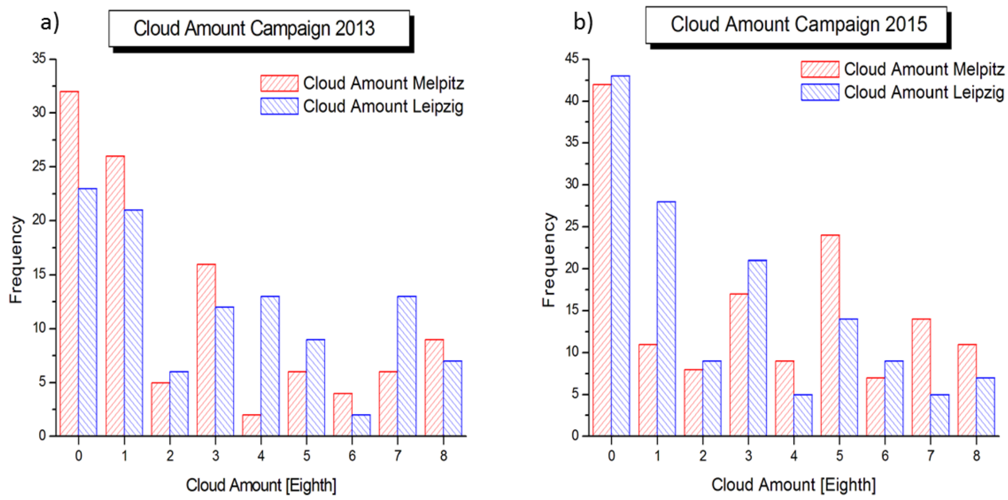

Figure 6.11: Cloud amount in eighth during the two measurement campaigns. Figure a) shows the cloud amount during the campaign in 2013, b) the cloud amount during the campaign in 2015. The red bars indicate the values from Melpitz, the blue ones from Leipzig.

6.4 Cluster analysis

In the following Section, the PBL top height as well as the PBL cloud base height will be analyzed for four different wind clusters during the two campaigns. The four clusters are already explained in Section 4.4 and two major cluster were chosen: an eastern and a western cluster. The two cluster were chosen to determine whether there is an influence of air mass origin to the PBL top and PBL cloud base height.
At first, the PBL top height concerning wind clusters for the campaign in 2013 are analyzed. From the upper part of Fig. 6.12 it can be seen that nearly half of the retrieved PBL top heights were observed during easterly flow (cluster 3), whereas the other values were observed during the 'typical' westerly flow (clusters 1, 2 and 4 added). The eastern cluster is broader than the other ones and enfolds directions from 0° up to 180°. This is the reason for the fact that nearly half of the measured values lie within the eastern cluster. When comparing between the western (Fig. 6.12 b)) and the eastern wind direction (Fig. 6.12 a)), some differences can be seen. For the eastern cluster there is a good correlation between both sites with no huge variance. For the western cluster it shows a good correlation, too, with slightly higher values in Melpitz. The graphic shows also that the PBL top height in the eastern cluster was a little bit higher (up to 400 m) than during wind directions from the western cluster. A possible reason for this may be the fact that during eastern flow directions drier air masses reach the sites. Those drier air masses may support better mixing than the wetter air masses from the western direction. Thereby, the PBL top height could grow more strong and higher. This graphic may suggest that the different wind directions could have a small influence on the PBL top height but this cannot be proven here.
In the lower part of Fig. 6.12 the cluster analysis for the summer campaign in 2015 is presented. The correlation between the eastern (Fig. 6.12 c)) and the western (Fig. 6.12 d)) cluster is comparatively good, as already seen in the upper part of the Figure. The PBL top height for both cluster is nearly equal with no visible differences. Nevertheless, during the summer campaign it turnes out that over half of the measurement values came from a westerly flow direction. Additionally, the maximum PBL top height in summer is nearly 500 to 600 m higher than during the autumn campaign. The reason for this may be the larger extent of surface air masses in summer compared to autumn.
It becomes apparent that seasonal differences concerning the different locations are small, except for the maximum height of the PBL.

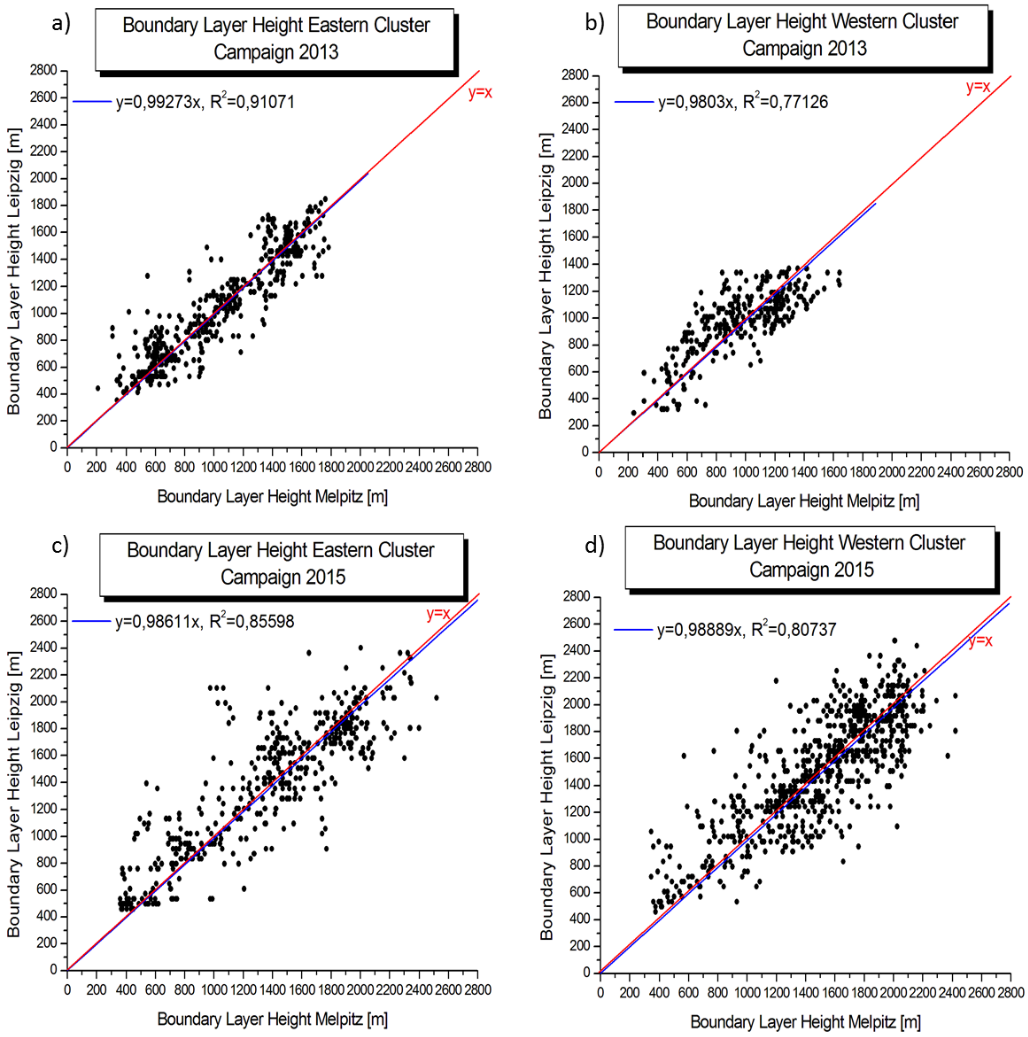

Figure 6.12: Correlation of the PBL top height between Leipzig and Melpitz for different wind cluster. a) Easterly wind cluster (see Section 4.4, cluster 3) during the campaign in 2013, b) westerly wind cluster (see Section 4.4) during the campaign in 2013, c) easterly wind cluster (cluster 4) during the campaign in 2015, d) westerly wind cluster during the campaign in 2015. Formula for linear regression (blue line) and 1:1 line (red line) is also shown. The data is averaged over ten minutes.

Next, the cloud base height for the eastern and the western cluster during the autumn campaign is shown (upper part of Fig. 6.13). It can be seen that the correlation between the different locations for both flow directions is comparatively good. For the easterly flow direction (Fig. 6.13 a)), the cloud base heights show a better correlation between both sites with only small differences than during the western direction.

Additionally, it can be seen that for the eastern cluster much less clouds have been observed than for the western cluster. The reason for this is the fact that the air masses coming from the eastern direction are significantly drier than the air masses from the west. The air masses from the east are not passing over a huge open water surface like they do when they come from the west. Because of this, they do not contain that much water vapor. Therefore, the cloud development is hindered and less clouds can form.
The lower part of Fig. 6.13 shows the PBL cloud base height for the eastern (Fig. 6.13 c)) and western (Fig. 6.13 d)) cluster during the campaign in 2015. The correlation between both measurement sites during both clusters is comparatively good but, as already seen in the upper part, worse than for the PBL top height. The maximum cloud base height between the two clusters was nearly the same and here, no differences between air masses coming from the east and west were found. Nevertheless, much less clouds were observed for the eastern cluster during the summer campaign. The reason is the same as for the campaign in 2013, much drier air masses that have reached the two sites from the east.
Likewise, the seasonal differences for the PBL cloud base height between both measurement sites are very small. Only some differences in maximum cloud base height between the seasons were present.

6.5 Lidar profiles

In the following Section, the lidar profiles for Melpitz and Leipzig during the autumn and summer campaign are analyzed.
The lidar profiles from the autumn campaign are shown in Fig. 6.14. Here, the backscatter coefficient at 532 nm wavelength for Melpitz (continuous line) and Leipzig (dotted line) is shown. The backscatter coefficient depends mainly on the size, the number and the refractive index. This means that the profile of the backscatter coefficient is an indirect measure for the height of the PBL.
The red lines indicate the 5th and 95th percentile, the black line characterizes the arithmetic mean and the blue line shows the median. A percentile subdivides a dataset into hundred pieces. This means that 95 % of all values lie under the 95th percentile. The median is the value in the middle of a sorted dataset which means that 50 % of the values are smaller or equal than this value and 50 % are larger or equal this value. On the other hand, the arithmetic mean is the average and can be

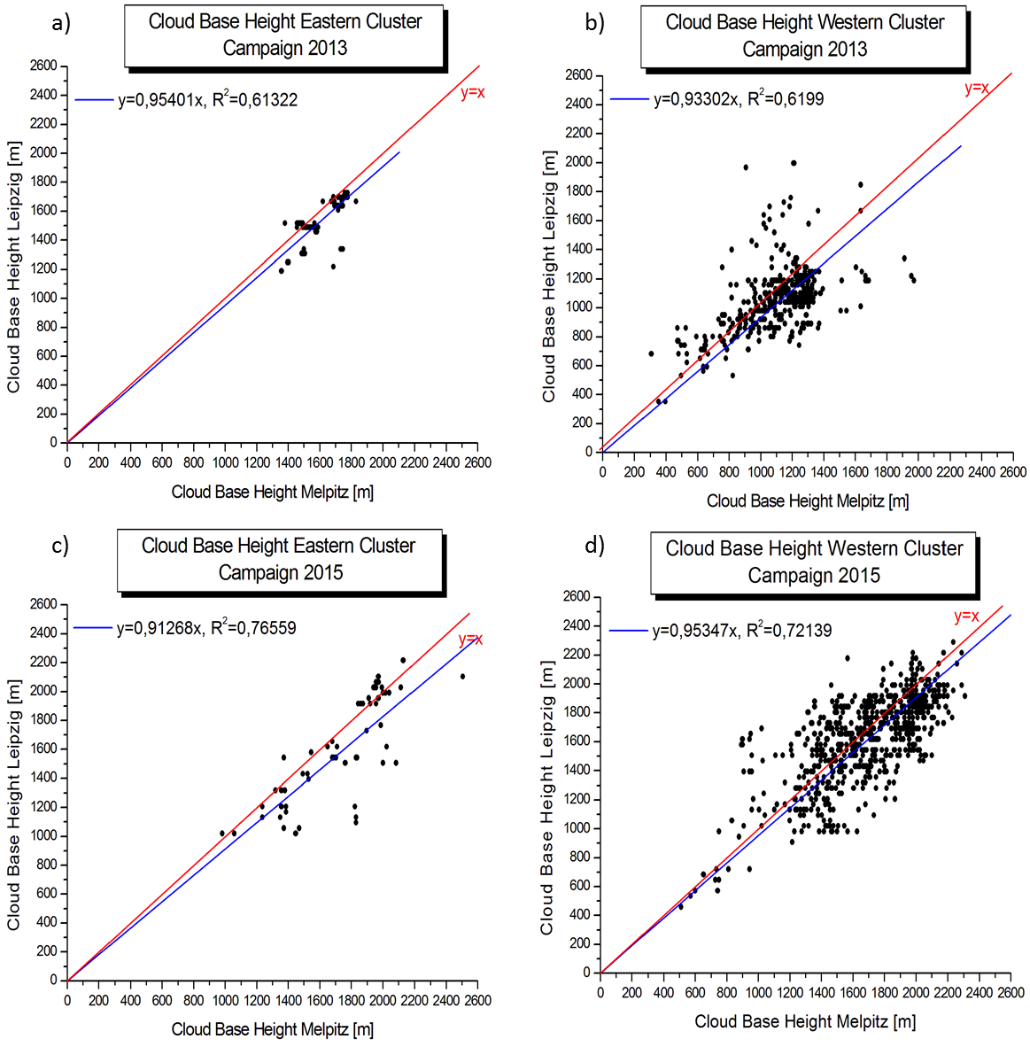

Figure 6.13: Correlation of the PBL cloud base height between Leipzig and Melpitz for different wind cluster. a) Easterly wind cluster (see Section 4.4, cluster 3) during the campaign in 2013, b) westerly wind cluster (see Section 4.4) during the campaign in 2013, c) easterly wind cluster (cluster 4) during the campaign in 2015, d) westerly wind cluster during the campaign in 2015. Formula for linear regression (blue line) and 1:1 line (red line) is also shown. The data is averaged over ten minutes.

calculated as quotient from the sum of all values (Fahrmeir et al., 1998).
Some differences between the two sites can already be seen. The mean height of the layer with the strongest backscatter is nearly 1700 to 2000 m high for both sites. Nevertheless, the mean backscatter coefficient in Melpitz is slightly higher compared to Leipzig. This may also be due to the higher relative humidity in Melpitz which may have led to bigger particles over Melpitz. They may scatter the light more

strongly back and cause a higher backscatter coefficient. Additionally, this graphic shows that the lidar measurements confirm the results obtained from the sun photometer (compare Fig. 6.1). The mean AOT measured by sun photometers was also higher in Melpitz compared to Leipzig.

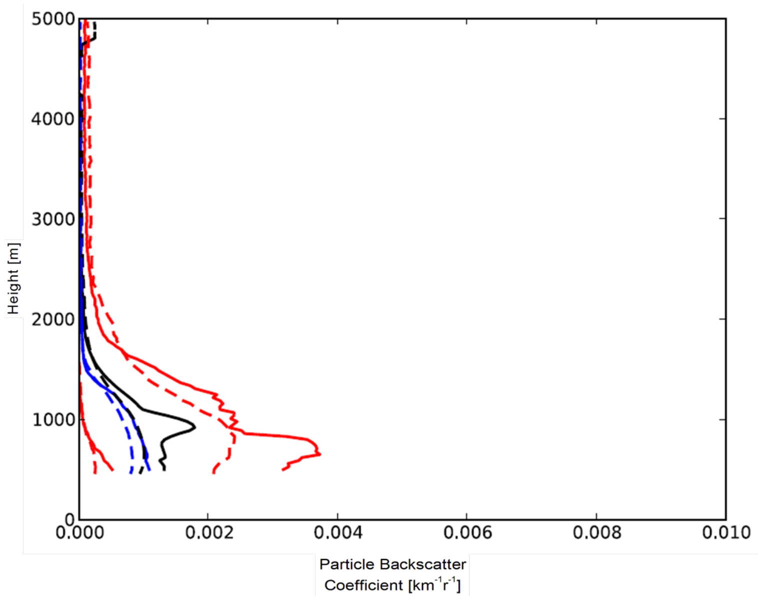

Figure 6.14: Lidar profiles during the autumn campaign in 2013. The continuous lines characterize the measurements from Melpitz, the dotted lines from Leipzig. The red lines indicate the 5th and 95th percentile, the blue lines characterize the median and the black lines the mean value.

The statistical results for the backscatter coefficient from the summer campaign in 2015 are also presented (Fig. 6.15, continuous line describes Melpitz, the dotted line Leipzig). The mean height of the layer with the strongest backscatter is in about 2300 to 2500 m height. This is about 500 m higher than in the autumn campaign. This might be caused by the larger extent of surface air masses due to the highest position of sun in the northern hemisphere in summer and enhanced incoming solar radiation. This leads to a higher heat flux, higher temperatures and a larger vertical extent of surface air masses in summer.
Also, there are some differences between the rural and urban site visible. The mean backscatter coefficient is higher in Leipzig than in Melpitz and it shows a smaller vertical gradient in Melpitz than in Leipzig.
Here, some differences between the two campaigns have become visible. In the autumn campaign, the mean particle backscatter coefficient in Melpitz was higher than

in Leipzig whereas during the summer campaign the reverse case occured. This may suggest that seasonal influences could be present but this is not proven.

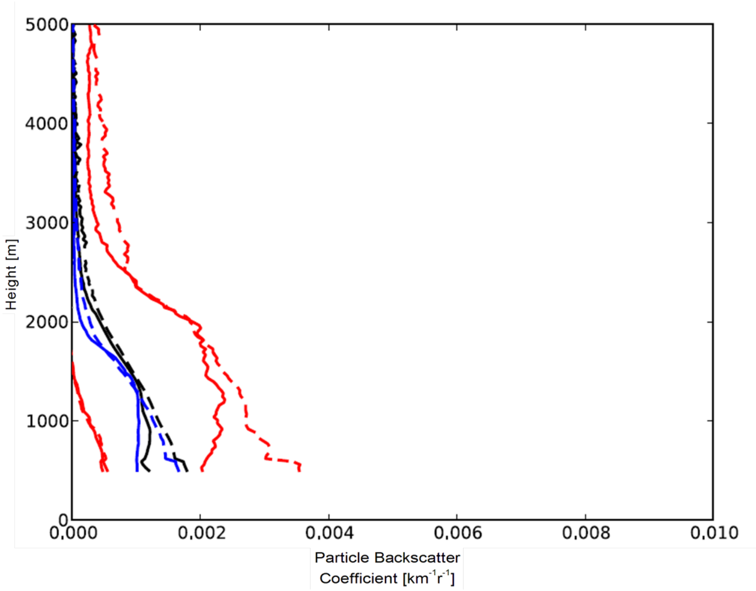

Figure 6.15: Lidar profiles during the summer campaign in 2015. The continuous lines characterize the measurement from Melpitz, the dotted lines from Leipzig. The red lines indicate the 5th and 95th percentile, the blue lines characterize the median and the black lines the mean value.

7 Conclusion and Outlook

In this work, differences between the city of Leipzig and the rural Melpitz with respect to aerosol were investigated by means of data from two measurement campaigns in autumn 2013 and summer 2015. In the framework of these two campaigns, lidars, sun photometers as well as ground-based in-situ instruments performed measurements. Ground-based in-situ measurements describe a point measurement on a certain place. On the other hand, sun photometers as well as lidars are ground-based remote sensing instruments. A sun photometer integrates about the whole atmospheric column above the instrument whereas a lidar measures vertically resolved. This means that every height (according to the resolution of the lidar) has a measurement value.

The data from the two campaigns revealed some interesting and unexpected results. It turned out that the total number concentration over the city is higher than over the rural site. The reason for this is the stronger polluted urban environment due to industry, households and traffic in contrast to the cleaner and less polluted rural environment. Additionally, it turned out, against all expectations, that during both campaigns a higher AOT has been detected in the rural location of Melpitz compared to urban Leipzig. This is caused by the higher relative humidity in Melpitz compared to Leipzig. Due to the higher relative humidity in Melpitz, the aerosol there can grow stronger. The higher relative humidity in the rural area is a result of the higher amount of natural vegetation. In Leipzig there are much more impervious and human made surfaces caused by the huge amount of streets and houses. They contain much less natural vegetation. Thus, over the city less evapotranspiration takes place and the relative humidity is smaller compared to the rural environment which resulted in a lower AOT over Leipzig during the two campaigns.

Measured lidar profiles during both campaigns were analyzed statistically to confirm the AOT measurements from the sun photometer. It turned out that during the autumn campaign the backscatter coefficient was higher in Melpitz which is consistent with the results from the sun photometer. For the summer campaign the reverse case showed up. The results showed that in Melpitz less aerosol was available but the relative humidity was higher over the rural area. This leads to enhanced scattering and thus a higher AOT was measured.

Also, different case studies during both campaigns were analyzed concerning PBL top and PBL cloud base height. Here, the PBL top as well as cloud base height showed mostly nearly equal heights between the two sites. Indeed, slightly enhanced PBL top and cloud base heights in Melpitz compared to Leipzig have been observed on some of the days. Nevertheless, the relative humidity during all observed cases was higher in Melpitz than in Leipzig.
Additionally, a statistical analysis has been performed concerning the PBL top and cloud base height. All in all, the differences in PBL top and cloud base height between Leipzig and Melpitz were mostly small and the two measurement sites showed equal PBL top and cloud base heights with only slightly enhanced cloud bases over Melpitz and no huge seasonal influence. The cloud amount during both campaigns was also analyzed. During the autumn campaign, the lower cloud amount was observed more often in Melpitz and the higher cloud amount more often in Leipzig. For the summer campaign the reverse was true. Here, only PBL cloud base heights were investigated.
Furthermore, the direction of air mass advection for both measurement sites during the two campaigns was investigated. Two major flow types have been observed, an eastern and a western flow. More than half of the measured values came from the west. Additionally, the PBL top and PBL cloud base height in dependence of the two wind cluster was investigated. Here, only small differences have become visible. For the eastern cluster there was a good correlation for the PBL top and cloud base height between Leipzig and Melpitz during both campaigns but for the western cluster the PBL cloud base height was slightly higher in Melpitz. Also, the maximum PBL top height during eastern wind conditions was slightly higher than during westerly conditions which might be due to drier air masses reaching the sites from the east.

All the results show that there are noticeable differences concerning the AOT, the relative humidity as well as the dry particle number concentration and small differences concerning PBL top and cloud base height. Almost no differences have been found concerning the origin of air masses between the urban and rural environment which may result from the urbanization. This urbanization is having an influence on the AOT, the PBL top and cloud base height. The mean AOT during the measurement campaign in 2013 for Melpitz was 0,111 and 0,107 for Leipzig whereas the mean AOT during the campaign in 2015 was 0,231 in Melpitz and 0,211 in Leipzig. The mean PBL top height between Leipzig and Melpitz during the campaign in

2013 was nearly equal with only two meters difference between Leipzig (1017 m) and Melpitz (1015 m) whereas the difference during the summer campaign was 17 m (1457 m in Melpitz and 1440 m in Leipzig). The mean difference for the PBL cloud base height was also small. Here, the mean difference for the campaign in 2013 was 59 m (1183 m in Melpitz and 1124 m in Leipzig) whereas it was 70 m during the campaign in 2015 (1696 m in Melpitz and 1626 m in Leipzig). Additionally, these results suggest that the seasonal influence is comparatively small. No huge differences between the autumn and the summer campaign were discovered.

Nevertheless, the results also revealed that not everything which would be expected from theory proved right. This shows that the connections and relations between and over the rural and urban environment are very complex. For that reason, further and longer investigations have to be done. The two measurement campaigns lasted on for only two and three months, respectively. This is actually a short time to make statistically reliable statements. Therefore, a measurement campaign over a longer period or during spring would be imaginable.

Bibliography

Althausen, D., R. Engelmann, H. Baars, B. Heese, A. Ansmann, and D. Müller, 2009: Portable Raman Lidar Polly^{XT} for Automated Profiling of Aerosol Backscatter, Extinction, and Depolarization. *J. Atmospheric and Oceanic Technology*, **26**, 2366–2378.

Angevine, W. M., A. B. White, C. J. Senff, M. Trainer, R. M.-Banta, and M. A. Ayoub, 2003: Urban–rural contrasts in mixing height and cloudiness over Nashville in 1999. *J. Geophys. Res.*, **108**, AAC 1–10,.

Ansmann, A., 10.12.2014: Lecture Notes Module 'Aktive Fernerkundung'.

Ansmann, A. and D. Müller, 2005: *Lidar - Range-Resolved Optical Remote Sensing of the Atmosphere*. 6th ed., Springer Series in Optical Sciences, Vol. 102, edited by C. Weitkamp, Springer Berlin/Heidelberg, 105-141 pp.

Baars, H., A. Ansmann, R. Engelmann, and D. Althausen, 2008: Continuous monitoring of the boundary-layer top with lidar. *Atmos. Chem. Phys.*, **8**, 7281–7296.

Baars, H., A. Foth, P. DiGirolamo, and B. Pospichal, 2015: Water vapour profiles from Raman lidar automatically calibrated by microwave radiometer data during HOPE. *Atmos. Chem. Phys.*, **15**, 7753–7763.

Bamberg, G., F. Baur, and M. Krapp, 2012: *Statistik*. 17th ed., Oldenbourg Verlag München, 1-2; 39-43 pp.

Barlow, J., C. Halios, S. Lane, and C. Wood, 2014: Observations of urban boundary layer structure during a strong urban heat island event. *Environmental Fluid Mechanics*, **15**, 373–398.

Bornstein, R., 1968: Observations of the Urban Heat Island Effect in New York City. *J. Appl. Meteorol.*, **7**, 575–582.

Demoz, B., et al., 1999: Determination of Cloud Base Height Using the GSFC Raman Lidar. *Ninth ARM Science Team Meeting Proceedings*, 1–8.

DWD, 1998: Automated Surface Observing System (ASOS) User's Gide. Tech. rep., German Weather Service, 23-31 pp.

DWD, 2010: Mittelung der Wolkenuntergrenzen des CHM 15k - cloudstat. Tech. rep., German Weather Service.

Ehrlich, A., 30.03.2012: Lecture Notes Module 'Measurement Techniques in Meteorology'.

Engelmann, R., et al., 2015: EARLINET Raman Lidar Polly^{XT}: the neXT generation. *Atmos. Meas. Tech. Discuss*, **8**, 7737–7780,.

Engler, C., W. Birmili, G. Spindler, and A. Wiedensohler, 2012: Analysis of exceedances in the daily PM_{10} mass concentration (50 μg m^{-3}) at a roadside station in Leipzig, Germany. *Atmos. Chem. Phys.*, **12**, 10 107–10 123.

Eresmaa, N., M. Rantamäki, and A. Karppinen, 2009: Comparison of urban and rural boundary layer height measurements by ceilometer. *The seventh International Conference on Urban Climate*, 237–243,.

Fahrmeir, L., R. Künstler, I. Pigeot, and G. Tutz, 1998: *Statistik*. 6th ed., Springer-Verlag Berlin Heidelberg, 53-59 pp.

Freudenthaler, V., et al., 2009: Depolarization ratio profiling at several wavelengths in pure Saharan dust during SAMUM 2006. *Tellus*, **61B**, 165–179.

Garratt, J. R., 1992: *The atmospheric boundary layer*. 1st ed., Cambridge Atmospheric and Space Science Series, Cambridge University Press, 1-12 pp.

Hänel, A., 2011: Untersuchungen zu vertikalen Aerosolprofilen nordöstlich von Peking anhand von Messungen mit dem Raman–Lidar Polly. Ph.D. thesis, Fakultät für Physik und Geowissenschaften der Universität Leipzig, 33-38 pp.

Hobbs, P. V., 1993: *Aerosol-Cloud-Climate Interactions*. First edition ed., Academic Press, Inc., Academic Press Limited, 3-16 pp.

Holben, B. N., et al., 1998: AERONET - A Federated Instrument Network and Data Archive for Aerosol Characterization. *Remote Sensing*, **66**, 1–16.

Jin, M. S., W. Keesonkiat, and G. Pereira, 2011: Satellite-Observed Urbanization Characters in Shanghai, China: Aerosols, Urban Heat Island Effect, and Land-Atmosphere Interactions. *Remote Sensing*, **3**, 83–99.

Klett, J. D., 1981: Stable analytical inversion solution for processing lidar returns. *Applied Optics*, **20**, 211–220.

Kreipl, S., 2006: Messung des Aerosoltransports am Alpennordrand mittels Laserradar (Lidar). Ph.D. thesis, Naturwissenschaftliche Fakultät der Friedrich-Alexander-Universität Erlangen-Nürnberg, 9-24 pp.

Mitev, V. M., I. V. Grigorov, and V. B. Simeonov, 1992: Lidar measurement of atmospheric aerosol extinction profiles: a comparison between two techniques - Klett inversion and pure rotational Raman scattering methods. *Applied Optics*, **31**, 6469–6474.

Oke, T. R., 1982: The energetic basis of the urban heat island. *Q. J. R. Meteorol. Soc.*, **108**, 7–24.

Pal, S. R., W. Steinbach, and A. I. Carswell, 1992: Automated method for lidar determination of cloud-base height and vertical extent. *Applied Optics*, **31**, 1488–1494,.

Poulain, L., G. Spindler, W. Birmili, C. Plass-üulmer, A. Wiedensohler, and H. Herrmann, 2011: Seasonal and diurnal variations of particulate nitrate and organic matter at the IfT research station Melpitz. *Atmos. Chem. Phys.*, 1–4,.

Pruppacher, H. R. and J. Klett, 1997: *Microphysics of Clouds and Precipitation.* 2d ed., Kluwer Academic Publishers, 225-226 pp.

Skupin, A., 2013: Optische und mikrophysikalische Charakterisierung von urbanem Aerosol bei (hoher) Umgebungsfeuchte. Ph.D. thesis, Fakultät für Physik und Geowissenschaften der Universität Leipzig, 9-41 pp.

Spindler, G., E. Brüggemann, T. Gnauk, A. Grüner, K. Müller, and H. Herrmann, 2010: A four-year size-segregated characterization study of particles PM_{10}, $PM_{2.5}$ and PM_1 depending on air mass origin at Melpitz. *Atmos. Environ.*, **44**, 164–173,.

Spindler, G., A. Grüner, K. Müller, S. Schlimper, and H. Herrmann, 2013: Long-term size-segregated particle (PM_{10}, $PM_{2.5}$, PM_1) characterization study at Melpitz – influence of air mass inflow, weather conditions and season. *Atmos. Chem. Phys.*, **70**, 165–195,.

UN, 2014: World Urbanization Prospects, United Nations, Department of Economic and Social Affairs, The Revision 2014.

Wendisch, M., 19.12.2013: Lecture Notes Module 'Theory of Atmospheric Radiative Transfer: A Comprehensive Introduction'.

Wiedensohler, A., 13.12.2013: Lecture Notes Module 'Atmosphärische Aerosole'.

Wiedensohler, A., B. Wehner, and W. Birmili, 2002: Aerosol Number Concentrations and Size Distributions at Moutain-Rural, Urban-Influenced Rural, and Urban-Background Sites in Germany. *Journal of Aerosol Medicine*, **15**, 237–243,.

Wiegner, M., et al., 2006: Mixing layer height over Munich, Germany: Variability and comparisons of different methodologies. *J. Geophys. Res.*, **111**, 1–17.

www.actris.eu, Status: 26.10.2015: *ACTRIS*. `http://www.actris.eu/l`.

www.arl.noaa.gov, Status: 18.02.2015: *HYSPLIT*. `http://www.arl.noaa.gov/HYSPLIT_info.php`.

www.cimel.fr, Status: 20.04.2015: *CIMEL Sun Photometer*. `http://www.cimel.fr/?instrument=multi-band-sunsky-photometer&lang=en`.

www.cosmo-model.org, Status: 25.02.2015: *COSMO model*. `http://www.cosmo-model.org/content/tasks/operational/dwd/default_eu.htm`.

www.epa.gov, Status: 22.06.2015: *Urban Heat Island*. `http://www.epa.gov/heatisland/resources/pdf/BasicsCompendium.pdf`.

www.hdcp2.zmaw.de, Status: 22.07.2015: *HOPE Melpitz Campaign*. `http://hdcp2.zmaw.de/`.

www.tropos.de, Status: 06.01.2015: *Lidar*. `http://www.tropos.de/forschung/grossprojekte-infrastruktur-technologie/technologie-am-tropos/fernerkundung/lidar/`.

www.tropos.de, Status: 13.02.2015: *Sun photometer*. `http://www.tropos.de/forschung/grossprojekte-infrastruktur-technologie/technologie-am-tropos/fernerkundung/sonnenphotometer/`.

www.tropos.de, Status: 24.07.2015: *Melpitz Column.* https://www.tropos.de/aktuelles/messkampagnen/melpitz-saeule-2015/.

www.welt.de, Status: 23.05.2015: *Air pollution in Czech Republic.* http://www.welt.de/wissenschaft/article114632484/In-Sachsen-stinkts-nach-tschechischem-Katzendreck.html.

List of Figures

Acknowlegdment

I would like to thank all people who supported and motivated me during the process of this master thesis.
First of all I would like to thank Dr. Holger Baars for his extensive and friendly assistance. He was supervising me and this work, introduced me into lidar and provided me all the data. Despite his familiar commitments, he always had time for me and my questions and helped with words and deeds. He also spent a lot of time proofreading and giving me suggestions how to improve this work. Thanks a lot for the time and effort you spent on this work.
I thank Dr. Heike Kalesse for the accurate proofreading of this work and the helpful hints.
Dr. Patric Seifert for enabling me the participation in the measurement campaign in Melpitz in 2015 and for providing me photos from the measurement site. I would also like to thank all the participants in the Melpitz measurement campaign 2015 for the inspiring discussions.
Kerstin Flachowsky and Achim Grüner for providing me ground-based in-situ data during the Melpitz measurement campaign in 2015.
The whole 'Lidar' team. They received me very friendly and I felt comfortable there.
Prof. Dr. A. Macke and Jun.-Prof. Dr. B. Pospichal for reviewing this master thesis.
My boyfriend Robby Göhler who supported me mental. He was very patient and understanding with me and encouraged me in difficult situations.
Last but not least I want to thank my family in German: Ein großes Dankeschön geht an meine Eltern und Großeltern. Sie haben mich in finanzieller, moralischer und verpflegungstechnischer Hinsicht unterstützt und immer an mich geglaubt. Sie hatten für meine Sorgen und Probleme immer ein offenes Ohr und die passende Lösung parat.

Selbstständigkeitserklärung

Ich versichere, dass ich die vorliegende Arbeit selbständig verfasst und keine anderen als die angegebenen Quellen und Hilfsmittel benutzt habe.
Alle Stellen, die wörtlich oder sinngemäß aus veröffentlichten oder noch nicht veröffentlichten Quellen entnommen sind, sind als solche kenntlich gemacht.
Die Zeichnungen oder Abbildungen in dieser Arbeit sind von mir selbst erstellt worden oder mit einem entsprechenden Quellennachweis versehen.
Diese Arbeit ist in gleicher oder ähnlicher Form noch bei keiner anderen Prüfungsbehörde eingereicht worden.

Ort, Datum

Unterschrift